ANL-6840
Reactor Technology
(TID-4500, 26 th Ed.)
AEC Research and
Development Report

ARGONNE NATIONAL LABORATORY
9700 South Cass Avenue
Argonne, Illinois 60440

# REACTOR DEVELOPMENT PROGRAM PROGRESS REPORT

January 1964

Albert V. Crewe, Laboratory Director
Stephen Lawroski, Associate Laboratory Director

| Division | Director |
|---|---|
| Chemical Engineering | R. C. Vogel |
| Idaho | M. Novick |
| Metallurgy | F. G. Foote |
| Reactor Engineering | L. J. Koch |
| Reactor Physics | R. Avery |
| Remote Control | R. C. Goertz |

Report coordinated by
R. M. Adams and A. Glassner

Issued February 15, 1964

Operated by The University of Chicago
under
Contract W-31-109-eng-38
with the
U. S. Atomic Energy Commission

## DISCLAIMER

## FOREWORD

The Reactor Development Program Progress Report, issued monthly, is intended to be a means of reporting those items of significant technical progress which have occurred in both the specific reactor projects and the general engineering research and development programs. The report is organized in a way which, it is hoped, gives the clearest, most logical over-all view of progress. The budget classification is followed only in broad outline, and no attempt is made to report separately on each sub-activity number. Further, since the intent is to report only items of significant progress, not all activities are reported each month. In order to issue this report as soon as possible after the end of the month editorial work must necessarily be limited. Also, since this is an informal progress report, the results and data presented should be understood to be preliminary and subject to change unless otherwise stated.

The issuance of these reports is not intended to constitute publication in any sense of the word. Final results either will be submitted for publication in regular professional journals or will be published in the form of ANL topical reports.

The last six reports issued in this series are:

| | |
|---|---|
| July 1963 | ANL-6764 |
| August 1963 | ANL-6780 |
| September 1963 | ANL-6784 |
| October 1963 | ANL-6801 |
| November 1963 | ANL-6808 |
| December 1963 | ANL-6810 |

TABLE OF CONTENTS

boiler zone was taken as that of saturated water with zero steam void. Problems were run for three different boiler fuel assembly configurations (see Figure 2): Case I, 8 flow rods, concentrated; Case II, 8 flow rods, dispersed; and, Case III, 12 flow rods. Values of $k_{eff}$ and superheater power fraction (normalized source integral), together with available excess reactivity and flooding worth, are listed in Table II.

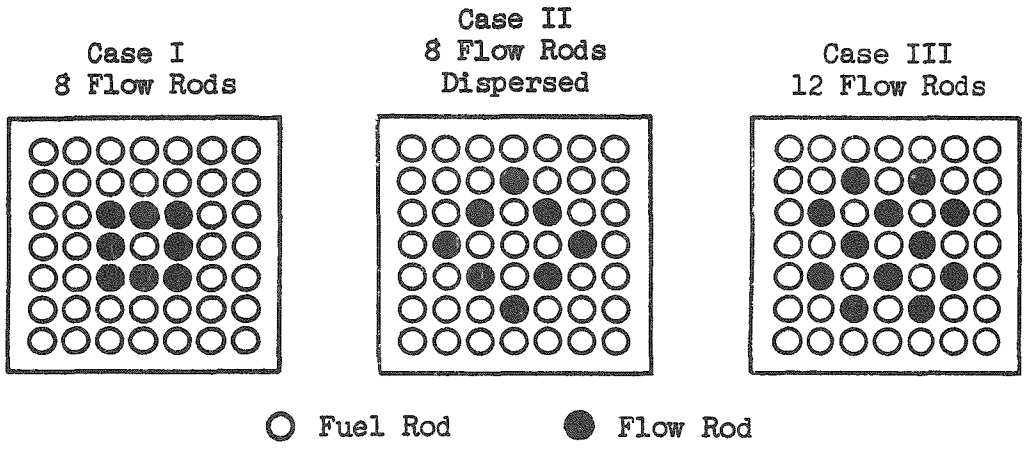


Figure 2. Flow Rod Configurations in Boiling Fuel Assembly for BORAX-V

Table II. Calculated Core Characteristics (Superheater Cores, BORAX-V; Zero Power)

| | Temp. °F | Superheater Fuel Loading (g $U^{235}$ per assembly) | Superheater Condition | Boiler Configuration | Superheater Power Fraction | $k_{eff}$ | Available Excess Reactivity % | Flooding Reactivity Worth % |
|---|---|---|---|---|---|---|---|---|
| Central Superheater | 70 | 680 | Flooded | III | 0.313 | 1.246 | 19.7 | 1.9 |
| | 70 | 680 | Dry | III | 0.219 | 1.217 | 17.8 | |
| | 489 | 680 | Flooded | III | 0.321 | 1.168 | 14.4 | 3.4 |
| | 489 | 680 | Dry | III | 0.215 | 1.123 | 11.0 | |
| | 70 | 430* | Flooded | I* | 0.213 | 1.181 | 15.3 | 0.6 |
| | 70 | 430* | Dry | I* | 0.152 | 1.173 | 14.7 | |
| | 489 | 430* | Flooded | I* | 0.229 | 1.107 | 9.7 | 1.7 |
| | 489 | 430* | Dry | I* | 0.160 | 1.087 | 8.0 | |
| | 70 | 430 | Flooded | III | 0.210 | 1.186 | 15.7 | 0.6 |
| | 70 | 430 | Dry | III | 0.151 | 1.178 | 15.1 | |
| | 489 | 430 | Flooded | III | 0.230 | 1.106 | 9.6 | 1.7 |
| | 489 | 430 | Dry | III | 0.161 | 1.086 | 7.9 | |
| | 489 | 430 | Dry | II | 0.161 | 1.083 | 7.7 | |
| | 489 | 680 | Dry | II | 0.215 | 1.121 | 10.8 | |
| Peripheral Superheater | 70 | 680 | Dry | II | 0.108 | 1.241 | 19.4 | |
| | 70 | 680 | Flooded | II | 0.140 | 1.250 | 20.0 | 0.6 |
| | 489 | 680 | Dry | II | 0.136 | 1.150 | 13.0 | |
| | 489 | 680 | Flooded | II | 0.172 | 1.161 | 13.9 | 0.9 |
| | 70 | 680 | Dry | III | 0.107 | 1.252 | 20.1 | |
| | 70 | 680 | Flooded | III | 0.138 | 1.260 | 20.6 | 0.5 |
| | 489 | 680 | Dry | III | 0.136 | 1.155 | 13.4 | |
| | 489 | 680 | Flooded | III | 0.171 | 1.166 | 14.2 | 0.9 |

*Reference loading for central superheater core CSH-1.

The desired power fraction in the superheater is 0.19. It is evident from the high values of superheater power fraction that the use of the 680 g $U^{235}$ per assembly superheater fuel in the central superheater location is not feasible without either removal of fuel from, or poisoning of, the superheater.

The power fractions calculated for the peripheral superheater are lower than desired. Previous experience has shown that a one-dimensional calculation of the peripheral superheater core may underestimate the power fraction in the superheater by 2 to 3% of the total power. The reference design of the peripheral superheater core included poison rods in the boiler to obtain the proper power split.[1] The proper power fraction probably can also be obtained by control rod manipulation alone.

The changes in available excess reactivity shown in Table II do not agree in either sign or value with the measured changes with the same flow rod configurations reported in Section 1.

3. Performance of Core CSH-1

Preliminary analysis of data from in-core and in-reactor vessel instrumentation measurements made during the brief power operation of central superheater core CSH-1 has been completed and is presented in the following sections.

a. Steam Temperature. The steam temperatures in the core as measured by two chromel-alumel thermocouples in each location of the first- and second-pass instrumented superheater fuel assemblies are presented in Table III.

Table III. Average Steam Temperatures in Instrumented Superheater Fuel Assemblies

| Reactor Power (MW) | Inlet Steam Temp (°F) | First-pass Exit Temp (°F) | Second-pass Entrance Temp (°F) | Second-pass Exit Temp (°F) |
|---|---|---|---|---|
| 1.9 | 480 | 605 | 593 | * |
| 5.2 | 486 | 636 | 618 | 755 |
| 7.0 | 485 | 671 | 602 | 775 |
| 7.3 | 487 | 640 | 618 | * |
| 10.2 | 487 | 635 | 620 | 770 |

*Data not available.

b. Flow in Boiling Fuel Assembly. Inlet velocity and flow in instrumented boiling fuel assembly I-1 in core position 33 are plotted in Figure 3 as based on recorded information furnished by the turbine-type inlet flowmeter. Recorded volumetric flow data were corrected for meter body expansion (increased flow area) and for reduced water density which causes a higher indicated flow in the ratio of $(\gamma_1/\gamma_2)^{1/2}$, the ratio of fluid specific weights at calibration and use conditions, respectively. Because of restrictions caused by the inlet and outlet flowmeters, the flow in a standard boiling fuel assembly in a symmetrical core location will be about 10% greater than in an instrumented assembly.

[1] Design and Hazards Summary Report, BORAX-V, ANL-6302.

c. Exit Void Fraction. Outputs from the inlet and exit turbine meters on the instrumented boiling fuel assembly I-1 in core position 33 furnished the data for calculating the exit void fractions shown in Figure 4. The void fraction $\alpha$ is defined as

$$\alpha = (v_{out} - v_{in})/v_{out},$$

where

$v_{out}$ = exit water velocity;

$v_{in}$ = inlet water velocity,

both being determined from recorded volumetric flow data.

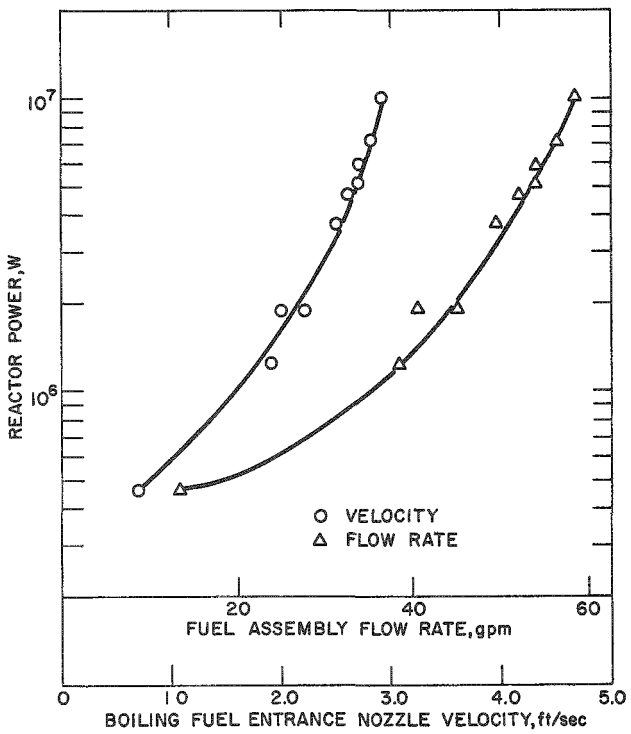


Figure 3. Inlet Velocity and Flow vs. Reactor Power for Instrumented Boiling Fuel Assembly I-1, Core CSH-1 of BORAX-V

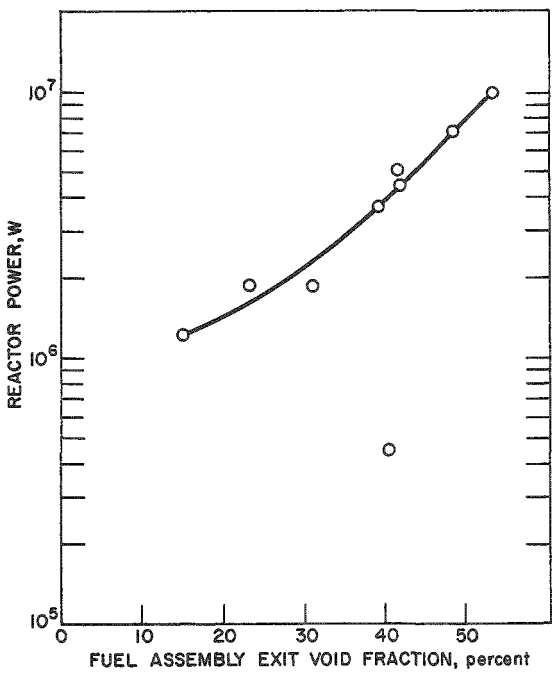


Figure 4. Exit Void Fraction vs. Reactor Power for Instrumented Boiling Fuel Assembly I-1, Core CSH-1 in BORAX-V

d. Boiling Fuel Rod Temperatures. Five boiling fuel thermocouple rods in the instrumented boiling fuel assembly and two in a standard fuel assembly were used to obtain the $UO_2$ fuel temperatures shown in Figures 5, 6, and 7. Note that the various axial locations, as well as radial core locations, allow an indication of the power density as a function of location. These fuel rods contained W-W/26% Re thermocouples in the axial center of the fuel.

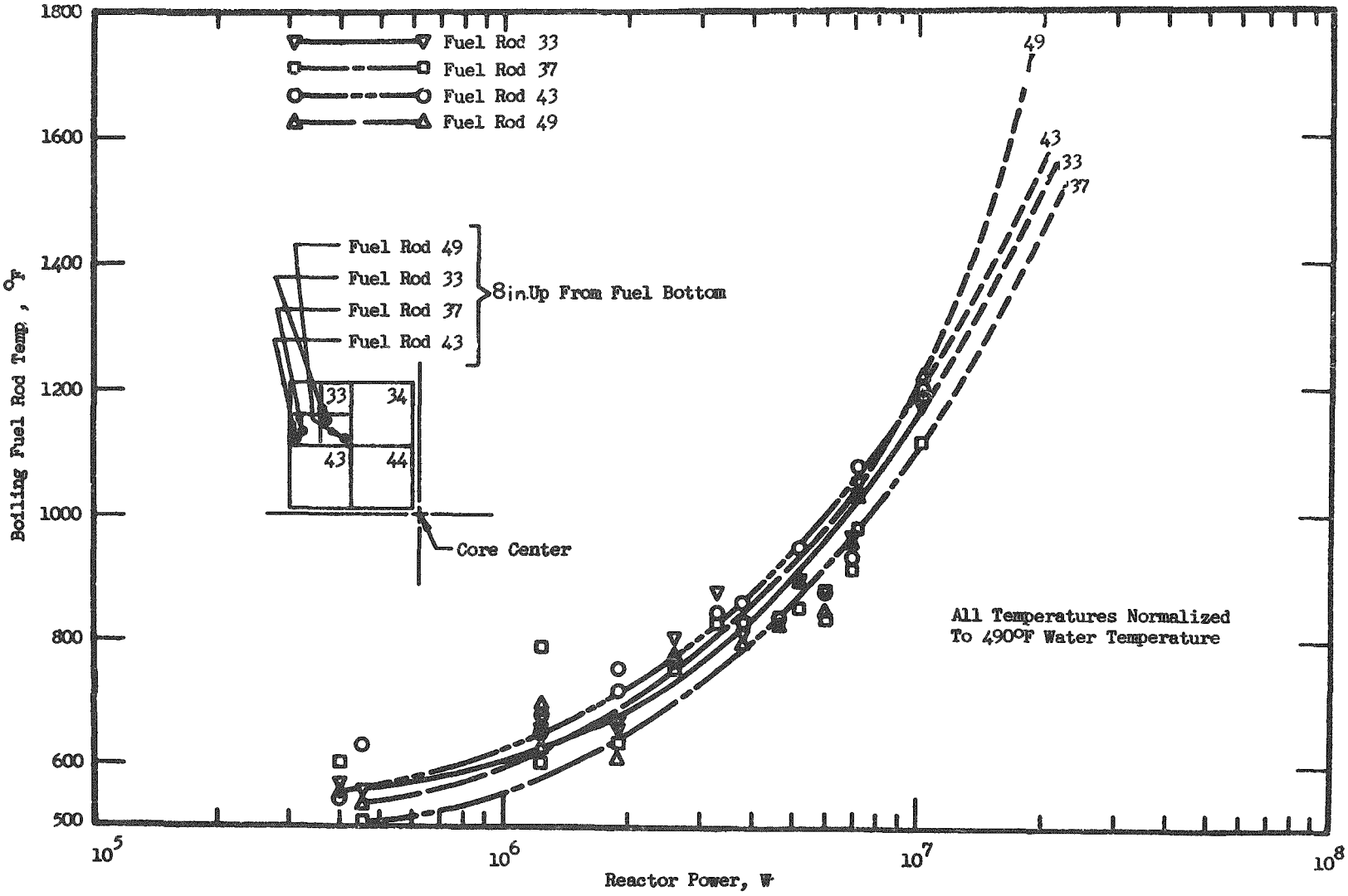


Figure 5. Boiling Fuel Rod Indicated $UO_2$ Temperature vs. Reactor Thermal Power for Core CSH-1 in BORAX-V

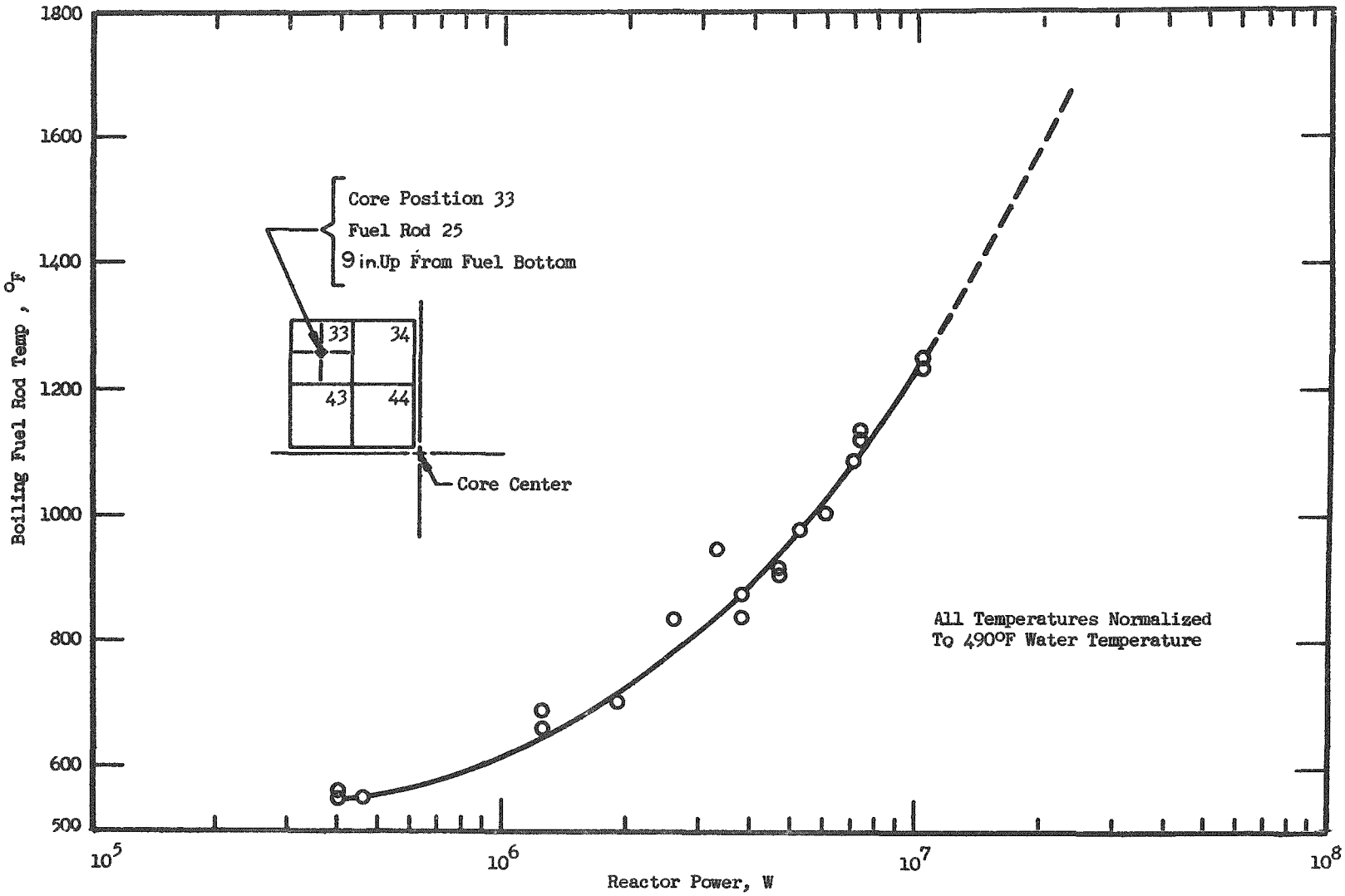


Figure 6. Boiling Fuel Rod Indicated $UO_2$ Temperature vs. Reactor Thermal Power for Core CSH-1 in BORAX-V

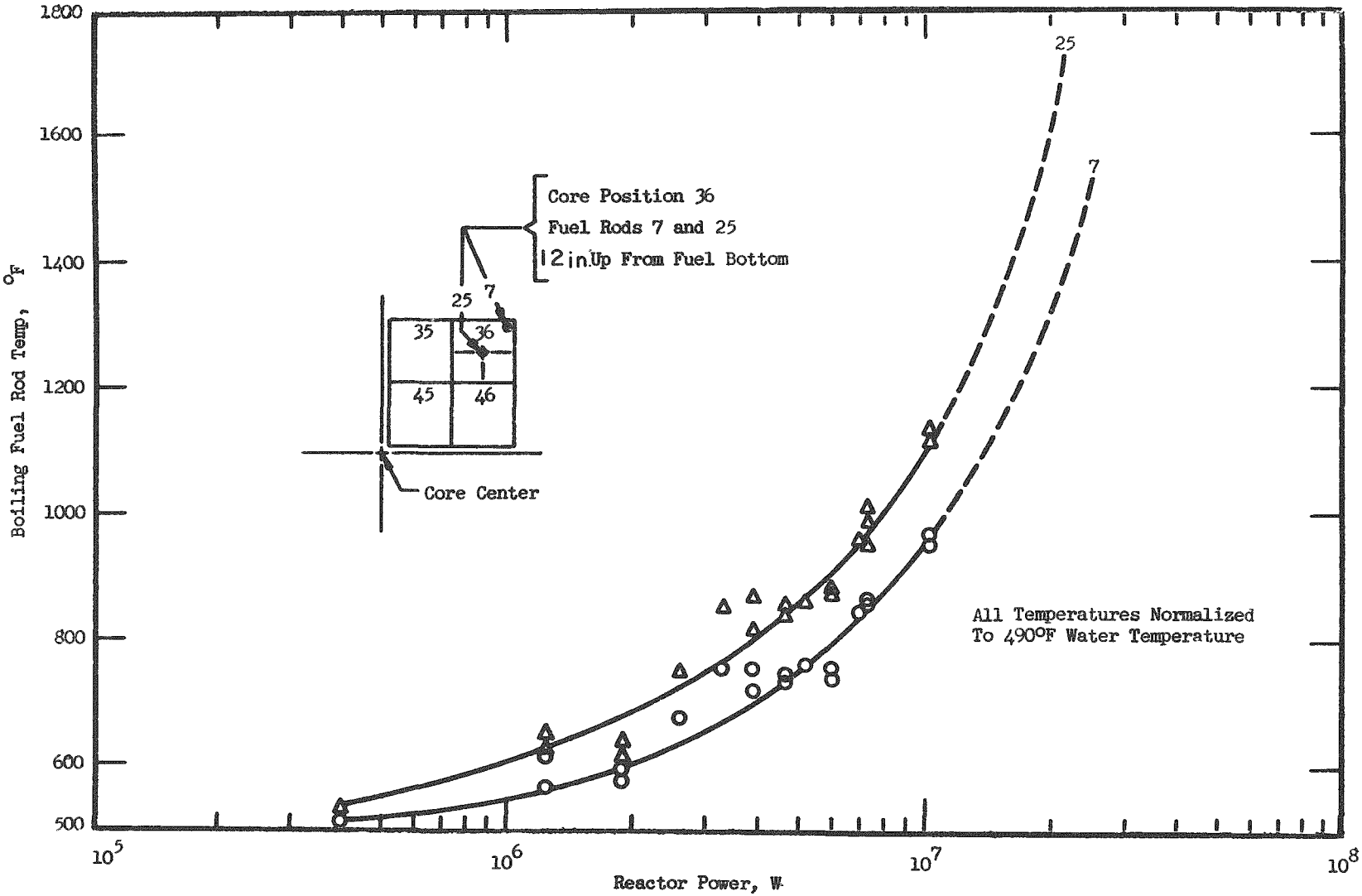


Figure 7. Boiling Fuel Rod Indicated $UO_2$ Temperature vs. Reactor Thermal Power for Core CSH-1 in BORAX-V

The total fuel burnup of these thermocouple fuel rods is below that experienced during boiling core B-2 operation by about a factor of 30, and none of the time- varying temperatures were observed as during core B-2 operation. (See Progress Report for March 1963, ANL-6705, p. 8, for a discussion of postulated fuel irradiation damage.)

e. Downcomer Velocity. Downcomer velocity measurements were made with a Stauschiebe tube located on the inner wall of the reactor vessel, 1 5/32 in. below the top of the core support plate. The associated differential-pressure cell had a full-scale pressure range of 4 in. of 68°F water.

To interpret the data, a duplicate of the Stauschiebe tube used in the BORAX-V reactor vessel to measure downcomer velocity was installed in a vertical flow test section of a circulating water loop to determine its calibration coefficient. The tube is constructed of $\frac{7}{8}$-in.-diameter stock, 4 in. in length, with two taps spaced 180° apart and centered on the probe length. All tests were made at atmospheric pressure with 70°F water.

Several traverses were made to determine velocity profiles in the test section. The final results showed a marked sensitivity to wall proximity. When mounted $\frac{3}{4}$ in. from the wall to centerline of probe (simulating reactor vessel installation), the flow calibration coefficient was 2.69, based on average stream velocity. At the point of average stream velocity, the coefficient was 1.88. The coefficient is defined as follows:

$$h = Cv^2/2g,$$

where

C = calibration coefficient;

h = measured differential pressure (ft of flowing fluid);

v = fluid velocity (ft/sec);

g = local acceleration due to gravity ($ft/sec^2$).

Because of the lack of sufficient data to establish reliability of measurements - in particular, the zero point - measurements of downcomer velocity are not reported.

f. Steam Carryunder. The volume fraction of steam carried under into the downcomer by natural circulation is shown in Figure 8. Water-cooled static pressure taps in the vessel downcomer sensed differential pressure between their 12-in. vertical separation to give a void fraction output on their differential-pressure transmitters.

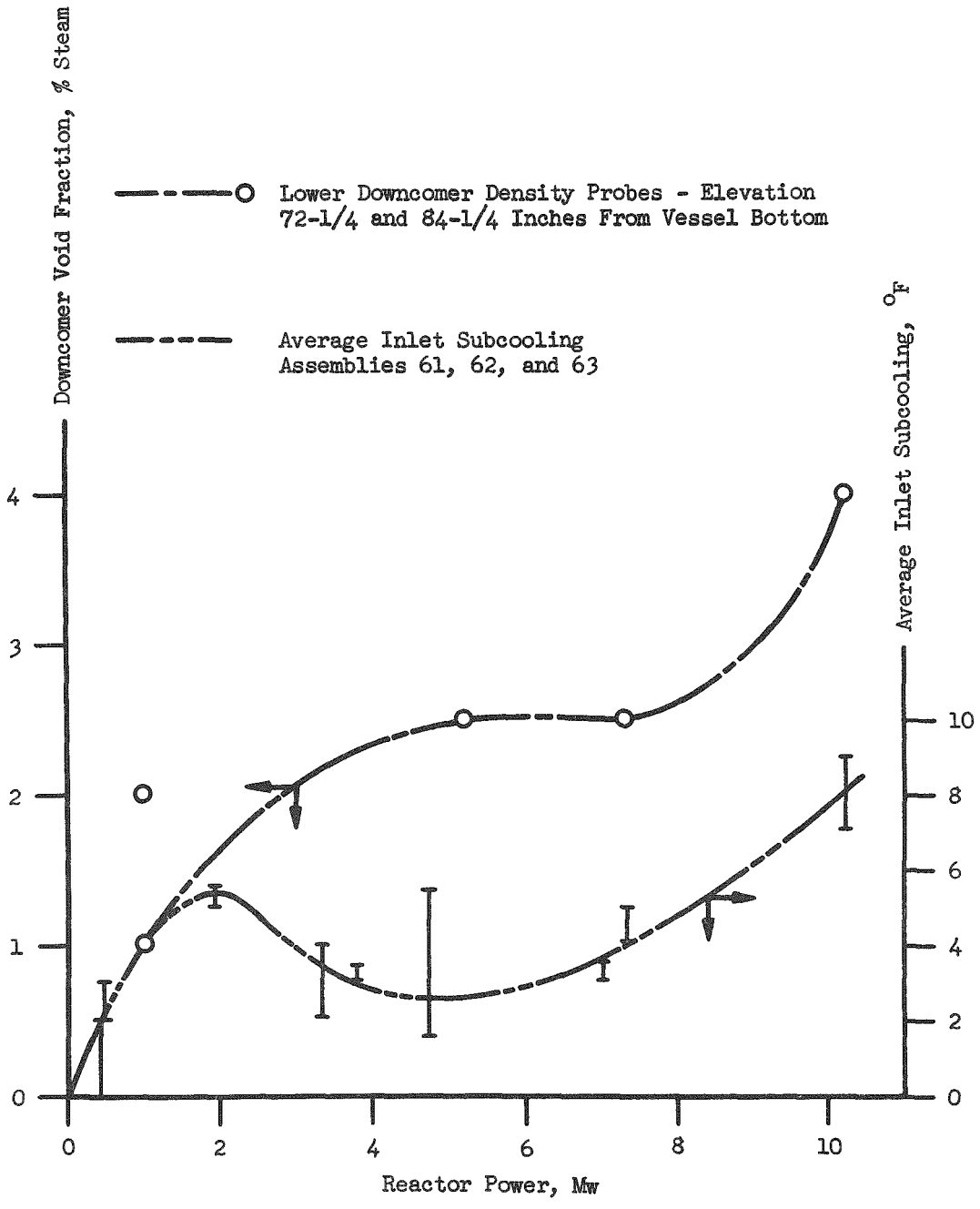


Figure 8. Downcomer Void Fraction and Core Inlet Subcooling vs. Reactor Power for Core CSH-1 of BORAX-V

g. Inlet Subcooling. Subcooling measurements were made with thermocouples sensing steam dome temperature and inlet water temperatures at fuel assembly positions 61, 62, and 63. Data were obtained from two thermocouples per inlet location for various reactor power levels. The curve shown in Figure 8, representing averages of these values, also indicates maximum and minimum values. The initial peak in the subcooling curve at low power appears to be a result of extra feedwater additions due to seal water, downcomer probe-cooling water, and operation of the reactor water demineralizer.

h. Reactor Water Level. Table IV gives a comparison of the reactor water levels measured by means of the standard operating instrument LR-1 and the special accurate ultrasonic water-level probe. This table gives an indication of the calibration errors which can be expected from use of standard pressure-compensated, differential-pressure sensing level indicators and recorders when applied to reactor water-level measurements. At higher powers and resultant void fractions, the errors might become significant, as was reported earlier for boiling core B-2 operation (see Progress Report for February 1963, ANL-6698, p. 9).

Table IV. Reactor Water Level

| Reactor Power (MW) | Water Level from LR-1* | Water-Steam Mixture Interface Elevation from Acoustic Probe | Water** Elevation from Acoustic Probe |
|---|---|---|---|
| 5.2 | 12'-10" | 13'-0" | 12'-6" |
| 7.32 | 12'-8" | 12'-11$\frac{1}{2}$" | 12'-$\frac{1}{2}$" |
| 10.2 | 12'-9" | Above 13'-2"† | Above 13'-2"† |

*Operating instrument. Saturation pressure-compensated, differential-pressure sensor, and circular chart recorder.

**Elevation at which mixture density approached that of saturated water, as evidenced by constant readings on acoustic probe indicator.

†Upper limit of probe travel.

# II. LIQUID-METAL-COOLED REACTORS

## A. General Fast Reactor Physics

### 1. ZPR-III

a. Experimental Program. Experiments continued with Assembly 44, the plutonium mockup of the French reactor RAPSODIE. The first phase of the program, concerning physics core experiments, was completed this month and the transition to the engineering core experiments was started.

Central reactivity coefficients were measured, and some sample-size effects were investigated. The worths of plutonium and uranium were measured at various core positions, and uranium foils were irradiated.

In the measurements of central reactivity coefficients, 2 x 2 x 2-in. samples of a number of materials were substituted for void at the core center by means of a sample-changer mechanism that allows continuous running of the reactor without separation of the machine halves for changing the samples. Table V lists some of the results of central reactivity coefficient measurements with the 8-cu in. sample space.

Table V. Central Reactivity Coefficients in Assembly 44 (RAPSODIE) with 2 x 2 x 2-in. Samples

| Material | Reactivity Coefficient, Ih/kg |
|---|---|
| Stainless Steel (Type 304) | -5.3 ± 0.5 |
| Aluminum | +8.6 ± 1.0 |
| Molybdenum | -21 ± 0.5 |
| Iron | -5.8 ± 0.5 |
| Sodium | +53 ± 5 |
| Carbon | +156 ± 5 |

Some reactivity coefficient measurements were made with 1/2 x 2 x 2-in. samples in a sample space across the front of the central core drawer (1 in. from the core center) to investigate the discrepancy between results with the 2 x 2 x 2-in. samples and previous experiments with 1/4 x 2 x 2-in. samples (see Progress Report for December 1963, ANL-6810, p. 5) aligned axially in the drawer. The results of the new, small-sample substitutions again gave values for steel and aluminum that differ by factors of three or four and are different in sign. The data are

still being analyzed, and it is difficult to state whether or not sample-size effects or orientations are the source of the differences or whether the temperature effects in the assembly mask the small reactivity changes with the small samples.

Worths of plutonium, enriched uranium, and depleted uranium at a number of positions in the core were obtained from substitutions of 1/8 x 2 x 2-in. plates for void. The positions, including the core center, were on the core midplane at the radial core edge and at 1/2 the core radius, and on the axis at the axial core edge. The results are given in Table VI.

Table VI. Local Worths of Plutonium, Enriched Uranium and Depleted Uranium in Assembly 44 (RAPSODIE)

| Position (in. from center) | | Reactivity Coefficients (Ih/kg) | | |
|---|---|---|---|---|
| Radial | Axial | Pu[a] | Enr. U[b] | Depl. U[c] |
| 0 | 0 | 854 | 479 | 17 |
| 3.1 | 0 | 688 | 406 | 37 |
| 6.6 | 0 | 335 | 233 | 23 |
| 0 | 6 | 426 | 258 | 27 |

[a] 95% $Pu^{239}$; 5% $Pu^{240}$.

[b] 93.3% $U^{235}$.

[c] 0.2% $U^{235}$.

In the irradiation experiments, enriched and depleted uranium foils and sodium capsules were positioned near the core center, at the core radial edge, and at 3 in. into the radial blanket, and irradiated during a 30 Whr run. Radiochemical analysis of the foils and activation measurements of the capsules gave the results in Table VII.

The critical volume of the physics core was found to be larger than predicted from earlier calculations. Consequently, it was expected that the addition of the gaps, channels, etc., or the transition to the engineering core would provide a critical core volume in excess of a limitation of about 40 liters in the RAPSODIE reactor. It was thus decided to increase fuel concentration in the Assembly 44 core composition to provide a smaller engineering core volume. This was accomplished by replacing a 1/4-column enriched uranium and a 1/4-column depleted uranium in each drawer with 1/2-column plutonium (see Progress Report for October 1963, ANL-6801, p. 9), giving two plutonium, two enriched uranium, and one depleted uranium column per drawer. The resulting composition is given in Table VIII. After

unloading about half the physics core volume, an approach to critical was made with the new composition; and criticality was obtained with 32 drawers in each half in a symmetrical cylindrical geometry.

Table VII. Results of Fission and Activation Measurements in Assembly 44 (RAPSODIE)

| Location | Fissions per g | | Captures per g | Sodium Captures |
|---|---|---|---|---|
| | Enr. U | Depl. U | Depl. U | per g |
| Core Center | $6.1 \times 10^{10}$ | $5.9 \times 10^{9}$ | $5.0 \times 10^{9}$ | $2.0 \times 10^{8}$ |
| Core Edge | $4.2 \times 10^{10}$ | $3.1 \times 10^{9}$ | $3.7 \times 10^{9}$ | $1.4 \times 10^{8}$ |
| 3 in. in Blanket | $1.8 \times 10^{10}$ | $5.0 \times 10^{8}$ | $1.9 \times 10^{9}$ | $8.5 \times 10^{7}$ |

Table VIII. Composition of Assembly 44 (RAPSODIE) Engineering Core

Core Unit Cell - 14.06 x 2.18 x 2.18 in
Volume - 1.0944 liters

| Material | Density in Core (g/cc) | Volume % |
|---|---|---|
| Pu[a] | 0.89 | 4.7 |
| $U^{235}$ | 1.75 | 9.4 |
| $U^{238}$ | 1.08 | 5.7 |
| Al | 0.46 | 17.2 |
| O | 0.52 | (20.4)[b] |
| Fe | 1.36 | 17.4 |
| Cr | 0.17 | 1.2 |
| Ni | 0.09 | 2.1 |

[a] 95.0% $Pu^{239}$, 4.5% $Pu^{240}$; 0.5% $Pu^{241}$.

[b] Assuming 100% density is $0.096 \times 10^{24}$ atoms/cc.

Preliminary measurements of edge core worth gave an estimated just-critical loading of about 31.5 drawers with a critical volume of 34.3 liters.

b. Examination of a Defective ZPR-III Plutonium Fuel Plate. A badly swollen ZPR-III Pu-1 w/o Al alloy fuel plate has been examined. It appears that swelling was most probably caused by reaction of the fuel alloy with water and organic liquids. The fuel plate, nominally 2.5 x 5 x 0.3 cm (1 x 2 x 1/8 in.) was nickel coated and canned in a 0.38-mm (0.015-in.)-thick stainless steel jacket. It was received by the Idaho Division on Dec 17, 1959, and on July 10, 1963 it was found to have swollen drastically.

Before dejacketing the plate, the can was punctured in an enclosure in order to sample the gas that caused the swelling. The fuel plate removed from the can is shown in Figure 9. Several small pimples were found on the plate. Also, the steel leaf spring supposed to position the fuel plate in the jacket was found in three pieces. In addition, both sides of the fuel plate were stained as from a dried liquid.

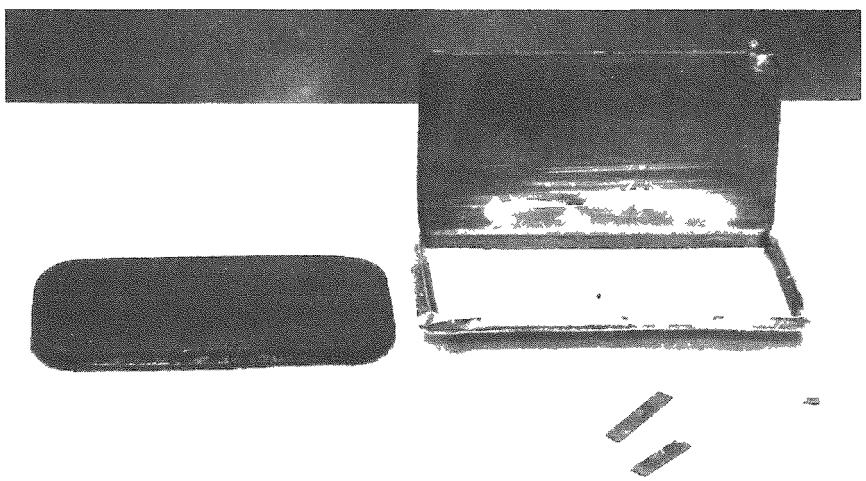

38173 ~1X

Figure 9. A Pu-1 w/o Al Alloy Fuel Plate (Left) Removed from the Stainless Steel Jacket (Right) of a ZPR-III Fuel Element That Had Swelled during Storage. The puncture in the bottom of the jacket was made to recover gases for testing. Below the jacket are three fragments of a steel spring that had been used to position the plate.

Mass-spectrographic analysis of the gas that caused the jacket to swell showed it to be mostly hydrogen and methane with smaller amounts of ethane, propane, and carbon dioxide (see Table IX).

A rough measurement of the lattice parameter of the powder found in the small pimples showed it to be either $PuH_2$ or $PuO_2$ with a trace of $Al_2O_3$. More precise measurements would have to be made to distinguish between $PuH_2$ and $PuO_2$, because of the similarity in their lattice parameters.

Table IX. Mass-spectrographic Analysis of Gas Sample Taken from Swelled Fuel Plate No. 235

| Gas | % |
|---|---|
| Hydrogen ($H_2$) | 70.7 |
| Helium (He) | 0.1 |
| Methane ($CH_4$) | 15.7 |
| Ethane ($C_2H_6$) | 8.6 |
| Propane ($C_3H_8$) | 2 9 |
| Carbon Dioxide ($CO_2$) | 1.2 |
| Mass 31 | 0.8 |

Normal fabrication procedure calls for cleaning the plate with trichloroethylene ($C_2HCl_3$) followed by evacuating to 1 $\mu$ to remove the solvent prior to canning. Ethyl alcohol and water might also be present from the routine bubble testing of the welds for leaks. These liquids can be trapped if the removal of trichloroethylene is not complete or if, instead of stripping off a can containing a pin-hole leak, an attempt is made to repair the defective can. The stains on both sides of the decanned fuel plate strongly suggest that a liquid was present. Studies elsewhere have shown that this problem can be practically eliminated if great care is taken to avoid trapping water and solvents

2. ZPR-VI

a. Facility. The ZPR-VI facility was modified for use with Assembly No 2, a 650-liter carbide core. The dual-purpose rods were relocated and four $B^{10}$ insertion safety rods were added to each reactor half. Equipment for determining the fatman effect was also installed. Fuel loading was started on January 8, 1964, and criticality was attained on January 14, 1964. Experimental measurements are now being made on the assembly.

b. Assembly No. 1 Results. Fuel columns in certain zones of Assembly 1 of ZPR-VI were bunched or unbunched (see Figure 10). By making some zones symmetrical and others unsymmetrical to the plane of the fuel, an attempt was made to separate the measured effects into two parts. It was assumed that the bunching effect was the sum of a real heterogeneity effect, due to transport phenomena, and a pure geometric effect, due to change of importance of the bunched fuel. The following steps were performed:

(i) Bunching was accomplished by rearranging the fuel in each drawer. To bunch, two 1/8-in. fuel columns in a drawer were combined into one 1/4-in. fuel column in the center of the drawer and the following drawers were bunched for each experiment:

(A) all drawers in one quadrant of the core symmetrical to its horizontal midplane (Section 1 of Figure 10);

(B) all drawers in the quadrant supplementary to Section 1, and symmetrical to the vertical midplane of the core (Section 2 of Figure 10);

(C) all drawers in the horizontal midplane of the core (Section 3 of Figure 10);

(D) all drawers in the vertical midplane of the core (Section 4 of Figure 10).

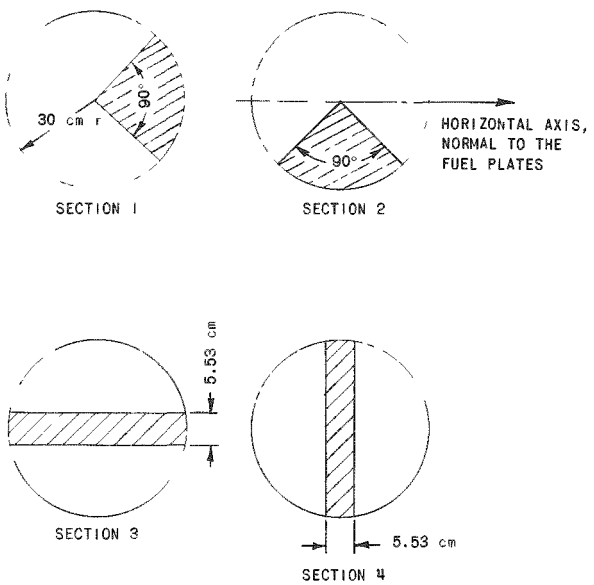


Figure 10

Cross Section through the Cylindrical Core of ZPR-VI Assembly 1. Bunched fuel zones are cross hatched.

(ii) The drawers in the remaining quadrants in (i)(A) and (i)(B) above were unbunched. The two 1/8-in. fuel columns per drawer were split into four 1/16-in. fuel columns and evenly distributed in the drawers.

(iii) The fuel columns in the six central drawers were unbunched further by a separation of the 1/8-in. fuel columns into 1/32-in. fuel columns.

The experimental results were corrected for changes in reactivity due to increased leakage and shift of the importance peak of the reactor. The errors indicated were estimated from reproducibility

experiments performed prior to the bunching experiments and from the uncertainties determined by the control-rod-calibration measurements. Changes in control-rod worth, up to 5%, were measured close to the bunched zones and were taken into account in the calculations. Further corrections were necessary to allow for the shape of the bunched sectors which deviate from a complete quadrant at the control rod positions and in the center of the core.

The results compiled in Table X are given in in-hours, where 480 Ih are equivalent to 1% $\Delta k/k$. The experimental results of either bunching or unbunching for the region of interest are shown in column 3. The separated effects of bunching as extrapolated for the whole core are shown in the last two columns, with the geometry effect shown in the second column and the heterogeneity effect shown in the third column.

Table X The Effect of Fuel Bunching on Reactivity

| Section No. | Description of Core Zones | Calculated Effect (Ih) on Core: Experimental Results on Region of Interest | Calculated Effect (Ih) on Core: Geometric Effect Extrapolated | Calculated Effect (Ih) on Core: Heterogeneity Effect Extrapolated |
|---|---|---|---|---|
| | Bunching 1/8 → 1/4 in. | | | |
| 1 | Quadrant Symmetrical to Horizontal Midplane | +97 ± 5 | +39 ± 22 | +361 ± 20 |
| 2 | Quadrant Symmetrical to Vertical Midplane | +112 ± 5 | | |
| 3 | Row in Horizontal Midplane | +57.5 ± 3 | +67 ± 21 | +304 ± 33 |
| 4 | Row in Vertical Midplane | +76.8 ± 3 | | |
| | Calculated by 1-group Approximation | | +28 | |
| | Unbunching 1/8 in. → 1/16 in. | | | |
| 1 | Quadrant Symmetrical to Horizontal Midplane | -55.8 ± 5 | -5.4 ± 23 | -212 ± 20 |
| 2 | Quadrant Symmetrical to Vertical Midplane | -58.5 ± 5 | | |
| | Calculated by 1-group Approximation | | -9 | |
| | Unbunching 1/8 in. → 1/32 in. | | | |
| | Central 6 Drawers with Diminished Fuel Content | -14.1 ± 3 | | |
| | Extrapolated to Regular Fuel Content | -17.3 ± 4 | | -215 ± 56 |
| | Calculated by 1-group Approximation | | -11 | |

## B. General Fast Reactor Fuel Development

### 1. Metal Fuels

#### a. U-Pu-Fs and U-Pu-Fz

(i) Properties. The structures, phases, and transformation kinetics of U-Pu-Fz alloys are being studied. The composition of the major second phase in U-10 w/o Pu-10 w/o Fz consists of about 40 w/o each of zirconium and uranium, and 10 w/o each of plutonium and ruthenium. In the U-10 w/o Pu-10 w/o Fs alloy, a composition corresponding to $U_2Ru$ predominated in the major second phase. The quantities of these phases were measured by point analysis, and found to be 8 and 10 v/o respectively.

The alloys were annealed for one week at 775°C and oil quenched prior to the analysis. An electron-beam microprobe analyzer was used at Mound Laboratory to measure the compositions.

(ii) Compatibility with Potential Cladding Materials. U-Pu and U-Pu-Fz alloys are being tested for compatibility with potential cladding materials to help in the selection of fuel and cladding materials for future fast reactors.

The fuel-cladding combinations of U-10 w/o Pu and U-20 w/o Pu-10 w/o Fz with niobium and of U-10 w/o Pu-10 w/o Fz with niobium, Nb-1 w/o Zr, molybdenum, vanadium, V-10 w/o Ti, V-20 w/o Ti, 304 stainless steel, and Hastelloy-X are being investigated in the temperature range from 550 to 650°C.

Information concerning several of these combinations has been reported earlier (see Progress Reports for May, June, October, and November 1963). Preliminary results of compatibility of U-10 w/o Pu-10 w/o Fz with vanadium, V-10 w/o Ti, and V-20 w/o Ti between 550 and 650°C are given in Table XI.

Table XI. Penetrations of U-10 w/o Pu-10 w/o Fz into Vanadium, V-10 w/o Ti, and V-20 w/o Ti Alloys

| Temp, °C | Penetrations ($\mu$) | | | | | |
|---|---|---|---|---|---|---|
| | Vanadium | | V-10 w/o Ti | | V-20 w/o Ti | |
| | 17 days | 42 days | 7 days | 17 days | 7 days | 17 days |
| 550 | nil | nil | - | - | - | - |
| 600 | nil | nil | 2 | 3 | 2 | 2 |
| 650 | - | 1 | 4 | 5 | 4 | 4 |

In the study of compatibility with vanadium, very little penetration into the vanadium is detected, but at 650°C a continuous gray band up to 11 $\mu$ thick was found on the fuel side of the couple. Electron microprobe analysis indicates that no vanadium is present in this band and that it is composed of a material having a rather low average atomic number containing large amounts of uranium and plutonium. Because of the high concentration of oxygen in the vanadium used (1300 ppm) it seems likely that this band is a solid solution of uranium and plutonium oxides.

Vanadium having a lower oxygen concentration (360 ppm) has been tested with U-10 w/o Pu-10 w/o Fz. Although some gray material was present in the fuel, a continuous layer was not formed. As would be expected, this combination showed measurable penetration into the vanadium

(about 1.5 $\mu$ at 650°C for 10 days). It seems quite likely that compatibility between vanadium and uranium-plutonium containing alloys is sensitive to the oxygen content of the vanadium.

V-10 w/o Ti and V-20 w/o Ti were penetrated more deeply by the fuel than was vanadium (about 5 $\mu$ at 650°C for 17 days for both alloys), but this is still very low when compared with niobium, for which the penetration was 30 $\mu$ at 650°C for 17 days. The difference in penetration characteristics between vanadium and V-Ti alloys may be due in part to their lower oxygen content (300 to 600 ppm), but the addition of titanium is probably more responsible. There was also some evidence for diffusion into the fuel of the V-Ti alloys, but this has not yet been substantiated.

b. Development of Metal Fuels for Use in Fast Criticals. Plate elements of U-25 w/o Pu-1.5 w/o Fe, jacketed in stainless steel envelopes, are being considered for use in ZPR-III and ZPPR. Cylindrical slugs of the same composition, jacketed in stainless steel, are being considered for the Mazurca reactor element. Because several tens of thousands of the plate specimens will be required, the fabrication method should be adapted to reasonably high production rates.

Preliminary tests of a precision casting method using copper chill and graphite molds have been successful. There appears to be a considerable difference in the structure of the metal cast in copper and that cast in graphite.

Preliminary rolling tests at 250°C were made with a billet heated to a temperature of 615 to 620°C. The rolls were set for 5 percent reduction per pass. Cracks occurred on the first reduction pass. The billet fragmented on the second pass through the mill.

The alloy was centrifugally cast directly into thin-walled, stainless steel cylindrical jackets with a plug welded into the bottom end. The surfaces of the jackets were protected by silver foil wrapped about the outer diameter. A graphite gate funnel was provided to protect the top of the jacket sleeve. Each jacket was clamped tightly in a copper chill mold, which was bolted to the centrifugal-casting machine rotor wheel. The alloy was vacuum melted at 680°C and superheated approximately 400°C for centrifugal casting. The rotor speed was 350 rpm.

After casting, the exposed sprue was counterbored below the jacket opening. The lip of the jacket was wiped clean and a stainless steel plug inserted. The specimens were then carefully wiped until all wipe tissues showed less than 500 dpm alpha. The plug was then TIG welded in place. The weld contamination level was 3000 dpm alpha. Difficulty in controlling contamination in the weld and on the surface of the jackets appears to be the principal problem of an in-jacket casting. The U-Pu-Fe

core shrank away from the stainless steel jacket very slightly. There was no evidence of bonding. The specimens were X-rayed and sectioned to evaluate mold filling which appeared to be satisfactory.

c. Experimental EBR-II-type Irradiation Specimens. An additional 32 samples were prepared of U-10 w/o Pu-10 w/o Fz alloy from pin-end remelts, which were cast from a strainer crucible into a billet mold and then remelted and injection cast into fuel pins. The castings were exceptionally good: the surface quality was good and the metal appeared extremely clean. A 100 percent yield on the basis of molds charged was obtained.

Fifty-five fuel tubes of Nb-1 w/o Zr alloy, of Nb-4 w/o V alloy, and of vanadium were cleaned, fitted with end plugs, and welded. A sodium-purifying train was set up in which the sodium is gettered and filtered. Two sodium samples were analyzed for oxygen contents, which were 175 ppm and 228 ppm, respectively.

d. Radiator-type Fuel Elements. Twelve specimens have been compacted from powdered U-15 w/o Pu-10 w/o Fz alloy. The specimens were of single-size-fraction powders with average densities as follows:

| NBS Sieve Size | Percent Theoretical Density |
|---|---|
| -325 | 59 |
| -200, +325 | 58 |
| -120, +200 | 60 |

The compacted-fuel column-length was 5 cm. The jackets were Nb-1 w/o Zr tubing of 0.4-cm inside diameter

The specimens were sodium bonded by use of the following sequence:

1. Load and vibratory compact metal power.
2. Extrude, measure, and weigh sodium wire.
3. Place sodium wire in specimen tube.
4. Evacuate tube.
5. Melt sodium
6. Pressurize with helium gas.

The sodium was heated to 200°C and the furnace pressurized with one atmosphere of helium, which forced the sodium down into the powder bed. Bond effectiveness was determined by comparison of measured bond level with a calculated bond level based upon the void fraction

of the powder column. In five tubes the bonded sodium level was within 0.16 cm of the level calculated for complete bonding. The effectiveness of the bond is being further evaluated by the preparation of a series of metallographic specimens. Similar specimens are being prepared for ultrasonic testing.

e. Vibratory Compaction. The results of the study of compaction of spherical shapes is summarized in Figure 11, in which void packing efficiency is plotted against ratio of diameter of container to first component, first to second, second to third, etc. The upper curve is the packing efficiency of the first component, which is a function of the ratio of diameter of container to diameter of the first component sphere, $D/d_1$.

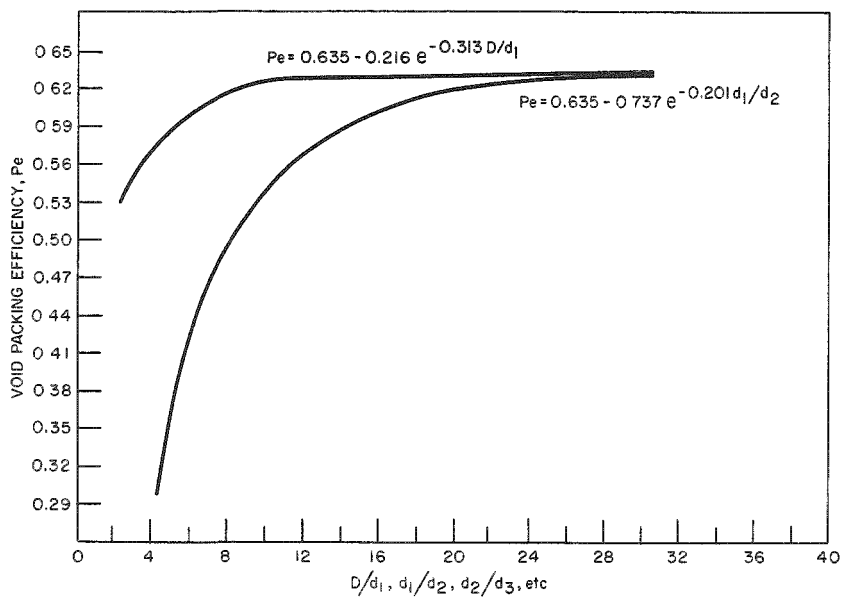


Figure 11. Void Packing Efficiency vs. Ratio of Diameter of Container to First Fraction ($D/d_1$), First Fraction to Second Fraction, etc.

The value 0.635 in the equation

$$Pe = 0.635 - 0.216\, e^{-0.313\, D/d_1}$$

is the limiting density to which spherical bodies will fill a void space. The void spaces within a matrix of packed spheres is a somewhat triangular pore path which permeates, and is continuous through, the entire structure offering an exaggerated boundary condition. The relationship between the void-packing efficiency and the ratio of first-to-second component is given by the lower curve in the figure, the equation being

$$Pe = 0.635 - 0.737\, e^{-0.201\, d_1/d_2}.$$

With the aid of these two equations, it is possible to calculate the packing efficiency of any multicomponent system of spheres as a function of diameter ratios. If the packing efficiency of spheres within a cylinder is

$$Pe = 0.635 - 0.216\, e^{-0.313\, D/d_1}, \tag{1}$$

the void fraction remaining is obtained as

$$V_f = 1 - Pe = 0.365 + 0.216\, e^{-0.313\, D/d_1}. \tag{2}$$

Since the void packing efficiency of the second component is

$$Pe = 0.635 - 0.737\, e^{-0.201\, d_1/d_2}, \tag{3}$$

then the total packing fraction is

$$0.867 - 0.079\, e^{-0.313\, D/d_1} - 0.269\, e^{-0.201\, d_1/d_2} - 0.159\, e^{-0.313\, d/d_1 - 0.201\, d_1/d_2}.$$

The value 0.867 is the limiting density for a binary system. The above equation was compared against 60 data points for a two-component system and was found to agree within a standard deviation of 0.013.

If the constant 0.635 in equations (1) and (3) is the limiting density to which spheres will pack into any void, and the value of the multiplier and exponent is determined by the void shape, one must conclude that equation (3) will express the void packing efficiency of all spherical systems, because the void shape is nearly the same within all spherical matrices. The above reasoning may be extended ad infinitum through multicomponent systems; however, the calculations become somewhat tedious beyond the quaternary. Without leading one through the involved algebra, and dropping terms which have an insignificant effect on the packing fraction, the following equation may be developed for the ternary system:

$$P_f = 0.951 - 0.029\, e^{-0.313\, D/d_1} - 0.098\, (e^{-0.201\, d_1/d_2} + e^{-0.201\, d_1/d_2}) - 0.198\, e^{-0.201\, [(d_1/d_2) + (d_2/d_3)]}.$$

In the ternary system, the limiting density is 0.951. The average difference between the calculated density and that achieved by experiment was 0.014.

The importance of the findings reported lies chiefly in the ability to predict achievable densities by a purely mathematical method. The obviation of graphical solutions or extrapolations greatly reduces the labor and inaccuracies involved in reaching desired densities in compacted bodies. The procedures employed lead to very regular packing densities which are repeatable to with ±0.015 for systems to the ternary.

## 2. Irradiation of Fast Reactor Fuels

All available instrumented irradiation facilities in the CP-5 reactor core are presently being used for irradiation experiments. A total of 36 separate specimens are being irradiated in six different capsules. The central fuel temperature range being investigated is from 500 to 680°C. One capsule, CP-32, contains U-20 w/o Pu-10 w/o Fs specimens which have attained a calculated 3.0 a/o burnup.

A recent nondestructive examination of these specimens shows the claddings to be intact. The cladding material of the specimens is Nb-1 w/o Zr having wall thicknesses of either 0.38 mm or 0.63 mm. Capsule CP-33 has claddings of the same thicknesses; however, the plutonium concentration in the fuel material has been varied between 10 w/o and 15 w/o. The maximum burnup calculated for the specimens is 2.6 a/o at central fuel temperatures of 500°C.

The cladding material of the specimens in the remaining capsules is of 0.23-mm thickness and is either Type 304 stainless steel lined with tungsten, Hastelloy-X lined with tungsten, or Nb-1 w/o Zr. The plutonium concentration in the fuel is either 20, 15, or 10 w/o. Selected claddings have been vented.

Capsule CP-35 differs from the others in that the fuel specimens either have a 1.4-mm axial hole or the annulus between fuel and cladding has been increased from 0.15 to 0.31 mm. The central fuel temperature of one of the specimens is being read directly with a thermocouple.

The instrumentation in capsule CP-34 recently indicated an apparent cladding failure of a specimen fueled with U-20 w/o Pu-10 w/o Fs and clad with 0.23 mm of Nb-1 w/o Zr. The specimen had been operating at a 580°C cladding temperature and had attained an estimated 2 a/o burnup. (Comparison specimens fueled with U-15 w/o Pu-10 w/o Fs and U-10 w/o Pu-10 w/o Fs are apparently intact.) Further study of this failure will be made by neutron radiography. On the basis of this examination, the capsule will either be returned to the reactor or will be disassembled for a detailed examination of the failure.

## 3. Refractory Alloy Fuel Jackets

a. Duplex Tubing. A 304 SS-V duplex tube (see Progress Report for December 1963, ANL-6810, p. 8) has been delivered to the Irradiation Testing Group for fuel-cladding studies. Quality evaluation by nondestructive testing (radiography and eddy current) disclosed this to be a good quality product. A good mechanical bond was present and only a few localized defects (voids) were observed.

b. Nb-1 w/o Zr Tubing. Nb-1 w/o Zr tubing has been fabricated with various inner diameters to provide stock for studies of fuel-element cladding in which various annular sizes between the fuel pin and cladding inner surface are used.

Drilled Nb-1 w/o Zr bars were ironed on a nondeformable mandrel to a ratio of approximately 15:1 for the diameter to wall thickness. The tubes were annealed and drawn over a ductile core (of copper) to slightly above the final size. After core removal the tubes were reannealed and given a slight sinking draw to final size. Sized tubing was again annealed for 2 hr at 1150°C, yielding an approximately 50% recrystallized structure. All tubing was examined by nondestructive testing. The results and sizes are as in Table XII.

Table XII. Dimensions and Test Results for Nb-1 w/o Zr Tubing

| OD | | ID | | Wall Thickness | | |
|---|---|---|---|---|---|---|
| cm | in. | cm | in. | cm | in. | Quality |
| 0.660 | 0.260 | 0.550 | 0.216 | 0.056 | 0.022 | Defects < 0.01 cm |
| 0.609 | 0.240 | 0.495 | 0.195 | 0.056 | 0 022 | Defects < 0 01 cm |
| 0.558 | 0.220 | 0.456 | 0.180 | 0.051 | 0.020 | Defects < 0.01 cm |
| 0.527 | 0.208 | 0.437 | 0.172 | 0.046 | 0.018 | No defects |
| 0.518 | 0.204 | 0.419 | 0.165 | 0.050 | 0.019 | No defects |

c. V-20 w/o Ti (TV-20) Alloy. Enhanced interest in TV-20 as a fast-reactor cladding material has increased the demands for tubing, sheet, and rod stock for early irradiation tests and property evaluation. To meet these demands, the most expeditious methods of consolidation, extrusion, and secondary fabrication of TV-20 are in various phases of development.

Two ingots were made by different techniques in an effort to evaluate alloy homogeneity. A 5.8-cm-diameter x 17.8-cm-long ingot (EB-14R5) was drip melted from a 5.8-cm vanadium rod to which strips of titanium had been welded. The second ingot (EB-15), 3.8 cm in diameter x 28 cm long, was prepared by drip melting a 3.18-cm diameter rod composed of compacted V-Ti briquets. Ingot evaluation has not been completed, pending receipt of chemical analysis.

The EB-14R5 TV-20 ingot was solution treated for 3 hr at 1500°C, machined to 4.47 cm diameter x 14.3 cm long, canned in a mild-steel jacket, and extruded at 1100°C at a 9:1 reduction ratio. The surface of the TV-20 bar was heavily striated but of uniform diameter. The striations are most likely a consequence of the large grain size. A double-extrusion technique is planned to achieve an extruded product requiring little if any surface conditioning prior to secondary fabrication.

4. Compatibility of Potential Cladding Materials with Molten Fuels

Safety considerations for EBR-II and other future fast reactors require information about the rate of penetration of prospective clad materials by molten uranium and plutonium-containing fuels.

Work has been done on the following: (1) U-5 w/o Fs fuel against Type 304 stainless steel, Type 430 stainless steel, and Armco iron, (2) molten uranium against Type 304 stainless steel and Armco iron, (3) molten U-36 a/o Fe against Armco iron, and (4) molten U-77 a/o Fe against Armco iron.

The compatibility of vanadium with molten uranium, U-10 w/o Pu and U-10 w/o Pu-10 w/o Fz in the 1100 to 1400°C temperature range is now under way. Preliminary results with vanadium versus molten U-10 w/o Pu-10 w/o Fz indicate penetration rates of about 1 to 5 $\mu$/sec in the above temperature range.

5. Corrosion of Fuel-cladding Materials

a. Vanadium-Titanium Alloys and Niobium. Additional weight change rates of a group of vanadium-titanium alloys and pure niobium (see Progress Report for November 1963, ANL-6808, p 11) are reported in Table XIII. Oxygen and carbon pick-up data are in Table XIV

Table XIII. Results of Exposure of Vanadium Alloys and Niobium to Flowing Sodium at 650°C and 195-ppm Oxygen

| Alloy (w/o) | Rate of Weight Loss ($mg/cm^2/mo$) | Equivalent Metal Loss | |
|---|---|---|---|
| | | cm/mo x $10^2$ | mils/mo |
| V-10 Ti (SR)* | 3.23 | 0.55 | 0.22 |
| V-10 Ti (RX)** | 2.76 | 0.47 | 0.18 |
| V-20 Ti (SR) | 3.33 | 0.58 | 0.23 |
| V-20 Ti (TX) | 3.72 | 0.65 | 0.25 |
| Nb (SR) | 41.6 | 4 95 | 1.95 |
| Nb (RX) | 52.8 | 6.55 | 2.58 |

*(SR) - Stress Relieved
**(RX) - Recrystallized.

Table XIV. Oxygen and Carbon Pick-up of Vanadium-Titanium Alloys and Niobium Exposed to Flowing Sodium at 650°C (195 ppm Oxygen - 9.0 Days)

| Alloy | Initial Impurity Conc, ppm* | | Final Impurity Conc, ppm* | | |
|---|---|---|---|---|---|
| | | | Oxygen | | |
| | Oxygen | Carbon | SR | RX | C (RX) |
| V-10 Ti | 800 | 486 | 2400 | 2080 | |
| V-20 Ti | 800 | 435 | 1465 | 1500 | 509 |
| Nb | 65 | 38 | 240 | 205 | 28 |

*Bulk metal concentration. Average of two analyses.

The samples were exposed to flowing (15 cm/sec) sodium for nine days at 650°C. Zirconium turnings in the sodium stream were used to getter oxygen. Oxygen concentration, erroneously given as 120 ppm in ANL-6808, was actually 195 ppm.

These data show that the vanadium-titanium alloys experienced rates of weight loss about an order of magnitude less than those apparently typical of niobium-base alloys exposed under similar conditions. The extensive intergranular attack frequently observed in niobium alloys was not observed in the vanadium-titanium alloys.

Samples used were too small to permit measurement of mechanical properties, e.g., room-temperature bend ductility. Microhardness traverses were taken. The behaviors of the stress-relieved samples and of the recrystallized samples were identical except that the base hardness of the stress-relieved material was higher. Within the limits of the measurements, the V-20 w/o Ti samples did not become harder as the result of the sodium exposure. Hardened layers about 60 $\mu$ thick were formed on the V-10 w/o Ti samples. The maximum hardness measured in this zone was about 1040 DPH (100 g load). Bulk metal hardness for the 1.46-mm-thick, recrystallized sample was about 190 DPH.

X-ray powder patterns of the surface films on the V-10 w/o Ti, V-20 w/o Ti, and Nb samples have been taken The surface films on the V-10 w/o Ti and V-20 w/o Ti appear to be a single phase, which was identified as VO. No titanium was found in the film by X-ray analyses. Other means of analysis will be tried in order to establish or disprove the suspected presence of a titanium oxide in the film.

The phase or phases present on the surface of the niobium samples could not be identified. (Formation of complex films in the loop being used for this work would not be surprising.)

Additional samples of V-10 w/o Ti and V-20 w/o Ti are in test in order to determine the effects of longer exposure. Other samples to study the effect of titanium and oxygen content on the corrosion behavior of the vanadium-titanium system have been prepared. Other alloying additions will also be studied.

b. Zirconium Alloys. Preliminary studies have been continued of the corrosion behavior of unpolarized zirconium-alloy samples in oxygenated sodium at 540°C and 650°C. The oxygen concentration in the 540°C sodium was nearly 3000 atom ppm, which is near the solubility limit. The concentration is maintained by addition of an excess quantity of sodium peroxide to the sodium at the beginning of the test.

Sodium flow rate is approximately zero except for slow convective stirring which is thought to occur due to a differential of about 30°C in the melt.

Samples of the alloys described below were supported in the sodium by tungsten hooks and a stainless steel rod, which were insulated from the nickel test chamber except through the sodium itself Evidence of possible electrolytic attack near the support point was seen on a sample of Zr-Cu-Fe alloy at 650°C.

Samples of Zr-3 w/o Ni-0.5 w/o Fe and Zr-1 1 w/o Cu-1.2 w/o Fe were tested at 540°C for a total of 12 days. After an initial period during which weight gains of 0.46 mg/cm$^2$ occurred, the weight gains were very low, amounting to a total of only 0 57 mg/cm$^2$ by the end of the test. In view of the occurrence of weight losses at higher temperature, it is likely that these gains do not reflect the true amount of corrosion Smooth, dark, adherent corrosion films were formed, having gray patches of (apparently) transformed corrosion product

Samples of the same alloys, together with Zircaloy-2 specimens were tested at 650°C for a total of 3 7 days. All samples lost from 30 to 40 mg/cm$^2$. The Zircaloys displayed a gray layered product that was relatively adherent, whereas the (apparently) transformed outer layer of the other samples was readily brushed away, leaving a dark coat

An attempt will be made to reduce the corrosion of the Zr-Cu-Fe and Zr-Ni-Fe alloys by means of polarization techniques, in which use will be made of low current densities through the intact films already formed.

## 6 Process Development for Fast Reactor Fuels

a. Melt Refining of Uranium-Plutonium-Fissium Fuels The recovery of discharged uranium-plutonium-fissium fuels by a melt refining

process performed beneath a molten salt layer is being investigated. In this process, rare earth elements are extracted into the salt phase without significant oxidation and extraction of the plutonium. Advantages found in small-scale experiments were high yields and low operating temperatures. The most satisfactory salt flux thus far tested was 75 m/o barium chloride-25 m/o calcium chloride, to which was added magnesium chloride in 10 percent excess of that required as a rare earth oxidant.

An experiment has been performed to determine the occurrence of any plutonium volatilization or plutonium transfer into the flux. An alloy of approximately 80 w/o uranium-10 w/o plutonium-10 w/o fissium was liquated for one hour at 1150°C in the presence of 81 w/o barium chloride-19 w/o calcium chloride flux. The amount of plutonium evaporated and recovered on an overhead condenser was only 0.05% of that charged, and the amount extracted into the flux was only 0.09% of that charged.

b. Skull Reclamation Process. Work was continued on the development of the skull reclamation process (see Progress Report for August 1963, ANL-6780, p. 22) for the recovery and purification of fissionable material in melt refining crucible residues (skull material). The latest run performed in the large-scale (1.5 kg of uranium) integrated equipment was the first continuous run attempted and was completed up to the final retorting step in about 35 hr. A modified procedure was used in which flux removal from the crucible is delayed until after the magnesium-50% zinc waste solution has been separated from the precipitated uranium. No major difficulty was encountered. Samples of product and waste materials from this run are being analyzed.

A molybdenum-30% tungsten transfer line which has been used successfully for 23 transfers of metal and salt solutions failed as a result of oxidation. Examination revealed that the stainless steel sheath had oxidized; possibly, a small leak existed through the threads in the transfer line elbow, allowing zinc or flux to attack the stainless steel.

A new transfer line has been installed which employs tapered joints rather than threaded joints at the elbow, with palladium brazing at the outside of the joints to hold the joint in place and complete the seal. The possibility of fabricating a transfer line by bending molybdenum-30 w/o tungsten pipe is also being explored. A 1/2-in.-diameter rod of molybdenum-30 w/o tungsten was bent at about 800°C, and metallographic examination of sections of the rod in the area of bending revealed no change in the crystal structure and no increase in hardness.

In several steps of the modified skull reclamation process (see Progress Report for November 1963, ANL-6808, p. 24), impurity-bearing metal solutions are pressure-siphoned from beneath frozen flux. Since magnesium (a component of two of these waste metal solutions) has

a fairly low density, density measurements were made to compare the densities of the skull reclamation process flux systems with the densities of magnesium-zinc alloys of various compositions. The most magnesium-rich alloy used (50 w/o magnesium-zinc) has a density of 2.6 g/cc.[2] This may be compared with the density of 2.3 g/cc found for a slurry of 47.5 m/o calcium chloride-47.5 m/o magnesium chloride-5 m/o magnesium fluoride to which 10 w/o magnesium oxide had been added to approximate the flux composition after reduction of skull oxides. The density difference, though small, should be adequate to assure separation of the phases.

In the skull reclamation process for recovering and purifying the fissionable material remaining in EBR-II melt refining crucibles, magnesium chloride-calcium chloride-magnesium fluoride is utilized as flux in the oxide reduction step. The solubility of magnesium fluoride in magnesium chloride-calcium chloride has been measured over the composition range from 0 to 100% magnesium chloride at various temperatures between 610°C and 830°C. The magnesium fluoride solubility decreases from about 15 m/o in pure calcium chloride to about 4 m/o in calcium chloride-35 m/o magnesium chloride, then increases to a value of 11 m/o in pure magnesium chloride. The temperature coefficient of magnesium fluoride solubility in this system between about 600 and 850°C appears to be negligible.

c. Blanket Processing Studies. An additional run (see Progress Report for October 1963, ANL-6801, p. 25) has been performed in the engineering-scale distillation unit for studying the retorting of magnesium-zinc-plutonium solutions generated near the end of the EBR-II blanket process. In this run, evaporation was continued nearly to dryness with the induction heating coil positioned to provide heating of the bottom 3 in of the still pot wall so that refluxing would minimize deposition of spattered solute on the walls. Only 2 percent of the solute, which was tin (used as a stand-in for plutonium), was found deposited on the walls and vapor baffles at the end of this run. Design studies are continuing on an improved distillation unit which will incorporate still pot reflux and promote concentration of the solute in the still pot heel.

d. Advanced Processes for Fast Reactor Fuels. Cadmium-zinc-magnesium alloys are being considered as process media for plutonium-bearing fast reactor fuels. The use of cadmium-rich alloys may allow operation at lower temperatures than those required in systems employing magnesium-zinc alloys and thus permit the use of stainless steel equipment without excessive corrosion. The uranium solubility at 600°C appears to be sufficiently high (greater than 2 w/o) to be of process interest in two composition regions of the cadmium-zinc-magnesium system. One region lies in the cadmium-rich corner of the ternary composition diagram, in

---

[2]Pelzel and Saverwald, Zeit. fur Metallkunde, 33, 229 (1941).

the area where cadmium concentration ranges from about 60 to 100 a/o, magnesium concentration ranges from 0 to 25 a/o, and zinc concentration ranges from 0 to 25 a/o. The other region lies in a cadmium-poor area of the diagram, where zinc and magnesium concentrations each range from about 40 to 65 a/o and cadmium concentration ranges from 0 to 20 a/o.

e. Properties of Molten Chloride Systems. The systems LiCl-KCl-$MgCl_2$ and LiCl-NaCl-$MgCl_2$ are being considered as fluxes in liquid metal processes for uranium-plutonium fuel. For good separation of rare earth fission products from uranium and plutonium, a flux containing more than 50 m/o magnesium chloride and having a melting point below 600°C is desired. Liquidus temperatures for the lithium chloride-potassium chloride-magnesium chloride mixture are being determined by thermal analysis techniques. Preliminary results indicate that liquidus temperatures as low as about 450°C exist in the lithium chloride-potassium chloride-magnesium chloride system at magnesium chloride concentrations that are sufficiently high to meet the needs of the process.

## 7. Sodium Coolant Chemistry

The distillation unit (see Progress Report for October 1963, ANL-6801, p. 25) has been used to process three pounds of sodium for the program aimed at elucidating the chemistry of the reactions that occur in liquid alkali metal solutions. The first sodium produced contained about 60 ppm carbon and 40 ppm oxygen. More experience with the unit should make possible the production of sodium with lower carbon and oxygen contents.

In a preliminary experiment, a sample of reagent-grade sodium was degassed at 300°C, and the gases evolved during heating were determined by mass-spectrographic analysis. The principal gases were hydrogen (93%), methane (1.9%), carbon monoxide (0.2%), and helium (4.5%).

Preliminary measurements were made of the solubility at 175°C of carbon in sodium saturated with oxygen (approximately 40 ppm oxygen). The average carbon concentration from three measurements was 121 ± 11 ppm.

One method of analyzing sodium for sodium oxide content is vacuum distillation of the sodium from the sodium oxide. The amount of this oxide is then determined by one of several chemical methods.

In the past, the distillation method has given divergent results. In analyzing the cause of this divergency, attention has been given to sampling technique. Normally, the sodium sample is withdrawn from the loop into a cup of a given volume with dependence on the overflow to give

a uniform volume of sample. It was suspected that the sample volume might vary due to a meniscus on the molten sodium drawn into the cup. To investigate this point, several samples were withdrawn from the loop into the cup in the hot distillation apparatus. The apparatus was then cooled to room temperature and the cup removed from the apparatus in the confines of a dry box. It was observed that the meniscus varied greatly from sample to sample with a resulting variance in weight between 16 to 20 g. It is evident that other methods of fixing the volume must be devised.

## C. EBR-I, Mark IV

The reactor was shut down and secured on December 30, 1963. Total power produced by the Mark IV loading was 577 MWh. Eleven fuel rods were removed from the reactor for return to the Metallurgy Division for examination of the irradiated plutonium fuel slugs.

The reactor is subcritical by 1.74% $\Delta k/k$ with the controls in their most reactive position and the reactor temperature at 30°C. Surveillance of the reactor blanket gas will be maintained during this indefinite, extended shutdown period.

Fifty irradiated Mark III fuel rods have been shipped from the facility for reprocessing, thus completing the removal of irradiated Mark III fuel.

## D. EBR-II

### 1. Reactor Plant

a. Primary Sodium Pumps. The temporary plug in the M-1 nozzle was removed from the primary tank on January 7. An inspection of the No. 1 pump before reassembly revealed that the baffles in the baffle assembly (located between the shield plug and the pump casing, and serving as a drain for sodium that is dislodged after migrating up the pump shaft) were found to be off center with respect to the pump shaft. On the advice of the pump manufacturer, the baffle assemblies of both pumps were remachined to center them and to provide additional clearance between the baffle and pump shafts.

The No. 1 pump was re-installed in the primary tank on January 10. Breakaway torque to turn the pump and motor manually was found to be 5 ft-lb with the pump submerged in the bulk sodium

The new shaft for the No. 2 pump, assembled with the impeller, was received at the site during the week of January 20. Dimensional tolerances are being checked.

b. Fuel Gripper. The fuel gripper was removed from the primary tank to investigate the cause of binding of the gripper shaft. A large amount of sodium and sodium oxide was found on the shaft of the gripper at a point just above the sodium level in the tank and the lower bearing position when the gripper is at the "operate" elevation. What appeared to be additional sodium oxide buildup was found at the center of the labyrinth on the bottom of the gripper shaft. No damage to the labyrinth itself is apparent The cause of the binding has not yet been determined, although it may be due to the sodium oxide deposit.

c. Control Rod Drives. The No. 8 control rod drive was removed preparatory to using this location for the oscillator drive assembly. The rod assembly appeared to be free of any oxide accumulation

The control rod shock absorbers have been reworked to improve dashpot plunger operation, facilitate plunger return to the "up" position, and to stabilize shock absorber oil level.

d. Thimble Cooling. An interconnecting line between the shield- and thimble-cooling systems has been installed. In the event of failure of both turbo-compressors, temporary cooling of the instrument thimbles at reduced flow rates can be provided by the shield exhaust blowers In the event of failure of both shield exhaust blowers, temporary cooling of the shield and rotating plugs at reduced flow rates can be provided by the turbo-compressors.

e. Seal Heater Control. Installation of the revised seal heater control system for the large and small rotating plug seals has been completed. Checkout of the system is proceeding Ammeters for detecting individual seal heater failures have been installed and will be checked out with the rest of the system.

f. Oscillator. The installation of the oscillator drive and associated control equipment is proceeding. The boron oscillator rod and thimble have been returned to Argonne, Illinois, for rework.

g. Sodium-purification System. Modification of the surge tank and associated piping for the sodium-purification system has been completed. A higher surge tank was installed for improved level control. The steel floor plates and beams in the immediate area of the surge tank were reworked to provide the space for the surge tank.

h. Fuel Element Rupture Detector Loop (Delayed-neutron Monitor). The E-3 nozzle plug assembly was reworked and reinstalled in the primary tank. The electromagnetic pump for this experimental loop was positioned and bus bars were fitted between the pump and the rectifier.

## 2. Sodium Boiler Plant

At the beginning of the month, the steam and sodium systems were at operating temperature and pressure. Measured plugging temperatures of the sodium remained in the range 475-500°F, even though the indicated flow through the permanent cold trap was less than 1/4 gpm.

The difficulty with the NaK heat-rejection system of the temporary cold trap was found to be a plug in the cooling coil of the crystallizer tank. The coil was cleaned and the NaK system was made operative.

The temporary cold trap was placed in operation, and in 4 days the plugging temperature of the sodium was reduced to about 275°F. The temporary cold trap was then shut down, and the plugging temperature was observed closely. It did not rise, indicating that the system has probably been cleaned to the best condition attainable at a temperature of 570°F. The system temperature was then increased for testing steam drum safety valves. The valves relieved simultaneously at an indicated pressure of 1330 psig.

During the period January 15-20, the steam and sodium systems were cooled and the sodium system drained. The steam generator was put in wet layup, completely flooded with water containing morpholine (pH 9.8) and about 60 ppm of sulfite for oxygen scavenging. The temperature of the storage tank has been maintained at 350°F.

Work is underway to remove the return bend in the yard piping and to join the secondary system piping to the intermediate heat exchanger. Replacement of the plugged secondary cold trap is also proceeding.

## 3. Power Plant

During the first half of the month, the steam generator was maintained at a saturation temperature around 570°F. Water level in the steam drum was maintained slightly above the centerline of the drum by intermittent addition of feedwater to replace losses. After the secondary sodium system was drained and the steam generator put in wet layup, the power plant systems were shut down.

The exhaust line from the relief valve of the condensate pump drive turbine was completed. Restrictions on operation of the turbine were lifted accordingly, and the pump was test-run satisfactorily.

A $1\frac{1}{2}$-in. bypass line and valve were installed around a 6-in. valve in the feedwater line, downstream of the feedwater heaters to permit utilization of the motor-driven feedwater pump if the start-up pump is not operable.

The before-and-after-seat drain lines from the trip-throttle valve of the turbine-driven feedwater pump were extended to the building drain system. Installation has started on the turbine lube oil purification and transfer systems and the additional turbine extraction line non-return valves.

4. Fuel Cycle Facility

The hoist drive for one of the Argon Cell cranes ceased to operate recently while removing the transfer basket from the large lock. The basket was transferred to the second crane by means of manipulators, and the nonoperative crane trolley was removed for examination. Circuit checks on the trolley and the current supply system indicated that a short-circuit existed in the cell at some point between the roof feeder lead-in wires and the bridge bus bars. However, repair cannot be attempted until the cell is entered.

Testing and modification of the fuel-decanning machine was continued. A modified scrap separator tube and chopper orifice appeared to operate somewhat better, but addition of a heater (see Progress Report for December 1963, ANL-6810, p. 15) to the separator tube did not facilitate movement of decanned fuel. Decanning of 100 elements with the original orifice and separator tube showed only 2.5 g of uranium in the scrap, corresponding to 0.04% of the uranium processed. Comparable data are not yet available for the modified orifice and separator. A marked increase in power consumed by the decanner roll drive motor was traced to roll and drive train wear.

The second melt-refining furnace ("B") was installed, and heatup and thermocouple calibration runs were made. A copper ingot was poured.

In the "A" furnace, ten melt-refining runs were made with charges ranging from 7 to 11 kg. Typical ingot yields were 95% Difficulty was experienced in charging sodium-coated pins which had been left several days in the charger. It was necessary to break them loose with a rod. A pyrolytic carbon-coated mold was used for several runs. The first ingot came out freely and in unusually good condition. Sample protrusions did not come out with the ingot in several cases, possibly due to inadequate relief in the mold.

Three additional runs, which were carried out remotely, have been completed in a melt refining furnace in the Argon Cell to prepare uranium-fissium alloy for use in the injection casting furnace. In all runs, the molten metal was held at 1400°C for about 1 hr. In the first run, 6,770 g of unirradiated, uranium-fissium pins were melt refined; the poured yield was 96.6 w/o. In the second run, the charge, which weighed 9,400 g (including 2,700 g of unirradiated, sodium-coated chopped uranium-fissium pins), was melt refined; the poured yield was 94 6 w/o. In the final run,

the charge, which consisted of 8,800 g of unirradiated, sodium-coated chopped pins was melt refined; the poured yield was 95.8 w/o.

Nine injection casting runs were made with yields of pins longer than 15 in. ranging from 0 to 100%, but mostly in the vicinity of 70%. Slag gaps were apparent in some cases, and there appeared to be some correlation of poor yields with a drossy surface condition of the heel (recycled pins were generally removed from the Argon Cell to be broken in air). Immersion thermocouple protection tubes of tantalum-tungsten alloy and of beryllia showed promise of withstanding molten fissium alloy.

The addition of a magnetic clutch to the pin-processor drive did not wholly solve gauging problems. The clutch did not appear to be strong enough, and alignment still requires correction. A group of 50 pins was processed successfully, however.

Both the EBR-II fuel-element-assembly machine and its remote controls were completed. The assembly machine consists of a 4-m (13-ft)-high vertical frame holding the following major elements:

1. an adapter sleeve that holds the lower blanket subassembly and adapter in position;

2. a platform with six radially mounted weld guns to arc spot weld the hexagonal tube to the lower adapter;

3. a fuel-bundle-assembly platform with gates and guides that are programmed to prevent incorrect assembly of the fuel bundle (this platform also is equipped with fixtures for holding and packing the fuel bundle as it is assembled and a blower for cooling the radioactively heated fuel bundle);

4. a screw elevator and force bridge to bring the hex tube and upper blanket assembly accurately over the fuel bundle and to position it for welding.

Electrical heating elements are provided to preheat the hexagonal tube A force transducer and torque limiter measure the closing force and prevent its exceeding a preset limit.

The core fuel elements, blanket elements, and control and safety elements may be assembled on this machine by exchange of the adapter sleeve and the assembly platforms. The electrical programmers and controls for assembling both the 61- and 91-pin fuel elements were constructed by the Metallurgy Division at Argonne National Laboratory. These are shown in Figure 12 together with the controls for the gauging and the tensioning operation which will test the assembly machine product.

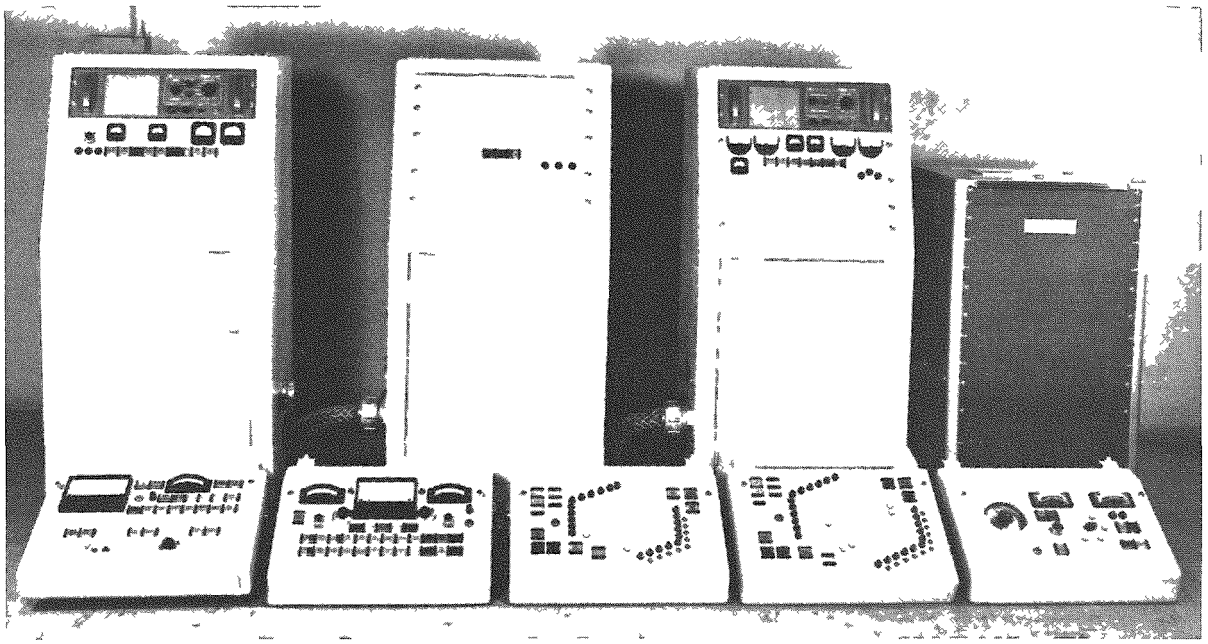

Figure 12. Programming and Controls for Assembling and Testing 61-pin and 91-pin Fuel Elements for EBR-II

The bonding and bond-testing machines were placed in operation, and a group of 29 canned reference rods was bonded for 30 min at 120 cycles/min and 500°C. Some of these contained known defects, and the remainder are to be used as reference standards. These were examined in the bond tester, yielding traces which are not completely interpretable.

Preparations are being made for admitting air to the Argon Cell in order to effect entrance by personnel during February to carry out crane and manipulator repairs, add cover plates to windows, and make other minor changes.

Plant-scale equipment for the oxidation of the residue (skull) remaining in the crucible after melt refining has been fabricated. The oxidation furnace and the process control system are being tested in the EBR-II mockup area at Argonne before being sent to Idaho for installation in the Argon Cell.

The transfer of a fuel subassembly between the transfer coffin and the EBR-II Air Cell is through a 6-in. opening in a shielding plug in the floor of the Air Cell. This shielding plug will be modified so that it can be lowered onto the top of the transfer coffin to provide shielding during fuel subassembly transfers. The hydraulic equipment for lifting and lowering the shielding plug has been ordered.

Drawings have been completed for the installation of a motorized drive on the sliding plug of the fuel transfer coffin. The sliding plug serves as a seal and a shield for the top part of the coffin. The motorized

drive will replace a manually operated drive and will eliminate the need for personnel to climb onto the coffin cart in order to operate the drive.

A mathematical analysis of the hoists for the cell cranes, the manipulators, the crane removal tool (blister hoist), and the electromechanical manipulators has shown that each hoist drive is capable of damaging its associated hoist mechanism. Such damage could result from a malfunction of the "up" limit switch on the hoist (see Progress Report for December 1963, ANL-6810, p. 16) or from an attempt to lift a severe overload with the hoist. To prevent overloading of the hoists under any circumstance, a slip clutch will be installed between the hoist drive motor and the drive gear reducer. Slip clutches have been designed for the hoist drives of the cell cranes (see ANL-6810, p. 16), the removal tool, and the electromechanical manipulators.

5. EBR-II Physics

An exploratory study was initiated to determine how to enhance fission rates in the radial blanket of the EBR-II. If fission rates commensurate with those in the core can be obtained in the blanket, the additional irradiation space, for testing prototype reactor fuel or fuel samples, might be extremely valuable in the future.

The specific calculations were carried out with multigroup diffusion theory in one-dimensional cylindrical geometry. To date, realistic requirements of heat removal have not been factored into the study, but results are generally encouraging. It was found that replacement of the absorbing depleted uranium over a large part of the radial blanket (e.g., a hexagonal sector) by a mixture of moderator (e.g., beryllium, carbon, and ZrH) and stainless steel with sodium coolant afforded a great deal of flexibility in fixing the peak fission rate and the neutron spectrum.

A reflector, containing approximately 85 v/o moderator, tends to produce unperturbed fission densities which can exceed those in the core by as much as a factor of 10. However, the composition of this reflector tends to degrade the neutron spectrum seriously and is undesirable in a fast flux irradiation facility. The peak reflector fission rate can be reduced by hardening the spectrum. This was accomplished by replacing some of the moderator with stainless steel. It appears that a blanket composition of approximately 20 to 40 v/o moderator, approximately 70 to 50 v/o steel, and approximately 10 v/o sodium can produce blanket fission rates commensurate with those in the core, even if the neutron flux is appreciably perturbed by the introduction of a typical large test assembly.

## E. FARET

### 1. General

The Laboratory has received and is reviewing the initial submission of Bechtel's control network and related documents, including general plans for Title II activities, the latest PERT efforts, and currently scheduled submission dates for ANL information necessary for Bechtel to complete the Title II work. This material will be refined and will provide the basis for all Title II work involving Bechtel and the Laboratory.

Bechtel has prepared a manual of construction drawing requirements for FARET to provide instructions for the Bechtel engineers in developing the Title II design drawings to meet the requirements of the Laboratory. Extensive comments have been prepared after evaluation of this manual and transmitted to Bechtel.

Current PERT work is centered around integration of fragmentary networks into a single control network for the entire project. The control network and associated information submitted by Bechtel is being evaluated to formulate the corresponding network for the Laboratory participation. A third major network, describing the activities of the construction contractor, will not be available until after such contractor has been selected.

A critical evaluation of the excavation and foundation plans for the facility indicates the possibility of substantial savings if a reduction in rock excavation and foundation simplification can be effected. Specifically, consideration is being given to raising the entire reactor building to an elevation where the proposed caissons or alternate pressure grouting would be essentially unnecessary.

The typical specifications received recently from Bechtel for ANL consideration as to format, general range, and adequacy of depth of technical content have been evaluated by the Commission. Their comments are being considered prior to finalizing these specifications with Bechtel.

General revisions and coordination of the Title II design by the Laboratory for the past month cover the following areas:

a. Cell-lighting problems are being investigated to determine the applicability of available fixtures and required intensity at various operating points in the cell.

b. Title I electric power system design is being extensively reviewed by the Laboratory and Bechtel. Cost analyses, short-circuit calculation checks, and relay studies are receiving considerable attention

and an alternative scheme of transformers is being investigated. It appears that somewhat more reliability might be achieved at a lower cost if the two transformers currently planned are replaced by three somewhat smaller units.

c. The inert gas system for FARET continues to receive considerable attention, particularly with respect to the nitrogen-removal components of the system and the overall regeneration problems.

d. Personnel access and general viewing are being studied. A demonstration at the Scott Aviation Company Research and Development Laboratory in Buffalo has been witnessed by a member of the FARET staff. Particular attention is being focused on breathing-air-supply systems and hardware, as well as reliability of various types of suits, masks, and provisions for emergency or auxiliary air supplies for in-cell operations.

e. The problems associated with sodium-system components, especially pumps and heat exchangers, are being studied.

f. Considerable backup and miscellaneous information has been transmitted to Bechtel regarding road cross sections, well-water quality, soil temperatures, stack-lighting problems, Hallam operational experience, shielding criteria, evacuation alarm system at EBR-II, etc.

Consideration has been given to the problems of stress in reactor vessel intervals:

A rotational stiffness of the cooling inlet pipe system was predicted mathematically.

Methods have been explored to decrease the deflection of the core support plate. For conservation of space, a single variable cross-section beam to increase the stiffness of the support plate was considered. Analysis for stress and deflection of the reinforcing beam has been completed, but no numerical results have yet been obtained.

Suggestions have been made for modification of the piping and vessel to improve stress conditions and simplify stress analysis, as well as to facilitate assembly of the vessel components

Suggestions were submitted for incorporation of features in the design and construction of the reactor plant which would permit investigation of various engineering mechanics problems of specific interest.

## 2. Materials for the Primary Sodium Loop

Of the many possible materials available for the primary sodium system for FARET, austenitic stainless steel Type 304 was judged to be adequate for the contemplated operations. These operations envision:

40,000 hr at 1000°F max;

40,000 hr between 1000°F and 1100°F;

10,000 hr (max) at 1200°F (max).

The selection of the alloy system was based on:

a. availability of products (plate, forgings, castings, welding electrodes);

b. status of the related arts (engineering design, shop- and field-fabrication procedures and techniques, and inspection);

c. materials (prior service applications, metallurgical stability, radiation damage);

d. economics.

At the contemplated FARET temperatures, the austenitic stainless steels are embrittled by the precipitation of: (1) carbides, and (2) sigma (and/or chi) phase. The sigma embrittlement is by far the most serious: resistance to impact at the elevated temperatures is almost as low as at room temperatures (falling to 5 to 10 ft-lb Charpy vee notch from 160+ ft lb). This embrittlement is a disadvantage, but the choice of the austenitic composition was resolved by considerations of metallurgical stability at elevated temperatures.

Studies of alloy thermal stability indicate that the long-time strength (creep, stress-to-rupture) and the ductility were better known for the Type 304 material than for the other members of the 300 series of alloys. From these studies, a 1150°F design temperature at a design stress level of 5750 psi was established; this design criteria is in exact agreement with the ASME Boiler and Pressure Vessel Code designs for equipment for long-lived equipment (i.e., 20 yr). The FARET primary system (pressure vessel and piping) meets all of the conventional design criteria of safety for operating temperatures up to and including 1150°F. In its final operational lifetime at 1200°F, the equipment can be operated for an additional 10,000 hr without failure by either creep or rupture at the design pressure stresses.

The available data also show a substantial variation in strength at the FARET temperatures which is apparently associated with the permissible alloy content of the Type 304 alloy. Further studies are in

progress to define the composition which will yield the strongest alloy consistent with thermal stability. Verifying test programs, both in- and out-of-pile, are contemplated to support the selection of the alloy composition.

Bechtel has been formally advised that the Laboratory's recommendation for all materials in contact with sodium in FARET is Type 304 stainless steel.

In addition to the consideration of various austenitic alloys, nickel- and cobalt-base super alloys, and Hastalloys were also evaluated and rejected due to unavailability, fabrication difficulties, or lack of long-time service at the required temperatures.

Refractory metals, although promising from strength consideration, were excluded because of their chemical reactivity and underdeveloped technology for long-time service applications.

### 3. Component Development

A proposed method for cooling a FARET fuel subassembly while in transit from a location in the reactor vessel to a storage location on the periphery of the reactor vessel utilizes forced-convection sodium as a coolant. An electromagnetic pump surrounding the subassembly during the fuel transfer provides for coolant flow. The pump would be a unique part of the fuel-handling mechanism, surrounding an open round tube, open at both ends, with the lower suction end of the pump always under the sodium level within the reactor vessel during the transfer operation. The fuel-handling gripper with subassembly attached would operate within the round tube. Sodium from the reactor vessel would be pumped upward, thereby cooling the subassembly, and returned to the reactor vessel by gravity.

A modified annular linear induction pump was investigated for this application. This pump would be modified by virtue of the absence of any internal magnetic structure normally found in a pump of this type. By sacrificing the magnetic flux return path, the center of the pump can consist of an open, round, straight tube. However, no pumping action would be expected unless some internal barrier were provided in the pump tube to prevent internal eddying of the sodium. An object such as a fuel subassembly, fitting loosely in the pump tube, could provide the internal barrier. To prove the principle, a prototype pump was constructed and tested.

The prototype pump incorporated certain design short-cuts in order to expedite construction. Among these were the use of a solid steel stator structure in place of a laminated one, and the use of conventional Class H

(180°C) insulated windings. Since the pump had no cooling system, operation in 350°F sodium was possible for short periods only. The test arrangement for the pump is shown in Figure 13.

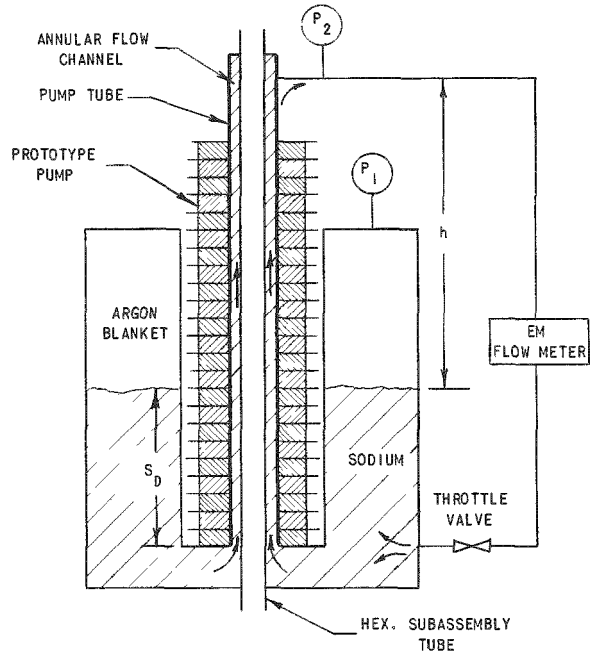


Figure 13

Schematic Arrangement for Testing Prototype Pump

The head developed by the pump is defined as the pressure $P_2$ plus the head of sodium, h, minus the argon blanket gas pressure, $P_1$. The flow rate was determined by electromagnetic flowmeter. The submerged depth of the pump inlet is defined as the distance $S_d$.

The results of the test indicate the following:

a. The pump will operate if certain minimum conditions are satisfied.

b. The pump inlet must be submerged 12 in. or more to insure starting of the pump.

c. Once the pump is in operation, any submerged level appears to be adequate so long as the inlet is covered.

d. The electrical resistivity of the central flow barrier (hex subassembly tube) had no significant effect on performance.

e. The excessive eddy-current heating caused by the solid steel stator structure prevented continuous operation of the pump at heads greater than 2 ft of sodium and a 20-gpm flowrate.

f. Variation of the sodium temperature had no significant effect on performance.

g. The pump developed 12 to 14 ft of sodium head at between 0 and 40 gpm for a maximum of 4 min before the windings became overheated.

h. At the maximum developed head (14 ft), the magnetic structure had not begun to saturate.

4. Cell Arrangement

The cell arrangement proposed in Title I plans has been revised by incorporation of more up-to-date information about the equipment to be installed. The functions of the operations to be performed in the cell have been studied to arrive at the space requirements with the cell. The presently conceived arrangement is shown in Figure 14 and is being used as a reference for the further development of the in-cell equipment.

5. Fuel Development

One of the first experiments in the FARET program schedule is concerned with the measurement of reactivity effects resulting from temperature changes in the fuel, sodium, and cladding, due to nuclear heating.

A zoned assembly is planned for the isolation of the Doppler coefficient. In this assembly, it is desired to measure reactor reactivity changes with respect to variations in test-zone fuel temperature, keeping other variables of fuel and cladding expansion, together with sodium temperatures, as nearly constant as possible. A thorough description of the experimental methods has been reported.[3]

In the test zone of the zoned assembly, it is proposed to use fuel elements in which the fuel is insulated from the cladding by a gas gap. Relatively large changes of fuel temperature can then be effected by varying either the gas pressure in the gap or the reactor power level. The fuel is fabricated in the form of short pellets to reduce effects of fuel expansion. Each may be supported independently by the cladding.

It is planned to irradiate samples of these gas-gap-insulated, fuel-pellet elements in a loop installed in CP-5. The experiments are required for the following reasons:

a. to measure the maximum heat flux which the pellets can withstand without cracking; the cracking may change the dimensions of the insulating gas gap between pellets and cladding for a given heat flux;

[3]Interim Report: FARET Experimental Program, ANL-6708 (April 1963).

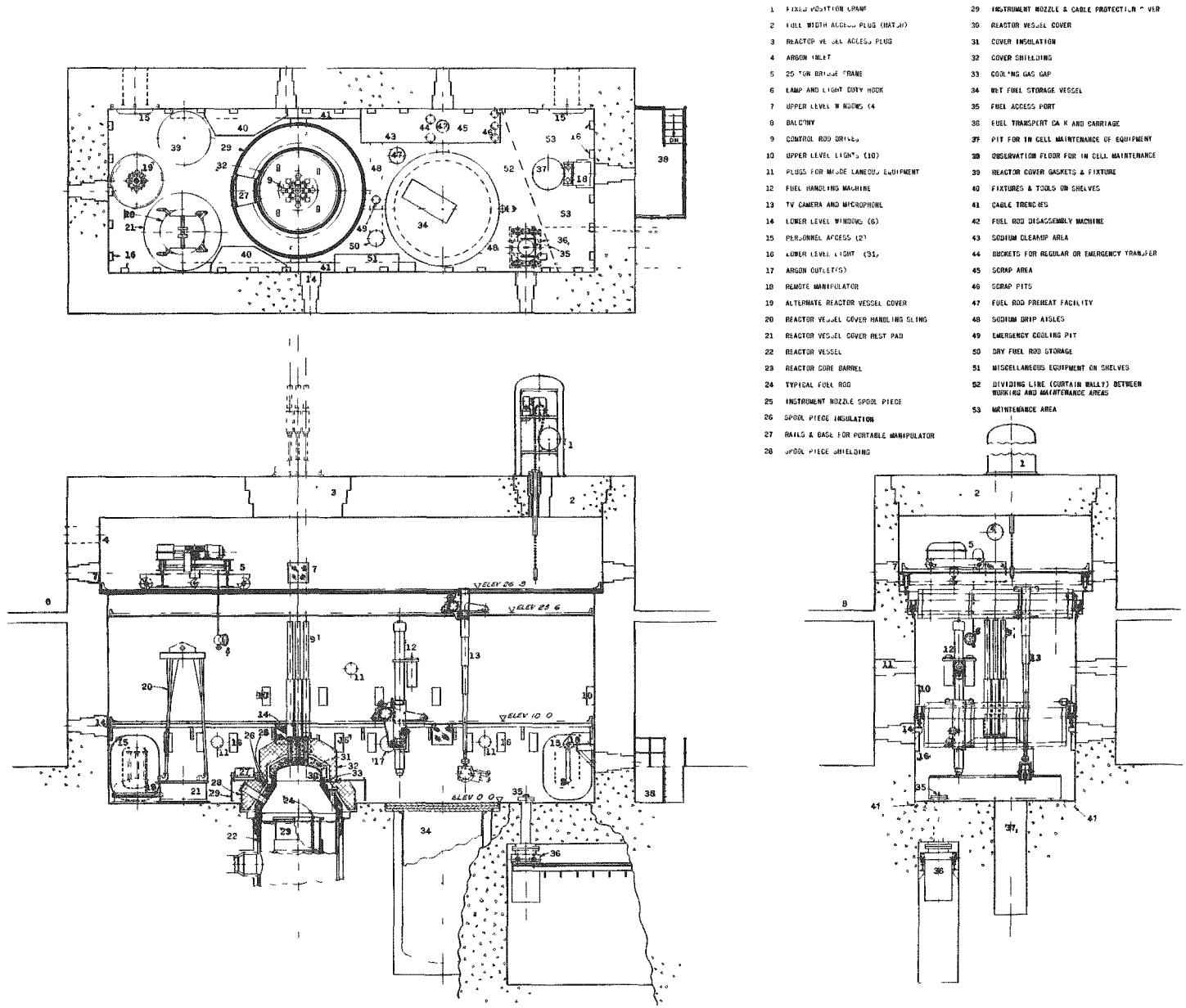


Figure 14. FARET Reactor Cell - General Arrangement

b. to verify the maximum temperature difference which can be obtained between the fuel and cladding for a given heat flux;

c. to test the integrity of the devices for support of the segmented pellets;

d. to test the performance of instrumentation and gas supply for the insulating gap under irradiation.

Bench tests with electrical heating have produced valuable data concerning the above items. However, the bench tests suffer from the following shortcomings which in-pile experiments should remedy:

a. electrical heating produces a different temperature (and stress) distribution in the fuel than nuclear heating.

b. the electrical heater radiates power between the segmented pellets where none occurs in the reactor.

c. the bench-test pellets, having four axial holes, (a central one for the heater, and three on a radius for installing thermocouples) differ from the reactor pellets, which have only a central hole for thermocouple installation.

The loop consists of the experimental assembly, gas systems, and instrumentation. The assembly shown in Figures 15 and 16, consists of four subassemblies, i.e., the fuel element capsule, the thimble, the outer tube, and the cadmium filter

The fuel-element capsule is the innermost subassembly. It contains segmented fuel which will consist of $UO_2$ or UC, enriched to 0.3% or 0.22% $U^{235}$. A thermocouple measures the center temperature of the fuel at the horizontal center plane. The fuel is clad by a stainless steel tube. A 20-mil fuel gas gap is formed between fuel and clad, and is filled with helium or argon. The gas pressure in the gap can be changed by using a vacuum pump system. Changes in the pressure between atmospheric and 10 $\mu$ cause a change in thermal conductivity of the gas which will effect a change in the fuel temperature. The cladding temperature will be indicated by means of two thermocouples brazed to the outside wall of the cladding at the horizontal midplane. For testing various fuels, the fuel element capsule can be removed from or inserted into the experimental assembly

The thimble is a stainless steel tube which contains the fuel-element capsule. A 6-mil gap is formed by the fuel-element cladding and the thimble wall, which is referred to as the cladding gas gap. This gap will be filled with helium and the pressure will be maintained in the same manner as in the fuel-gas-gap system. Changing the gas pressure will affect temperatures of the cladding and also of the fuel.

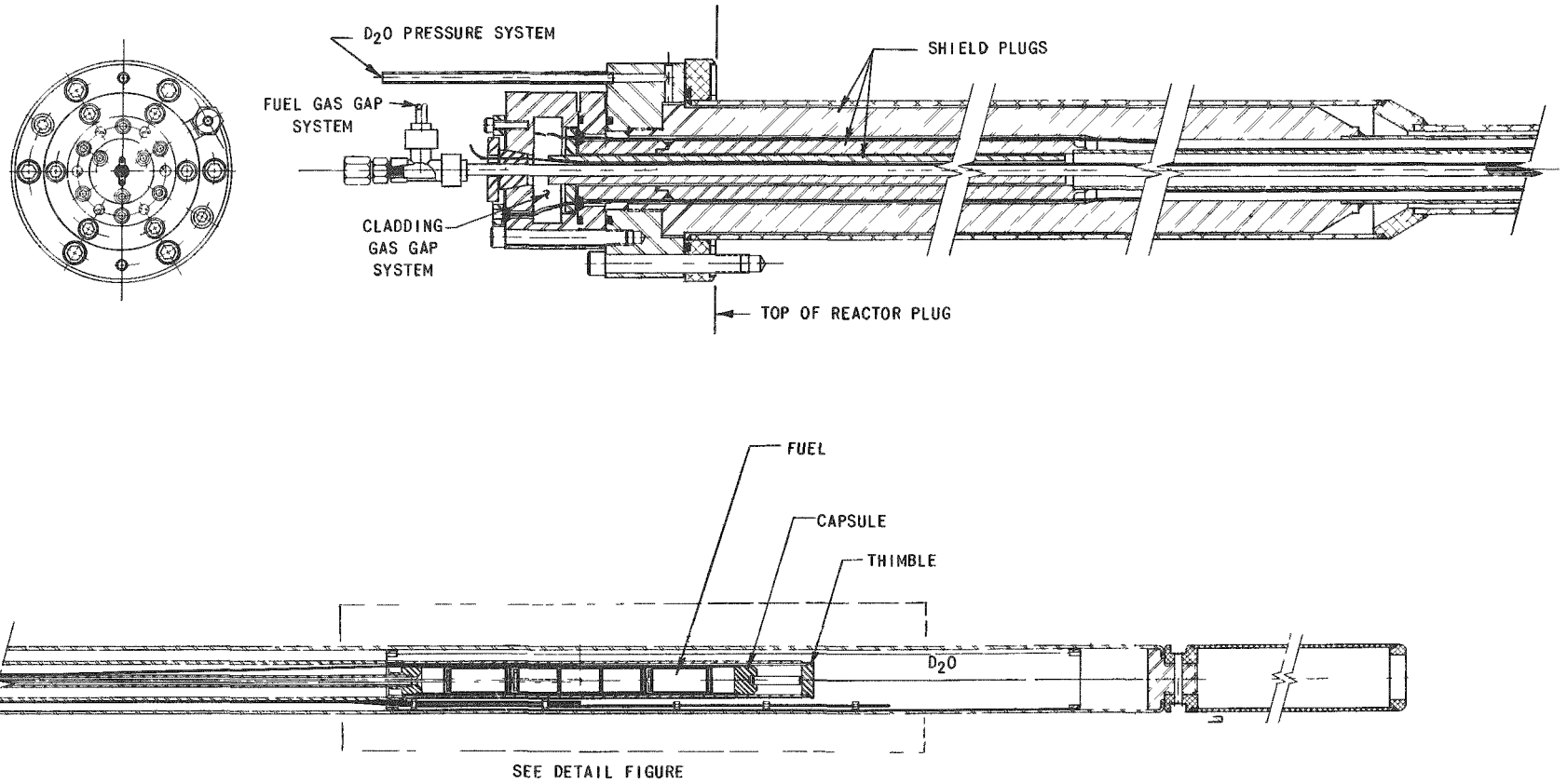


Figure 15. Irradiation Facility for Proposed FARET Fuel

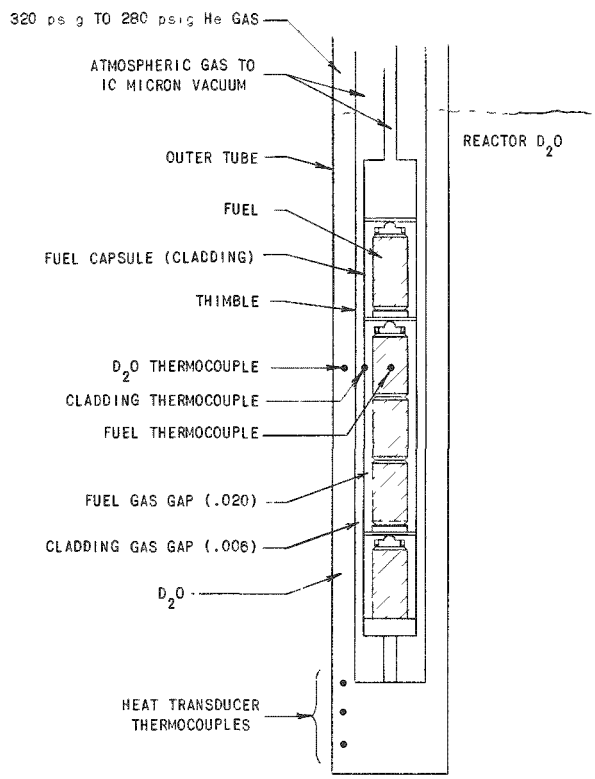


Figure 16
Detailed View of
Fuel Arrangement

Attached to the outside wall are two thermocouples for measurements of wall temperature at the horizontal center plane of the fuel. Adjacent to these couples is one thermocouple to measure the $D_2O$ temperature in the gap formed by the thimble and the outer tube.

Attached to the thimble are five thermocouples which make up the heat transducer. Two thermocouples are located at the bottom of the fuel-pellet plane in the $D_2O$. Another pair is located 2 in. down from the bottom plane of the fuel, also in the $D_2O$. The fifth thermocouple is located about 4 in. from the bottom plane of the fuel in the $D_2O$. The temperature difference ($\Delta T$) between the thermocouples at the different levels will be an indication of the heat flux generated in the fuel.

The transducer will require in-pile calibration. An electrical heater element will replace the fuel capsule, and with the reactor operating, the heater will be turned on and the power input will be compared with the thermocouple $\Delta T$'s. Several $\Delta T$'s vs. power points will determine a calibration curve for the transducer. The heater will then be removed.

The outer tube is the receptacle for the thimble and fuel capsule. The thimble and outer tube form a 9/32-in. gap filled with $D_2O$. The $D_2O$ will be pressurized with helium to 300 psi because the temperature of the $D_2O$ will be above atmospheric boiling plant. The temperature of the $D_2O$ is measured by a thermocouple immersed in the $D_2O$ at the midplane of the fuel.

The pressure of the gas in the two gaps, one between the fuel and cladding, and the other between the cladding and thimble, can be varied from atmospheric pressure to a vacuum sufficient to reduce heat transfer to that of radiation only. This corresponds to a vacuum of about 10 $\mu$. Therefore, various fuel and/or cladding temperatures can be obtained by regulation of the gas gap pressures. The $D_2O$ in the outer tube will be pressurized so that temperatures above the atmospheric boiling point can be obtained.

In order to test fuel of higher enrichment, a neutron filter is used. This filter is a cadmium tube clad with 304 stainless steel. The cadmium will be drilled with holes in order to adjust the neutron flux for a desired heat generation.

## 6. In-core Instrumentation

The necessary in-core instrumentation for the capsule has been considered. A test was performed to evaluate the adequacy of the stainless steel-alumel lead-wire combination for thermocouple lead wires. A sample connector, a thermocouple made up of a tungsten-3% rhenium wire and a tungsten-25% rhenium wire, together with the stainless steel (302)-alumel lead wire, were operated at temperatures up to 650°C.

The results of the test have not been completely evaluated, but the following preliminary conclusions have been reached. First, the sample connector performed as expected, retaining a high value of insulation resistance. Secondly, the resistance-welded hot junction remained intact throughout the test, as did the resistance-welded joints at the stainless and alumel connector pins. After the test was completed, the thermocouple was handled and showed no signs of extreme brittleness. The maximum error due to the combination thermocouple and lead wire would be, as reported previously, about 2% of the measured temperature if the hot junction is above 1000°C. This error occurs only at the extremely low splice temperatures. The last observation was that the emf output at the high splice temperatures (500 to 650°C) were slightly lower than those measured in the previous test. This could be due to the use of No. 302 stainless steel instead of the No. 308 as lead wire, or to a less uniform temperature distribution along the connector length. To check the alloy composition of the No. 302 and No. 308 wires used, samples of each are being analyzed chemically. Further investigation of this discrepancy will be pursued.

## 7. Fuel Assembly Sodium Flow Test Facility

The final design for a pump is a 100-hp centrifugal type with a 4-in. discharge, a 5-in. suction, and a single 20-in. impeller. The rated flow is 800 gpm of sodium at 1200°F at a head of 111 psi. Pending delivery of this

pump, a temporary pump will be used. The pump case for the temporary pump has been received and the internals are due about the middle of February.

A new 900-gal dump tank has been designed and now awaits checking. The pressure vessel and internal details are settled to a point where requisitions for basic materials have been sent out for quotations. Considerable detailing of the pressure vessel complex remains to be done. A tentative layout of the pit facility has been made and now awaits an analysis of the stress due to piping expansion. A preliminary study indicates that heat must be added for the preliminary 15-hp pump arrangement and must be removed for the 100-hp arrangement. A fin-tube heat exchanger will be used in the pump-discharge line with shrouding so that air can be circulated over the fins and ducted out of the building.

# III. GENERAL REACTOR TECHNOLOGY

## A. Experimental Reactor and Nuclear Physics

### 1. High-conversion Critical Experiments

Experiments with 3 w/o enrichment $UO_2$-fueled cores were continued (see Progress Report for November 1963, ANL-6808, p. 33; Progress Report for December 1963, ANL-6810, p. 26). The 1.13-cm pitch triangular grid was removed and the 1.27-cm grid was reinstalled. Additional measurements by the thermal activation technique are being made of $\rho_f^{25}$ and $\rho_c^{28}$, the ratios of epi- to sub-cadmium fission and capture in $U^{235}$ and $U^{238}$, to improve the confidence in these values. The $U^{238}$ capture cadmium ratio ($C_{28}$ = 1.07) was measured and used to derive the value of the epi-cadmium to sub-cadmium capture ($\rho_c^{28}$ = 14.4) in the 1.13-cm triangular-spaced stainless steel clad core.

Plots of cadmium ratios are nearly linear with the atomic ratio of hydrogen moderator atoms to $U^{235}$ fuel atoms. A plot of cadmium ratios versus the ratio of hydrogen atom density to thermal cross section of fuel atoms produced a linear distribution within the accuracy of the data. Reasonably accurate intermediate values may now be obtained by interpolation.

Measurements of the effect of gaps produced by foil insertion into fuel elements have indicated there is a net effect of about 1%. A comparison of activation measurements of the foils and the $UO_2$ pellet slices (which produced no gap, since they were from the fuel elements) were made by radiochemical measurements of fission product and $Np^{239}$ yields.

### 2. Fission-ratio Measurements at JUGGERNAUT

A series of measurements have been made at the JUGGERNAUT reactor to obtain preliminary data for a standard fast flux facility. The facility, contained in a beam hole in the reactor, was built to provide a known fast flux in which counters could be calibrated. It consists of a moderator layer of Benelex, a converter plate of natural uranium, and a thin Boral plate which prevents thermal neutrons from being scattered back into the converter plate. The counter is enclosed in a cadmium tube, which is contained in a hafnium cylinder. The cylinder is placed immediately behind the Boral plate to shield the counter from any neutrons except those which originate in the converter plate. Counters up to 2 in. in diameter can be calibrated in this facility.

The flux data were obtained by determining a number of fission ratios in the facility through the use of solid-state fission counters, containing $U^{233}$, $U^{235}$, and a number of threshold detectors. Three separate sets of measurements were made under different conditions.

In the first set of measurements, 1 in. of Benelex and 3 in. of natural uranium were placed between the counter and the neutron beam. The counter was also enclosed in a cadmium tube.

For the second set of measurements, the thickness of the Benelex was increased to 2 in., and the thickness of the natural uranium was reduced to 2 in. For these measurements, the cadmium tube around the counter was omitted.

For the third set of measurements, the thickness of the Benelex remained at 2 in., and the uranium thickness was increased to 3 in. The cadmium tube was replaced for the measurements shown in Table XV.

Table XV. Calibration Data for Standardizing the Fast Flux Facility

| Fission Detectors | I<br>1-in. Benelex, 3-in. Natural Uranium (Cadmium Tube) | II<br>2-in. Benelex, 2-in. Natural Uranium (No Cadmium Tube) | III<br>2-in. Benelex, 3-in. Natural Uranium (Cadmium Tube) |
|---|---|---|---|
| $U^{233}/U^{235}$ | 2.016 | 1.962 | 1.921 |
| $U^{234}/U^{235}$ | 0.184 | 0.284 | 0.178 |
| $U^{236}/U^{235}$ | 0.090 | - | - |
| $U^{238}/U^{235}$ | 0.0251 | 0.0395 | 0.253 |
| $Np^{237}/U^{235}$ | - | 0.183 | 0.139 |

## B. Theoretical Reactor Physics

### 1. Orthonormal Expansion of Neutron Spectra from Foil-activation Measurements

The investigation of orthonormal expansion methods (see Progress Report for December 1963, ANL-6810, p. 27) has continued. For the previously chosen test problem, the approximation of the spectrum $\phi(\epsilon)$ in the form

$$H_n(\epsilon) = \sum_{i=1}^{n} \gamma_i U_i(\epsilon) \qquad (1)$$

was determined by a least-squares method. For this particular test problem, the set of orthonormal functions $\{U_i(\epsilon)\}$ was chosen as the associated Laguerre polynomials of the second kind.

With the same set of cross sections employed with the Gram-Schmidt method (ANL-6810, p. 29), the relative error

$$E_n = \int_0^\infty |H_n - \phi(\epsilon)|\, d\epsilon$$

was determined for the least-squares method by numerical integration. Figure 17 presents the relative error $E_n$ as a function of n for the chosen test problem. A comparison of the approximation $H_8(\epsilon)$ with the original spectrum $\phi(\epsilon)$ is given in Figure 18.

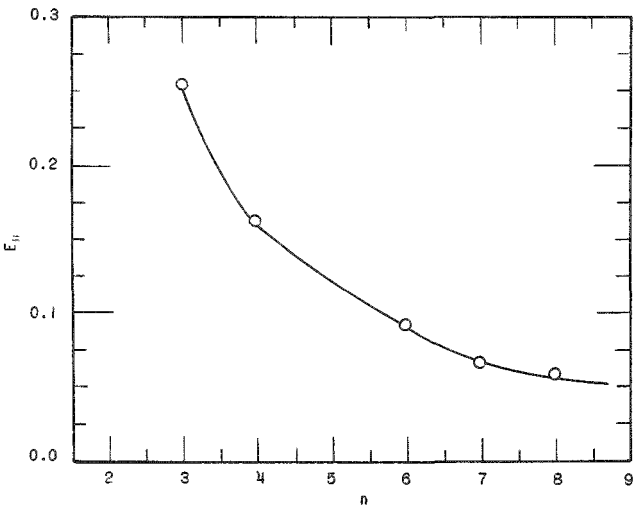


Figure 17

$E_n$ vs. n for the Least-squares Method

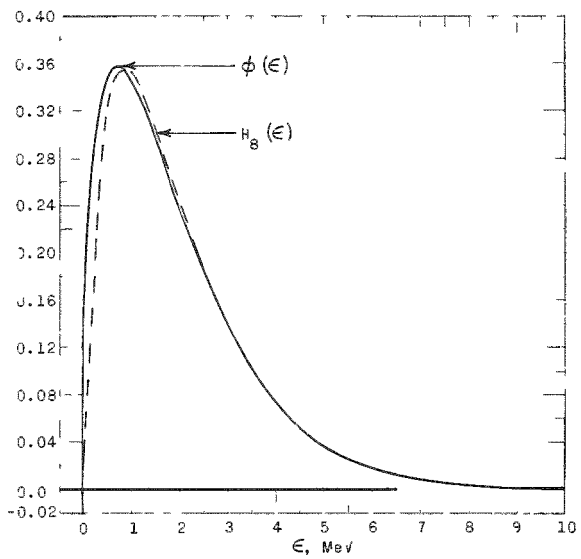


Figure 18

Comparison of $H_8(\epsilon)$ and $\phi(\epsilon)$ for the Least-squares Method

These results imply that the least-squares method is superior to the Gram-Schmidt method. However, as previously stressed, these results do not include any effects due to experimental error. The relative merit of either method will also depend on the sensitivity exhibited to uncertainties in the cross sections that are employed. Indeed, the general applicability of orthonormal expansion methods for furnishing adequate approximations may significantly depend on this factor. The computer program will be extended to investigate both the Gram-Schmidt and least-squares method from this viewpoint.

## 2. Fuel-cycle Studies

One of the more serious uncertainties in the study of fast reactor power breeder fuel cycles is in the value of the capture cross section of $Pu^{240}$. Besides affecting the breeding ratio, particularly of the core, and the economics of the fuel cycle, the relative abundance of this isotope can have a strong effect on the size of the important sodium void coefficient. An uncertainty of 30% in this capture cross section being easily credible, an arbitrary upper limit of 50% was selected as a variation to be examined. This upper limit was applied to the equilibrium fuel cycle of a 875-liter plutonium-uranium monocarbide reactor. In this study the ANL code CYCLE was used with a 16-group cross-section set based on the work of Yiftah et al.[4] It was found that for this reactor the change in cross section reduced the average abundance of $Pu^{240}$ in the core by 25% while increasing that of $Pu^{241}$ by approximately 21%. This increase in $Pu^{241}$ concentration tends to improve the sodium void reactivity coefficient.

## 3. Equation of State for Mixtures

The equation of state appropriate during a sharp power burst has been studied for a mixture of several materials in a fast reactor. It was assumed that the equations of state for the individual components were known. Two equations of state for the mixture were determined for two extreme but simple cases:

(1) where materials are finely dispersed and reach the same temperature locally (isothermal case), and

(2) where materials can be considered separated for the sharp burst considered; only the fuel is heated and changes in the diluent are adiabatic.

In both cases expression of energy $e$ in terms of pressure $p$ and specific volume $v$ were derived.

In the isothermal case this relation was obtained by first expressing the energy and specific volume of each material in terms of pressure and temperature, and then using addition to obtain both the energy and specific volume of the mixture. Finally, from these two relationships, temperature was eliminated and an equation relating pressure, energy, and specific volume was obtained.

In the adiabatic case, both energy $e_d$ and specific volume $v_d$ of the diluent can be expressed in terms of pressure $p$. If the functional

---

[4] S. Yiftah, D. Okrent, and P. A. Moldauer, Fast Reactor Cross Sections, Pergamon Press (1960).

dependence of pressure on energy $e_f$ and specific volume $v_f$ of the fuel is designated by the letter p:

$$p = p[e_f; v_f],$$

energy and specific volume of the diluent can be eliminated by addition and the equation of state obtained for the mixture:

$$p = p\left[\left(1 + \frac{md}{mf}\right) e - \frac{md}{mf}\, e_d(p); \quad \left(1 + \frac{md}{mf}\right) v - \frac{md}{mf}\, v_d(p)\right],$$

where (md/mf) is the ratio of mass of the diluent to that of the fuel.

In the relationships of energy, pressure, and specific volume, only small changes of the latter quantity were deemed of interest. Finally, these relationships were approximated by a linear dependence of specific heat on an artificial "temperature" and by linear dependence of pressure (after threshold for its generation) on density and "temperature."

## 4. Analysis by Numerical Methods

Integration rules which are exact for rational functions have been further explored. A geometric mean integration formula has been described in ANL-6717 (Reactor Development Program Progress Report for April 1963, p. 39). For the large class of functions which obey a generalized Riccati differential equation:

$$y'(x) = -[\alpha(x)y^2 + \beta(x)y + \gamma(x)],$$

the geometric mean formula leads to a quadratic equation which may be solved explicitly for y(x). The errors of the resulting approximations are proportional to $x^3$, but for many functions are appreciably smaller. Thus, for example,

$$e^x = 1 + x\left(1 + \frac{x^2}{4}\right)^{1/2} + \frac{x^2}{2} + \epsilon,$$

where

$$\epsilon = \frac{1}{24}\, x^3 + \frac{1}{24}\, x^4 + \ldots .$$

This error is one fourth that of the first three terms of the power series, and one-half that of the first diagonal Pade approximant. The following approximations may be obtained in similar fashion:

$$\ln x \approx x^{1/2} - x^{-1/2};$$

$$\tan x \approx x \left(1 + \frac{5}{12} x^2 \sqrt{1 - \frac{4}{25} x^2} - \frac{x^2}{12}\right) \Big/ \left(1 - \frac{x^4}{6}\right);$$

$$\operatorname{erf}(x) = \frac{2}{\pi^{1/2}} \int_0^x e^{-t^2} dt = \frac{z e^{-z^2}}{3\pi^{1/2}} \left[6 + \left(5\sqrt{1 - \frac{4}{25}(z^2 - z^4)} - 1\right) z^2 + 2z^4\right].$$

All these approximations have appreciably smaller error coefficients than the corresponding truncated power series or the formulas obtained by the trapezoidal rule.

Three-point formulas which are valid for ratios of quadratics have also been investigated. The resulting rules are considerably more accurate, but are algebraically complex when written explicitly and may break down when two consecutive integral values are equal.

## 5. Tungsten Cross Sections

The calculational program to analyze the sensitivity of experimentally measurable parameters to differences in tungsten cross sections has been completed. The parameters studied included the critical mass, central material worth coefficients, fission ratios, prompt-neutron lifetime, and effective capture cross sections. The study was carried out for three proposed tungsten-containing ZPR-IX assemblies, and it made use of five different tungsten cross-section sets.

A sample of the calculated results for one of the three proposed ZPR-IX assemblies is presented in Table XVI.

Table XVI. Parameters Calculated for the 7* Tungsten, 7 Aluminum, and 2 Oraloy ZPR-IX Assembly

| | Tungsten Cross-section Set Used in Calculations | | | | |
|---|---|---|---|---|---|
| Calculated Parameters | No. 30 | No. 35 | No. 37 | No. 40 | No. 43 |
| Critical Volume (liters) | 190 | 188 | 177 | 179 | 185 |
| Critical Mass (kg $U^{235}$) | 351 | 348 | 328 | 330 | 342 |
| Prompt-neutron Lifetime x $10^8$ (sec) | 12.26 | 10.38 | 10.44 | 10.42 | 10.51 |
| Effective Capture of Tungsten (b) | 0.135 | 0.176 | 0.166 | 0.166 | 0.166 |
| Central Boron Worth (Relative Units) | 0.327 | 0.311 | 0.327 | 0.317 | 0.312 |

*Number of $\frac{1}{8}$-in.-thick plates per assembly drawer. The assembly is reflected by 30 cm of 94% density aluminum.

Besides showing calculated differences which can be traced back to the differences of the five considered sets of tungsten cross sections, Table XVI also illustrates the fact that agreement in one experimental parameter (say critical mass) doesn't necessarily "prove out" a cross-section set. Compensating errors are possible and probably common; thus, comparing, for example, calculated results for sets No. 30 and No. 37, it is seen that set No. 30 has the lower $\overline{\sigma}_c$ for tungsten, but contrary to first expectations produces a larger calculated critical mass. This means that for the assembly in question the lower $\sigma_{TR}$ cross-section values of set No. 30 in reactivity terms outweigh the lower $\overline{\sigma}_c$ values.

One of the major conclusions of this study has been that it is preferable (for purposes of proving tungsten cross sections) to make a few select measurements on a number of differing tungsten-containing assemblies rather than study some particular assembly at great length. This is because most of the measurable parameters (such as fission ratios) are affected only indirectly by the presence of tungsten, that is, they are affected only to the extent that tungsten influences the overall core spectrum. Experimentally, it is thus more profitable to vary the spectrum (by constructing different assemblies) and do a few select measurements rather than obtain essentially the same information by performing multiple measurements in some particular spectrum.

## 6. Comparison of DSN and DTK Reactor Calculations

A comparison of criticality was made by use of the DSN and DTK computing codes for the unreflected Godiva and reflected Topsy systems (see Tables XVII and XVIII). Angular approximations N of 4, 8, and 16, and convergence criteria of $10^{-5}$ for Godiva and of $10^{-5}$ and $10^{-6}$ for Topsy were used in the calculations. An SNG case was also studied. The analyses were based on 16 energy groups and criticality was obtained by varying the radii for all regions.

Table XVII. Critical Dimensions of Godiva Determined from Computer Codes DSN and DTK

| Code | N | Convergence | Critical Core Radius, cm |
|---|---|---|---|
| DSN | 4 | $10^{-5}$ | 8.7557 |
| DTK | 4 | $10^{-5}$ | 8.7080 |
| DSN | 8 | $10^{-5}$ | 8.8032 |
| DTK | 8 | $10^{-5}$ | 8.78425 |
| DSN | 16 | $10^{-5}$ | 8.8133 |
| DTK | 16 | $10^{-5}$ | 8.8053 |

Table XVIII. Critical Dimensions of Topsy Core Determined from Computer Codes DSN, DTK, and SNG

| Code | N | Convergence | Critical Outer* Radius, cm |
|---|---|---|---|
| DSN | 4 | $10^{-5}$ | 26.3206 |
| DTK | 4 | $10^{-5}$ | 26.3870 |
| (SNG) | 4 | $10^{-5}$ | 26.4424 |
| DSN | 4 | $10^{-6}$ | 26.3206 |
| DTK | 4 | $10^{-6}$ | 26.3872 |
| DSN | 8 | $10^{-6}$ | 26.6343 |
| DTK | 8 | $10^{-6}$ | 26.6023 |
| DSN | 16 | $10^{-5}$ | 26.70925 |
| DSN | 16 | $10^{-6}$ | 26.7092 |
| DTK | 16 | $10^{-6}$ | 26.6901 |

*Outer radial dimension of the Topsy reflector. Ratio of core radius to outer radius is 0.2291.

The differences in critical radii as given by the DSN and DTK codes at N = 4 are essentially caused by the low angular approximation and not due to inadequate convergence criteria. In the tables it is seen that for the case of the bare system (Godiva) the DTK code gives smaller critical radii than DSN for the low approximation, N = 4, whereas for the case of the reflected system (Topsy), the DSN code gives smaller critical radii than DTK for the low approximation, N = 4.

### 7. Reactor Control

A synthesis of an optimal nuclear reactor control system has been developed. In developing this concept, a one delayed-group theory is used to describe the kinetics of a nuclear reactor. Further, the performance index which is minimized is the integral of a weighted square error and of the "control-effort" $(n\rho)^2$, where n is the neutron density output and $\rho$ is the excess reactivity in $. In this development, the optimal control input function which drives the reactor is expressed in a form suitable to be realized as a closed loop system. To simplify the controller, an infinite time of operation was assumed but for such a case, it was necessary to investigate the stability of the overall system. In conclusion, the stability criteria of the stationary system are given.

## C. High-temperature Materials Development

### 1. (Th,U) Phosphides

Studies have continued of the effect on the lattice constant of heating uranium phosphide in a vacuum. Heating UP above 1500°C invariably resulted in a change in the lattice constant; the original value of 5.589 Å

showed a measurable decrease, which generally became more significant with treatment at higher temperatures. The decrease in cell dimension is attributed to irreversible loss of phosphorus from the structure. However, the relationship between lattice constant and heating temperature is more complicated, since another effect became noticeable when heating was carried out above 1800°C. Some samples fired at 2000°C exhibited the same lattice constant as those fired at 1800°C. Also, a specimen of UP containing about 10% of $UO_2$, treated at 2200°C for 4 hr, showed a difference in lattice constant between material from the interior and that from the outer surface. The surface material was free of $UO_2$ and exhibited a lattice constant of 5.584 Å, whereas UP from the interior, which was in contact with $UO_2$, had a value of 5.579 Å. Finally, UP fired at 2000°C for one hour had a lattice constant of 5.578 Å, which increased to 5.583 Å with an additional 4 hr at this temperature.

The above phenomena can be explained in the following manner. Above 1500°C, UP loses phosphorus, resulting in a contracted lattice; above 1800°C, another substance is expelled from the structure, producing an expanded lattice, and this latter effect somewhat offsets the former one. Dissolved oxygen and nitrogen are most likely the anions expelled at elevated temperatures, and, since they are much smaller than phosphorus, their elimination would result in a lattice expansion. The amount of oxygen and nitrogen dissolved in the UP structure should not exceed 0.10 or 0.15% on the basis of metallographic and chemical analyses. Therefore, the UP lattice should continue to contract at higher temperatures once the dissolved anions have disappeared.

2. PuC and (U,Pu)C

Present work is directed to the development of methods for producing (U,Pu)C solid solution. Because of the extremely high rates of atmospheric corrosion of partly carburized U-Pu alloy, its carburization does not seem promising as a method of production of (U,Pu)C. Additional work has been done on the diffusion of PuC and UC in an effort to obtain single-phase solutions. Metallographic examination of an equal mixture of PuC and UC powders fired at 1900°C and at 2000°C showed diffusion of PuC into the UC grains. Additional firing at 2075°C showed grain growth of the UC-rich grains, but some PuC still remained in the grain boundaries.

A UC-20 w/o PuC powder mixture was fired at 2000°C for a total of 40 min in 10-min intervals. After each 10-min interval, the furnace was cooled and the fused cake was removed, sampled, and reground to the initial particle size of 80 NBS mesh. After 20 min of reaction time, little PuC was observed under metallographic examination. The fourth firing gave a much denser product than was previously observed. This product is being evaluated.

3. Irradiation of US and UC-PuC

An instrumented, temperature-controlled irradiation capsule containing four uranium sulfide specimens and two UC-20 w/o PuC specimens was inserted into the MTR reactor. The uranium sulfide was in the form of pressed and sintered pellets, whereas the carbides were vibratory-compacted physical mixtures of depleted uranium carbide and of both hypo- and hyperstoichiometric plutonium carbide. The overall specimen dimensions are 7.2 mm in diameter and 7.6 cm in length. All specimens are clad with 0.30 mm Nb-1 w/o Zr alloy. Target burnup for these specimens is 10 a/o of the metal atoms at a cladding surface temperature of 600 ± 50°C.

The capsule has a double-wall construction with a mixture of helium and nitrogen flowing between the inner and outer capsule walls. Specimen temperature is controlled by varying the composition of the flowing gas and hence the thermal conductivity of the annulus. A stainless steel-sheathed chromel-alumel thermocouple is adjacent to the midplane of each fuel section to monitor the cladding surface temperature. One uranium sulfide specimen contains a tungsten-coated tantalum center thermocouple well into which was placed a W-5 Re/W-26 Re thermocouple to monitor the temperature at the fuel center. Although all thermocouples were operating properly when the capsule was shipped to the reactor site, the center thermocouple did not function properly after reactor startup. All other thermocouples are functioning properly. The specimens are operating at slightly below the desired cladding surface temperatures at the limit of control possible with this capsule, and the capsule will be moved to a higher flux position.

A capsule of identical construction and containing a similar series of specimens is being readied for irradiation. A uranium sulfide specimen will again contain a center thermocouple Target burnup for specimens in this capsule is 5 a/o of the metal atoms at a cladding surface temperature of 800 ± 50°C.

4. The Thorium-Uranium-Plutonium Phase Diagram

The remarkable lowering of the alpha-beta transformation of thorium by plutonium additions that was reported by Russian workers could not be confirmed by US-UK investigators. In Progress Report for November 1963, ANL-6808, p. 42, we indicated that solid solutions of plutonium in beta thorium occur at 700 and 900°C. The plot of the lattice parameter of alpha-thorium versus composition of quenched ternary alloys shows discontinuities that can reasonably be explained by assuming that the beta-thorium phase is present at these temperatures.

An example for a series of thorium-base alloys with 4 w/o U and various percentages of plutonium is shown in Figure 19. From the

measurements of the lattice parameters combined with metallographic examinations, the two partial sections through the ternary phase diagram shown in Figures 20 and 21 were obtained. From these the rather weak breaks in the lattice parameter versus composition plots for the binary thorium-plutonium alloys (see Figure 22) were located, yielding in turn, the partial phase diagram of Figure 23. All the data are consistent.

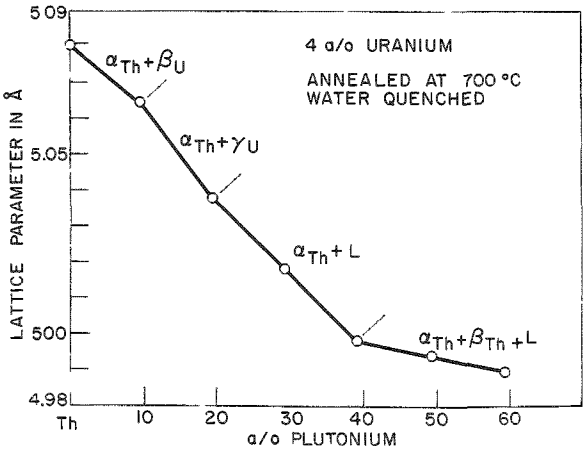


Figure 19

Lattice Parameters of $\alpha$-Thorium Phase of Th-4 a/o U-Pu Alloys. (The high-temperature phases are indicated.)

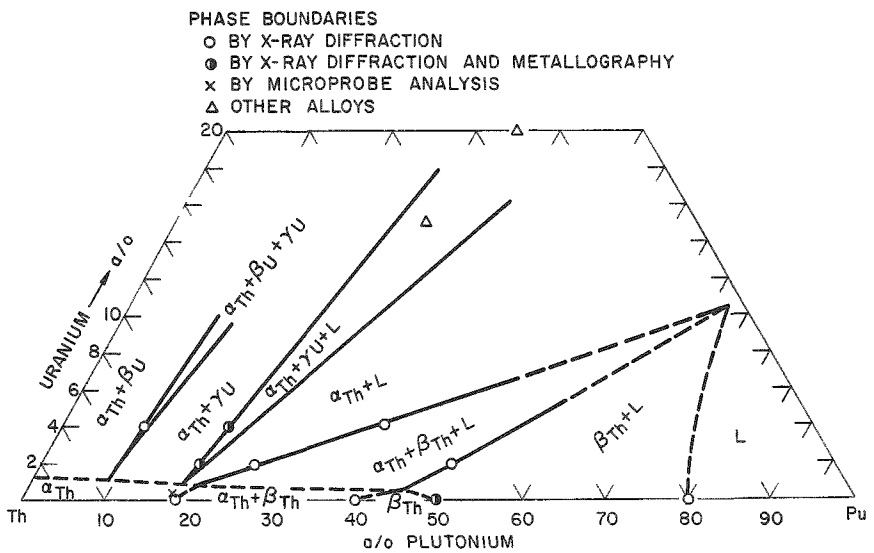


Figure 20. Preliminary Phase Diagram of Thorium-Plutonium-Uranium at 700°C

Additional confirmation was obtained from an electron microprobe analysis (see Table XIX) of the alloy Th-20 w/o U-35 w/o Pu, which showed the actual composition of its alpha phase to agree with the phase diagrams of Figures 19 and 20.

The two ternary phase diagrams show clearly the restricted range of ternary alloys useful as high-temperature fuels. They are those alloys in which no liquid phase occurs at elevated temperatures.

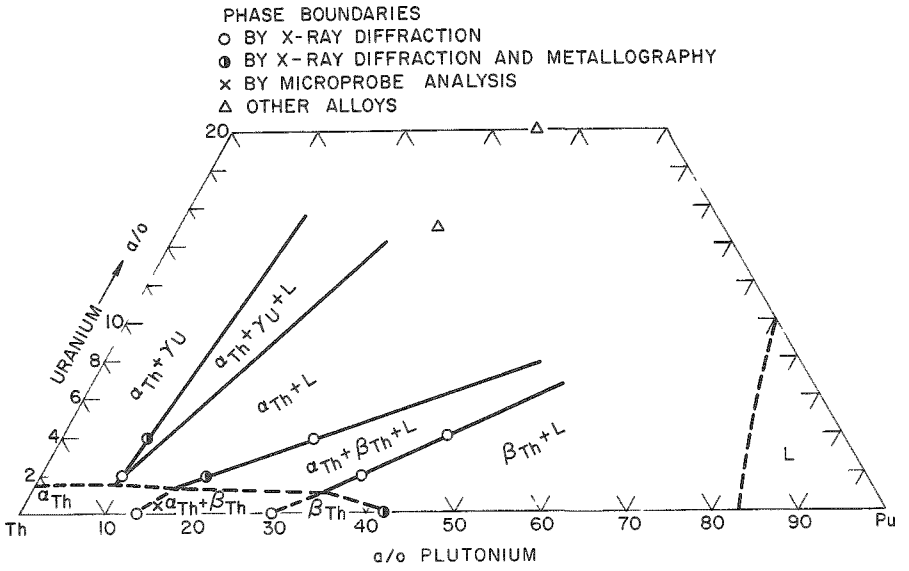


Figure 21. Preliminary Phase Diagram of Thorium-Plutonium-Uranium at 900°C

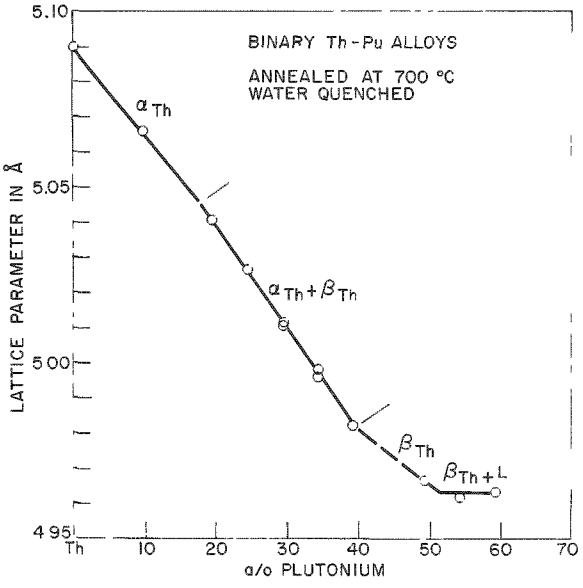


Figure 22. Lattice Parameters of $\alpha$ -Th Phase of Th-Pu Alloys. (The high-temperature phases are indicated.)

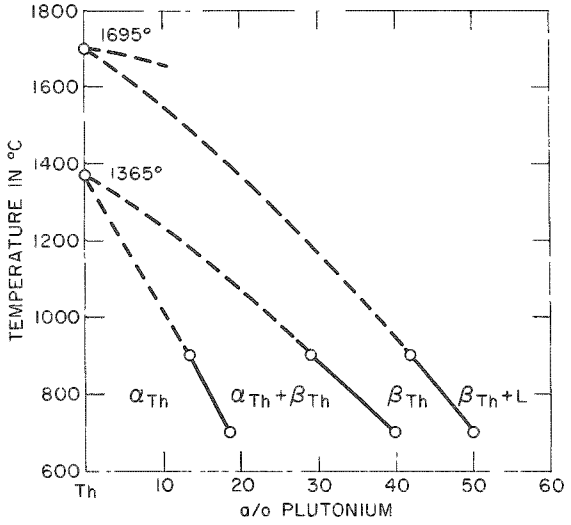


Figure 23. Portion of Binary Thorium-Plutonium Phase Diagram Showing the $\beta$ Phase between 700° and 900°C

Table XIX. Composition of the Alpha Phase in an Alloy with 45 w/o Th-20 w/o U-35 w/o Pu

| Quenching Temperature (°C) | Composition of $\alpha$ Phase | | | |
|---|---|---|---|---|
| | By Microprobe Analysis | | From Phase Diagram | |
| | w/o Pu | w/o U | w/o Pu | w/o U |
| 700 | 18.2 | 0.6 | 18.5 | 1.0 |
| 900 | 15.6 | 0.4 | 16.0 | 1.2 |

5. Fuel Jackets

Three tungsten sleeves were extruded at 1100°C to provide stock for secondary fabrication as follows:

| Ext. No. | Billet Components | | | Extrusion Ratio |
|---|---|---|---|---|
| | Jacket | Annulus | Core | |
| 244 | 304 SS | - | Mo | 13.1:1 |
| 245 | 304 SS | $Al_2O_3$ | Mo | 13.1:1 |
| 246 | 304 SS | - | 304 SS | 13.1:1 |

Radiographs of the extruded bars showed the tungsten sleeve to be uniform and free of defects. The cross section showed slight ovality. The use of Type 304 stainless steel cores could materially reduce billet can costs, and also permit lower extrusion constants and higher extrusion ratios. The initial attempt to use 304 SS as the core material (Ext. No. 246) was very successful and will be evaluated further.

During the reporting period a series of cast Stellite hot swaging dies were received. The die design is essentially the same as that used commercially for hot swaging of tungsten rod. Sizes of the twelve dies range from 1.385 cm (0.545 in.) to 0.401 cm (0.158 in.) with intervals of 20% reduction. Each die was given a preliminary check by hot swaging a piece of tungsten rod. The surface quality was fair considering no protective coating was used to prevent contamination.

Currently, a series of extruded tungsten tube composites, i.e., tubing jacketed with 304 SS and supported by a molybdenum core, are being hot swaged for tube pointing evaluation.

## D. Other Reactor Fuels and Materials Development

### 1. Corrosion of Ferrous Alloys in Superheated Steam

Various percentages of aluminum were added to Type 304 stainless steel in an effort to improve the corrosion resistance. About 4% Al was required (as shown in Table XX) to make a substantial improvement.

Table XX. Corrosion of Modified Type 304 Stainless Steel in 650°C, 42-kg/cm$^2$ Steam (30 ppm $O_2$)

| Alloy 304, % Al | Defilmed Metal Loss - 28-day Exposure, mg/cm$^2$ | Alloy 304, % Al | Defilmed Metal Loss - 28-day Exposure, mg/cm$^2$ |
|---|---|---|---|
| 0 | 18.0 | 4 | 0.06 |
| 1 | 17.0 | 5 | 0.03 |
| 2 | 8.8 | | |

Unfortunately the alloys containing 4 and 5 w/o Al were brittle after hot rolling into sheet form.

Alloys of Incoloy 800 modified with aluminum were obtained from the International Nickel Company. The results of the corrosion exposure are shown in Table XXI.

Table XXI. Corrosion of Modified Incoloy 800 in 650°C, 42-kg/cm$^2$ Steam (30 ppm $O_2$)

| Alloy 800, % Al Added | Defilmed Metal Loss, mg/cm$^2$ | |
|---|---|---|
| | 7.0 Days | 15.9 Days |
| 0 | 8.30 | |
| 1.05 | 4.67 | 4.21 |
| 1.7 | 0.33 | 0.61 |
| 2.4 | 1.06 | 1.04 |
| 3.7 (+0.3 w/o Ti) | 0.52 | 0.46 |
| 3.9 | 0.25 | 0.26 |

These alloys were ductile in sheet form and heliarc welds of the 3.9 w/o Al material were not brittle. Samples are being prepared for evaluation in flowing steam.

A wrist-pin failure in the feedwater pump has delayed testing in flowing steam. The new high-temperature semistatic steam autoclave is completed and in the process of being tested.

2. Nondestructive Testing

a. Application of Infrared Radiation. Investigation of the possible use of infrared in nondestructive testing has continued. The optical head of the mechanically scanned infrared imaging system (see Progress Report for November 1963, ANL-6808, p. 49) is being redesigned to permit much higher chopping speeds so as to improve the resolution and the signal-to-noise ratio.

b. Neutron Imaging. Several unirradiated plutonium fuel pins and one irradiated, radioactive reactor fuel capsule were inspected. An attempt was also made to compare the neutron attenuation properties of several reactor control materials to the neutron attenuation of cadmium by use of several neutron-detecting materials in order to vary the neutron energies involved. The initial attempt was encouraging, and further studies are planned.

c. Ultrasonic Imaging. Imaging round inspection objects by ultrasonic methods will be useful primarily for relatively large-diameter (4 cm or more) material. The inspection of round material of smaller diameter is complicated by the fact that the material itself acts as an ultrasonic lens and the image information is difficult to interpret.

Further studies of flat material have verified that much improved visual flaw detection can be realized by orienting the sample at an angle of 15 to 20° from the direction of the ultrasonic beam. Much of this improvement may be the elimination of multiple reflections between sample and detector.

Further efforts are now under way to determine the inspection speed possible for flat inspection objects.

The application of ultrasonic techniques to the inspection of small-diameter tubing is usually restricted to diameters of 0.64 cm or larger. Below a diameter of 0.64 cm, the ultrasonic beam is so severely scattered that insufficient energy is propagated in the tube wall. One possible approach to the solution of this problem lies in the design and construction of special-purpose transducer probes.

With this approach in mind, tubular and rectangular crystal elements, which shapes appear to offer the most promise, were purchased. Several probes were fabricated with curved and rectangular crystals of lead zirconate-titanate (Clevite's PZT-4).

Preliminary tests on Nb-1 w/o Zr tubing (of 0.51-cm diameter) with a 2.25-Mc line-focused probe were successful. Further tests will be conducted on a variety of small-diameter tubing.

During the testing of the Nb-1 w/o Zr tubing, the 2.25-Mc focused probe became erratic and eventually failed completely. Sectioning of the probe disclosed that the silver-loaded epoxy used for the ground connection had settled during curing. Apparently, the narrow gap between the crystal faces had broken down after a period of time under load.

To prevent the possibility of similar breakdowns in the future, a wire is silver-soldered directly to the crystal face to serve as a ground lead. A second 2.25-Mc line-focused transducer with a wire ground has been operating normally for several weeks.

d. Detection of Sodium Level by Ultrasonics. Several methods to determine the level of sodium within a stainless steel container during a transfer operation were tested and compared. A low-frequency (from 0.4 to 1 Mc range) ultrasonic transducer used on the side of a tank yielded erratic results during the actual transfer of sodium. However, subsequent work with this type of device appeared promising.

A good indication of the sodium level can be obtained by moving the transducer along the wall of the tank through the sodium-level area and observing the reflection of the ultrasound from the inner steel wall of the container. Above the sodium level, a good reflection is obtained. Within the sodium area, the reflection is much reduced as the ultrasound enters the sodium. The one question still unanswered concerning this method is whether or not the sodium will wet the inner surface of the tank sufficiently to observe the sodium level during the actual transfer.

Other methods used to observe the sodium level included probing with a thermocouple and the use of a thermal-sensitive phosphor applied to the outside of the tank. The phosphor, activated by ultraviolet and quenched by the heat of the sodium entering the transfer container, yielded a continuous indication of the sodium level during the transfer. Subsequent tests of sodium level with the thermocouple method, and with the phosphor and the ultrasonic technique yielded indications within ±1 cm.

e. Correlation of Heat-transfer Properties and Bond Quality. To measure thermal conductivities, it is necessary to determine Q, the amount of heat absorbed at the front surface of the specimen. In a calibration a value for Q of 0.5234 cal/cm$^2$ was found by using 2S-aluminum, copper, and nickel as standards, for their densities and specific heats are well known.

Two specimens, 1.9 cm square, were sectioned from an Argonaut fuel plate. One consisted entirely of the core, which is a dispersion of $UO_2$ in aluminum. The other had a cladding of 801-aluminum alloy roll-bonded to one side of the core. Each specimen was scanned, point by point, over its entire surface, and as all measurements were within 5 percent (there is a possible 5 percent experimental error in the measurements), average values are given. For comparison, values for 2S-aluminum are also given in Table XXII.

Table XXII. Thermal Conductivity Measurements on Components of Argonaut Fuel Plates

| Specimen | Sample Thickness, L(cm) | Thermal Diffusivity, $\alpha$(cm$^2$/sec) | Maximum Back Surface Temperature Rise, $T_m$(°C) | Thermal Conductivity, K(cal-cm/cm$^2$-sec-°C) |
|---|---|---|---|---|
| Al (2S) | 0.1278 | 0.860 | 7.02 | 0.502 |
| Argonaut: Core | 0.1263 | 0.597 | 6.66 | 0.371 |
| Argonaut: Core and cladding (cladding facing heat source) | 0.1267 | 0.625 | 6.71 | 0.385 |
| Argonaut: Core and cladding (core facing heat source) | 0.1267 | 0.619 | 6.70 | 0.382 |

As values for the full plate specimens are within 10%, which is within the accuracy of the system, it can be concluded that the bonding of the clad to the core has not affected its heat-transmission properties.

This last series of measurements has indicated the need for maintaining a more stable and rigid thermocouple contact at the back

surface of the specimen. As the specimens are scanned, the contact resistance must be maintained at its lowest value or spurious values of $T_m$ can result. Modifications are presently being made on the thermocouple supporting structure.

## E. Heat Engineering

### 1. Heat Transfer in Double-pipe Heat Exchangers

The previous analytical studies of heat transfer in double-pipe heat exchangers (e.g., see Monthly Report for October 1963, ANL-6801, p. 53) have concentrated on the use of plug flow models of the fluids. The introduction of an "effective conductivity approximation" made it possible to apply the results of these analyses to the turbulent flow of liquid metals when Peclet numbers are less than 1000. The extension of the analysis to Peclet numbers larger than 1000, and the need for a more definitive investigation of the range of applicability of the "effective conductivity approximation," led to consideration of an interesting class of "two-region" Sturm-Liouville systems. This type of system results when attempts are made to find analytical solutions for the turbulent and laminar cocurrent-flow double-pipe hext-exchanger problems by use of the classical method of separation of variables.

The following "two-region" Sturm-Liouville problem illustrates some of the highlights of the recent work.

(1) Let $y_1(\lambda,x)$ and $y_2(\lambda,x)$ be defined as the functions which satisfy the differential equations

$$y_i'' + g_i(x)\lambda y_i = 0; \quad i = 1,2,$$

with the boundary condition

$$y_i'(\lambda,0) = 0; \quad i = 1,2.$$

Primes denote differentiation with respect to x, the $g_i(x)$ are arbitrary non-negative functions of x defined for $0 \leq x \leq 1$, and $\lambda$ is an arbitrary real parameter.

(2) Let $\lambda_n$, with n = 1,2,3, ..., be the non-zero positive roots of

$$y_1(\lambda,1)y_2'(\lambda,1) + \alpha y_1'(\lambda,1)y_2(\lambda,1) + \beta y_1'(\lambda,1)y_2'(\lambda,1) = 0,$$

where $\alpha$ and $\beta$ are positive real constants. There will be a denumerably infinite number of these roots.

(3) Define the functions

$$E_{1n}(x) = y_2'(\lambda_n, 1)y_1(\lambda_n, x)$$

and

$$E_{2n}(x) = -\alpha\, y_1'(\lambda_n, 1)y_2(\lambda_n, x),$$

which obviously satisfy the differential equations and boundary conditions of (1). It can be shown that they also satisfy the boundary conditions

$$\alpha E_{1n}'(1) + E_{2n}'(1) = 0$$

and

$$\beta E_{1n}'(1) + E_{1n}(1) - E_{2n}(1) = 0.$$

(4) The functions $E_{1n}$ are eigenfunctions corresponding to the eigenvalues $\lambda_n$ for a "two-region" Sturm-Liouville system. The two regions are identified by the two functions $g_1$ and $g_2$. When these functions are equal, the system reduces to the usual Sturm-Liouville type. The equivalent of an orthogonality condition for the two region system is given by

$$\int_0^1 (g_1 E_{1n} E_{1m} + \frac{1}{\alpha}\, g_2 E_{2n} E_{2m})dx = 0 \text{ for } n \neq m$$

$$= N_n \text{ for } n = m,$$

with $N_n$ a normalizing factor. For completeness, $\lambda_0$ is taken as zero and $E_{i0}$, with $i = 1,2$, are taken equal to unity.

(5) The above makes it possible to represent two arbitrary functions $f_1(x)$ and $f_2(x)$ as expansions of the form

$$f_i(x) = \sum_{n=0}^{\infty} C_n E_{in}(x),$$

with

$$C_n = \frac{1}{N_n} \int_0^1 \left(f_1 g_1 E_{in} + \frac{1}{\alpha}\, f_2 g_2 E_{2n}\right)dx.$$

As applied to the cocurrent-flow double-pipe heat exchanger, $f_1$ and $f_2$ represent inlet temperature distributions for the two fluids. For the

laminar flow case, $g_1$ and $g_2$ are proportional to the fluid velocity distributions. For the turbulent flow case these functions depend on both eddy diffusivity and velocity distributions. The "two-region" Sturm-Liouville system outlined above makes it possible to obtain a practical solution for these cases based on various available approximation methods for estimating eigenvalues and eigenfunctions.

2. Studies of Boiling Liquid Metals

Assembly of the 10-kW radiant-heated NaK loop is progressing. An argon-purification system, consisting of a magnesium perchlorate moisture remover, a NaK bubbler, and a NaK vapor trap, is being installed. Some difficulty has been encountered in locating thermocouples in the heated section. Presently, chromel-alumel thermocouples in a 0.060-in. sheath are being investigated for this application.

A small-scale electron-bombardment heated-pool boiler is being designed. This system consists of a 16-in. heated length with four 0.060-in. sheathed chromel-alumel thermocouples located in the anode wall. The boiling liquid metal will be condensed by use of a coil condenser. The aims of this experiment are:

(1) to gain experience with electron bombardment heating at higher power levels,

(2) to investigate the measurement of temperatures in tube walls, and

(3) to obtain boiling of alkali metals.

3. Stability in Parallel-channel Flow Systems

In a boiler or a boiling water reactor, the makeup water introduced to the channels may be (several degrees) below saturation temperature. Consequently, boiling does not occur immediately at the channel inlet, and a portion of the length of the channels may have subcooled liquid. In such cases, the analytical methods[5] which assume that all water in the reactor is at saturation temperature cannot be applied directly.

A more realistic case, in which the water enters the channels at a constant subcooled temperature, may be studied by such techniques provided the conservation equations are written with different unknowns,[6] namely,

---

[5]C. K. Sanathanan, Dynamic Analysis of Coolant Flow in Boiling Water Nuclear Reactors, Ph.D. Thesis submitted to Case Institute of Technology (1963).

[6]J. E. Meyer, Conservations Laws in One-dimensional Hydrodynamics, Bettis Technical Review (Sept 1960).

$\overline{\rho}(z,t)$ the average density, $H'(z,t)$ the mixing-cup enthalpy, and $G(z,t)$ the mass flow rate per unit area. The variables in Ref. 5, namely, $\alpha(z,t)$, the void fraction, and $V_f(z,t)$ and $V_g(z,t)$, the velocities of water and steam, respectively, may then be indirectly obtained. The proposed system would have a boundary condition $\Delta H'(0,t) = 0$ for $t \geq 0$ to ensure constant inlet enthalpy. Slip-flow conditions are considered in an indirect manner.

The equations describing the dynamics of the subcooled system may now be solved, since the new variables are continuous and differentiable in space and in time. (The void fraction $\alpha$ would have a zero zone in z for a subcooled case.)

4. Shipping Cask Heat Transfer

Redesign of the proposed EBWR shipping cask has necessitated a complete revision of the original heat transfer analysis. Calculations made to date indicate that the cask surface-temperature restriction may cause a limit in the fuel loading. Elimination of paint on the exterior surfaces of the cask reduces radiant heat transfer and increases solar absorptivity, both to a marked degree. A simple steady-state calculation under maximum solar-heating conditions is no longer sufficient to demonstrate that significant heat loads from the fuel can be tolerated. The approach now being attempted is a transient study which considers the massive heat capacity of the cask and the diurnal radiation cycle. Results from this study should allow a more realistic estimate of the allowable fuel capacity of the cask.

5. Boiling Sodium Heat Transfer Facility

The temporary facility for checking out the 150-kW power supply has been essentially completed. Some conceptual design work for shutters and actuators for the liquid metal loop heat exchanger is underway.

## F. Chemical Separations

1. Chemistry of Liquid Metals

a. The Lanthanum-Cadmium System. Five intermetallic compounds are known to exist in the system lanthanum-cadmium: $LaCd_{11}$, $La_2Cd_{17}$, $La_3Cd_{13}$, $LaCd_2$, and LaCd. The equilibrium pressure of cadmium over the following two-phase regions has been measured: $LaCd_{11}$-$La_2Cd_{17}$, $La_2Cd_{17}$-$La_3Cd_{13}$, $La_3Cd_{13}$-$LaCd_2$, and $LaCd_2$-LaCd. The temperature range of the measurements was from 356 to 490°C. The data will be used to calculate the thermodynamic properties of these phases.

b. Liquid Metal Distillation. Vaporization from the liquid-vapor surface of a liquid pool without the formation of vapor bubbles (nonturbulent vaporization) is a method of vaporization that is of interest in relation to

retorting steps of pyrometallurgical recovery processes, since the method will very likely involve little entrainment. Study of the nonturbulent vaporization of mercury from a 1-in.-diameter, 12-in.-deep liquid pool has been continued. The temperature at the liquid surface has been measured at high and low vaporization rates by means of a modified liquid metal thermocouple. A large difference in temperature existed across the vaporizing surface; at a high vaporization rate, the maximum and minimum temperatures differed by 18°C. The temperature isotherms were asymmetric with respect to the pool center, particularly at high vaporization rates.

## 2. Fluidization and Volatility Separation Processes

### a. Recovery of Uranium from Low-enrichment Ceramic Fuels

(i) Laboratory-scale Fluid-bed Fluorinations. Laboratory support work has been directed toward the establishment of optimum conditions for the fluid-bed fluorination of mixtures of $U_3O_8$ and plutonium dioxide (see Progress Reports for November and December 1963; ANL-6808, p. 53, and ANL-6810, p. 37). Recent fluid-bed experiments have been made to determine the effect on the retention of plutonium on alumina of the following:

(a) the use of mixtures of $PuO_2$, $U_3O_8$, and fission product oxides in which the $PuO_2$ and $U_3O_8$ were mixed as separate compounds and were not obtained from the oxidation of a solid solution of $PuO_2$ and $UO_2$ prior to mixing with fission product oxides, as was the case in previous experiments;

(b) the use of a low fluorination temperature and a low rate of feed material during the feeding-fluorination period.

The concentration of plutonium in the $U_3O_8$-$PuO_2$ mixtures was about 0.4 w/o, and the concentration of 11 fission product oxides ($La_2O_3$, $CeO_2$, $Pr_6O_{11}$, $Nd_2O_3$, $Sm_2O_3$, $Eu_2O_3$, $Gd_2O_3$, $Y_2O_3$, BaO, $ZrO_2$, and $MoO_3$) was about 0.9 w/o. In these runs, alumina was added to the mixture prior to being fed to the fluid-bed reactor. The fluorination reaction consisted of two steps. The first step was a feeding-fluorination period during which the feed material was continuously transported into a $1\frac{1}{2}$-in.-diameter fluidized bed of alumina and simultaneously reacted with 20 v/o fluorine in nitrogen. The second fluorination step was carried out with 100% fluorine, which was recycled through the fluid bed.

The feeding-fluorination period was performed at 450°C over a period of 3.8 hr (feed-material flow rate was 1.3 g/min). This period was followed by three successive recycle-fluorination periods of 5 hr at 450°C, 5 hr at 500°C, and 10 hr at 550°C. After this series of

recycle fluorinations, the residual plutonium and uranium contents of the alumina were 0.006 w/o and 0.003 w/o, respectively. The results of this run have shown the following:

(1) No appreciable difference in the level of plutonium retention on the alumina resulted from the use of a mixture of plutonium dioxide, $U_3O_8$, and fission product oxides prepared either by mixing separate components or by using $PuO_2$ and $U_3O_8$ obtained from the oxidation of $PuO_2$-$UO_2$ solid solutions prior to mixing with the fission product oxides.

(2) Retentions of plutonium on alumina as low as 0.006 w/o were indicated with the utilization of both a low fluorination temperature and a low feed-material rate during the feeding-fluorination period.

b. Engineering-scale Studies of Two-zone Oxidation-Fluorination Processing Scheme for Clad Uranium Dioxide. The alumina bed from a previous two-zone oxidation-fluorination run (see Progress Report for October 1963, ANL-6801, p. 60) was subjected to a second cleanup fluorination step for further removal of uranium (see Progress Report for November 1963, ANL-6808, p. 55). In this run, the fuel charge consisted of twelve 11.6-in.-long simulated sheared pieces of Type 304 stainless steel-clad uranium dioxide pellets (3.25 kg uranium dioxide). The alumina in this run had been used as fluid-bed material in a previous run (see Progress Report for July 1963, ANL-6764, p. 53) and consisted mainly of small particles, 86% of the particles being in the size range of -120 +200 mesh. Prior to the first fluorination cleanup step, the stainless steel cladding was removed from the reactor. The first cleanup step resulted in reducing the residual uranium concentration in the alumina to 0.72 w/o, which is greater by a factor of 10 than the uranium retained by the alumina in other runs. The second fluorination cleanup step was carried out at the same temperature as the first, 500°C, for an additional period of 5.5 hr (a total of 10 hr for the two cleanup steps), with fluorine added to a maximum concentration of 83 percent (68% fluorine in the first step). This reduced the residual uranium concentration in the alumina to 0.035 w/o, which indicates that a satisfactory removal of uranium from alumina (after second usage) can be achieved by a cleanup step with fluorine in about 10 hr.

c. Recovery of Uranium from Highly Enriched Uranium-Alloy Fuels by Chlorination and Fluorination Steps

(i) Bench-scale Studies. Studies of the feasibility of using a fluid-bed chlorination-fluorination scheme for the recovery of enriched uranium from uranium-alloy fuels were continued. Presently, tests are being carried out with uranium-aluminum and uranium-Zircaloy fuels in a $1\frac{1}{2}$-in.-diameter fluid-bed reactor, with the alloy subassembly being submerged in an inert bed.

An additional run with a multiplate uranium-aluminum fuel subassembly has been carried out (see Progress Report for November 1963, ANL-6808, p. 55) to test the effect on the retention of uranium by alumina of a fluorination procedure utilizing low rates of fluorine feed, which could result in the elimination of a fluorine recycle step. The charge consisted of four uranium-aluminum subassemblies (total weight, 188.5 g; 5.2 w/o normal uranium), each subassembly being 5 in. long. The fluid-bed reactor contained 320 g of -40 +120 mesh sintered alumina (Tabular Alumina T-61, Aluminum Company of America); the packed bed filter contained 534 g of -14 +20 mesh fused alumina (Type 38 Alundum, Norton Company). The alumina in the fluid-bed reactor and the packed-bed filter had been used in previous runs.

The following reaction sequence was used in the run: hydrochlorination, hydrofluorination, and fluorination. The hydrochlorination reaction (with hydrogen chloride containing 1100 ppm water) was carried out while maintaining the fluid bed at a temperature of 250°C and the filter bed at 200°C. During the hydrochlorination period, two subassemblies were reacted over a period of $2\frac{1}{2}$ hr, after which the other two subassemblies were charged to the fluid-bed reactor and reacted over a period of $4\frac{1}{2}$ hr. The hydrofluorination step (with 25 to 50 v/o hydrogen fluoride in nitrogen) was conducted at a fluid-bed temperature of 350°C for 1 hr. During the fluorination step, the fluorine feed rate was 0.15 liters/min (at 21°C and 1 atm), which corresponded to about 6 kg of fluorine per kg of uranium recovered. This fluorine feed rate was less than one-tenth the feed rate previously used. The fluorination period was conducted in three steps over a 4-hr period, as follows: (1) the temperature of the fluid bed and the filter bed was gradually increased from 250°C to 500°C over a period of $1\frac{1}{2}$ hr while feeding a 5 v/o fluorine-nitrogen mixture, (2) the nitrogen diluent in the 5 v/o fluorine-nitrogen mixture was then gradually reduced to zero during the following $\frac{1}{2}$-hr period, while maintaining the same fluorine feed rate and the same temperature (500°C) of the system, and (3) the alumina bed of the fluid-bed reactor was then maintained as a settled, packed bed for the final 2 hr at 500°C while flowing a 95 v/o fluorine-nitrogen mixture at a low rate of fluorine feed (0.15 liters/min) which was insufficient to fluidize the alumina in the reactor.

The retentions of uranium by the alumina in the fluid-bed reactor and the packed-bed filter were very low: 0.005 w/o and 0.004 w/o, respectively. The results with the low rate of fluorine feed would indicate that a fluorine recycle step may not be needed. The low retentions of uranium by the alumina are comparable with the results obtained in a previous run (see Progress Report for September 1963, ANL-6784, p. 53) in which the uranium retained by the alumina in the fluid-bed reactor and the packed-bed filter were 0.004 w/o and 0.003 w/o, respectively. The alumina bed of the reactor in the previously reported run was fluidized during the fluorination period.

## 3. General Chemistry and Chemical Engineering

a. Conversion of Uranium Hexafluoride-Plutonium Hexafluoride Mixtures to Uranium-Plutonium Oxides: Preparation of High-density Particles. Plans are being made to develop a fluid-bed method for producing high-density particles from mixtures of plutonium hexafluoride and uranium hexafluoride by reaction with steam and hydrogen. This work is to be carried out in a 2-in. diameter fluid-bed reactor to be installed in the engineering-scale plutonium handling facility (see Progress Report for December 1963, ANL-6810, p. 38).

Current investigations are being made with uranium hexafluoride alone in preparation for the study with the $UF_6$-$PuF_6$ mixture and are being carried out in a 3-in.-diameter fluid-bed reactor. Recent work has investigated an oxidation-reduction procedure for the fluid-bed preparation of dense seed particles as an alternative to the present method of mechanical grinding (see Progress Report for September 1963, ANL-6784, p. 54). The runs were carried out with fluid beds of -18 +80 mesh uranium dioxide particles (tapped bulk density, ~6.2 g/cc).

In all runs, the fraction of -80 mesh particles increased with increase in the extent of oxidation. About 65 to 84 percent of the starting bed material was reduced to -80 mesh particles after 1.2 times the stoichiometric amount of oxygen required for the complete oxidation of $UO_2$ to $U_3O_8$ was added. Tapped bulk densities as high as 5.5 g/cc were achieved after the reduction step.

b. Alpha Decomposition of Plutonium Hexafluoride. The effect of alpha-induced decomposition of plutonium hexafluoride is being investigated as a part of a fundamental study of the radiation behavior of plutonium hexafluoride. Additional data have been obtained on the rate of alpha decomposition of gaseous plutonium hexafluoride to plutonium tetrafluoride and fluorine (see Progress Report for October 1963, ANL-6801, p. 58). The decomposition rates for plutonium hexafluoride were determined in runs which investigated the following: (1) the effect of storage container volume, (2) decomposition time, (3) the presence of plutonium tetrafluoride in the spheres from previous alpha-decomposition runs, (4) storage temperature, and (5) surface-to-volume ratio of test spheres (nickel wool was packed into some of the spheres to increase the surface-to-volume ratio). The runs were carried out in prefluorinated, nickel spheres whose volumes were either about 125 cc or 5.96 liters. The spheres were filled with varying amounts (55 mm, 75 mm, or 100 mm Hg) of plutonium hexafluoride and held for 75 to 571 days at decomposition temperatures which ranged from about 25°C to 82°C. In nickel spheres which were packed with nickel wool, the geometric surface-to-volume ratio was increased tenfold.

The results of the runs are summarized in Table XXIII and show the following effects on the average decomposition rate of plutonium hexafluoride:

(1) An increase in the volume of the storage sphere resulted in a decrease in the decomposition rate.

(2) The average rate of decomposition decreased with time, as was expected. A value of approximately 50 percent for the total decomposition of plutonium hexafluoride was being approached at the longer decomposition times (571 days).

(3) The presence of plutonium tetrafluoride resulted in a decrease in the decomposition rate, which substantiated previously obtained data (see ANL-6801, p. 58).

(4) The decomposition rate was increased when the decomposition temperature was increased (from 25 ± 2°C to 82 ± 2°C), which leads to the belief that some thermal decomposition of the plutonium hexafluoride is taking place at the higher temperature, since pure radiation-induced decomposition should be independent of temperature.

(5) The decomposition rate was previously found to be significantly increased when alpha-induced decomposition occurred in spheres that contained nickel wool and pure plutonium hexafluoride (see Progress Report for October 1963, ANL-6801, p. 59). In the current series of runs, the rate was noted to be less in spheres that were packed with nickel wool and contained plutonium tetrafluoride initially present from the previous decomposition of plutonium hexafluoride as compared with spheres that contained nickel wool and pure plutonium hexafluoride.

Table XXIII. Summary of Data on Alpha-induced Decomposition of Plutonium Hexafluoride

Prefluorinated, nickel spheres were used for sample storage vessels

| Sphere Volume (cc) | Temp (°C) | Initial $PuF_6$ Pressure (mm Hg) | Initial $PuF_4$ (mg) | Average Decomposition Rate (%/day) | |
|---|---|---|---|---|---|
| | | | | 75 to 77 Days | 571 Days |
| ~125 | ~25 | 100 | 0 | 0.19[a] | - |
| ~125 | ~25 | 100 | 28-57 | 0.14[a] | - |
| 5960 | ~25 | 100 | 0 | 0.11 | - |
| ~125 | ~25 | 100 | 0 | - | 0.044 |
| ~125 | ~25 | 100 | 3.8, 7.6[b] | - | 0.091 |
| ~125 | ~25 | 75 | 0 | - | 0.095 |
| ~125 | ~25 | 75 | 4.8 | - | 0.090 |
| ~125 | ~25 | 50 | 0 | - | 0.067 |
| ~125[c] | ~25 | 100 | 44 | 0.16 | - |
| ~125[c] | ~25 | 100 | 0 | 0.30[a] | - |
| ~125 | ~82 | 100 | 0 | 0.64 | - |
| ~125 | ~82 | 100 | 21-35 | 0.53 | - |

[a]Previously reported data (see Progress Report for October 1963, ANL-6801, p. 59).

[b]The quantity of plutonium tetrafluoride from previous $PuF_6$ decomposition tests initially present in each of the two spheres tested.

[c]Spheres packed with nickel wool; surface-to-volume ratio increased 10-fold.

### 4. Calorimetry

As part of a continuing program to determine the heats of formation of refractory substances by fluorine bomb calorimetry, calorimetric combustions of hafnium diboride in fluorine have been initiated. Techniques for the combustion of yttrium in fluorine have been developed, and a series of calorimetric combustions is in progress.

Preliminary combustions of uranium monosulfide in fluorine have been performed in a fluorine flow reaction vessel, a test vessel which is being evaluated for the combustion of materials which react spontaneously with the oxidizing gas. The sample was held in an inert atmosphere inside the vessel until reaction was desired; then a stream of fluorine at low pressure was directed onto the surface of the sample from a jet and reaction was initiated. In addition to the low pressure used and the avoidance of spontaneous reaction of the uranium monosulfide with fluorine, an advantage of this technique was the sweeping away of the volatile products of the reaction by the gas stream. Results of these combustions were favorable enough to warrant detailed examination of the combustion of uranium monosulfide in the fluorine flow reaction vessel.

## G. Plutonium Recycle Program

### 1. Doppler Reactivity Effects

Doppler reactivity effects have been evaluated for a realistic control rod configuration in the plutonium recycle loading of EBWR in which all but one of the corner rods are fully inserted. In this configuration, about 70% of the power resides in the quadrant with the rod removed. At zero burnup, the introduction of sufficient reactivity to yield a 200 Mw-sec energy output produced a feedback of about -0.8% $\delta k$, whereas with a plutonium zone burnup of 0.006, with the same energy output, the reactor yielded a feedback of about -0.9% in $\delta k$.

The Doppler reactivity worths were used in RP-129 kinetics calculations, which indicated that for the rod configuration above, a step reactivity insertion of about 1% will release about 190 MW-sec, which leads to fuel melting at the hottest point in the core. This 1% reactivity corresponds to a reactor period of about 6 msec.

ARGUS calculations for the above event indicate that the zirconium clad does not reach the melting point and probably will not be ruptured owing to the resulting thermal stresses. For example, the maximum temperature difference across the clad is calculated to be about 210°C. If the room-temperature value for Young's modulus of elasticity is used, which will give an upper limit to the stresses produced, the maximum

stress in the clad is calculated to be about 17,500 psi. This can be compared with the room-temperature elastic limit for zirconium of 44,800 psi and the value 18,300 psi at 230°C.

Further calculations were made of the boric acid worths for various conditions. The results are summarized below.

For the initial system at the hot operating condition, the void coefficient of reactivity, $\delta k/\delta V_{Pu}$, is approximately -0.33, where $\delta V_{Pu}$ refers to changes in the plutonium-zone void with relative changes in the other zones so as to maintain the initial void distribution. In terms of average core void, the value of the coefficient is about -0.45, which corresponds to a power coefficient of reactivity, $\delta k/\delta P$, of about -0.001 $MW^{-1}$.

At room temperature, the density coefficient of reactivity, $\delta k/\delta \rho$, is about -0.10. This value decreases as boric acid is added to the water, but remains negative for an addition of 10 gm of boric acid per gallon of room-temperature core water. Table XXIV gives $\delta k/\delta \rho$ for various boric acid contents for the initial system.

Table XXIV. Cold Density Coefficients of Reactivity for Various Boric Acid Contents[7]

| Boric Acid Concentration, gm/gal (cold) | $\delta k/\delta \rho$ |
|---|---|
| 0 | -0.10 |
| 1.0 | -0.094 |
| 5.0 | -0.059 |
| 10.0 | -0.024 |

The boric acid worth for the cold, initial system is about -1% in $\delta k$ for an addition of 1 gm/gal of core water to the unpoisoned system and about -0.8% for an addition of 1 gm/gal for the system when it contains 9 gm/gal. The boric acid worth decreases as the water density decreases, owing to hardening of the spectrum. At the hot operating temperature, but with no voids (water density $\rho$ = 0.788 gm/cm$^3$), the boric acid worth is about -0.68% for an addition of 1 gm/gal of equivalent room-temperature density water ($\rho$ = 1 gm/cm$^3$). Owing to nonlinearity of boric acid worth with concentration, an addition of 12 gm/gal of unit density water produces a $\delta k$ of about -7.6%, corresponding to an effective worth of about -0.63%/gm/gal over this range. For the cold system, at an assumed density of 0.788, this amount of boric acid produces a $\delta k$ of about -8.8%, corresponding to an effective worth of about -0.73%/gm/gal.

[7]These results correct the information given in the Progress Report for December 1963, ANL-6810, p. 40.

For the system at a burnup of 0.006 and at the hot operating condition, the void coefficient of reactivity, $\delta k/\delta V_{Pu}$, is about -0.38. In terms of the average core void, the coefficient is about -0.39, corresponding to a power coefficient, $\delta k/\delta P$, of about -0.0013 $MW^{-1}$.

At room temperature, the density coefficient of reactivity, $\delta k/\delta \rho$, is about -0.16. Table XXV shows the influence of boric acid on the density coefficient of reactivity for the system at a burnup of 0.006. As in the case of the initial system, the reactivity coefficient, though appreciably smaller than for the unpoisoned case, is still negative for boric acid contents as high as 10 gm/gal of core water at room temperature.

Table XXV. Cold Density Coefficients of Reactivity for Various Boric Acid Contents and a Burnup of 0.006

| Boric Acid Concentration, gm/gal (cold) | $\delta k/\delta \rho$ |
|---|---|
| 0 | -0.16 |
| 1.0 | -0.16 |
| 5.0 | -0.13 |
| 10.0 | -0.026 |

The boric acid worth is about -1% in $\delta k$ for an addition of 1 gm/gal to the cold unpoisoned system for a plutonium-zone burnup of 0.006. An addition of 1 gm/gal to the system which contains 9 gm/gal results in a $\delta k$ of about -0.7%. For the cold system at an assumed water density of 0.788 $gm/cm^3$, a boric acid addition of 12 gm/gal of unit density water produces a $\delta k$ of about -8.4% corresponding to an effective worth of about -0.70%/gm/gal over this range. By comparison with the corresponding results for the system at zero burnup, this addition would correspond to a worth of about -0.6%/gm/gal of unit density water for the hot system.

The cold density coefficient of reactivity, $\delta k/\delta \rho$, for the plutonium critical configuration with a burnup of 0.006 is about -0.11 for the system containing about 6 gm of boric acid per gallon of core water at room temperature, which corresponds to the initial clean critical condition. The boric acid worth is about -1.3% in $\delta k$ for a 1-gm/gal addition to the unpoisoned system and about -1% for a 1-gm/gal addition to the system which contains 9 gm/gal.

The Safety Analysis report for the plutonium recycle experiment is being prepared.

## 2. EBWR "T" Modification

In the original design for EBWR, provision for forced circulation was made by providing T's in the bottom of the pressure vessel. These T's have acted as a receptacle for radioactive crud and steps are being taken to cut off the T's and replace with reducers. This new arrangement permits flushing. As very limited space is available for T removal, it was necessary to simulate this operation in the shop.

The mockup has been completed, and shop personnel have successfully removed the 6-in. pipe cap by a guillotine saw. A special "T"-cutting tool is being installed. Following the "T" removal and subsequent rebeveling of the pipe end, the new 6X1 reducer will be welded in place. This entire operation simulates exactly what must be done with the EBWR reactor.

# IV. ADVANCED SYSTEMS RESEARCH AND DEVELOPMENT

## A. Argonne Advanced Research Reactor (AARR)

### 1. Core Physics

The latest revised values of the equilibrium concentrations of $Xe^{135}$ and $Sm^{149}$ present after startup at 240-Mw total power are given in Table XXVI. The annular core regions are numbered in consecutive order beginning with the innermost core region, with inner radius 7 cm. Core regions 1 through 9 and 11 through 14 represent successive individual plates near the inner and outer core edges, respectively, where $U^{235}$ loading is varied to achieve radial power flattening. Core region 10 represents the bulk of the core.

Table XXVI. Calculated Equilibrium Concentration of $Xe^{135}$ and $Sm^{149}$

| Annular Core Region No. | Outer Radius (cm) | $Xe^{135}$ Concentration ($10^{15}$ atoms/cm$^3$ core) | $Sm^{149}$ Concentration ($10^{16}$ atoms/cm$^3$ core) | $s_\ell$ |
|---|---|---|---|---|
| 1 | 7.1883 | 6.76 | 4.14 | 0.17590 |
| 2 | 7.3718 | 8.99 | 5.32 | 0.22828 |
| 3 | 7.5508 | 11.93 | 6.86 | 0.29319 |
| 4 | 7.7257 | 15.88 | 8.88 | 0.37420 |
| 5 | 7.8967 | 21.29 | 11.62 | 0.47550 |
| 6 | 8.0641 | 28.81 | 15.39 | 0.60148 |
| 7 | 8.2281 | 39.41 | 20.73 | 0.75588 |
| 8 | 8.3887 | 54.43 | 28.41 | 0.93988 |
| 9 | 8.5467 | 72.22 | 37.83 | 1.10000 |
| 10 | 23.2172 | 98.05 | 62.79 | 1.00000 |
| 11 | 23.613 | 65.64 | 37 14 | 1.10000 |
| 12 | 23.8084 | 53.25 | 30.18 | 1.09982 |
| 13 | 24.0022 | 32.35 | 19.11 | 0.75047 |
| 14 | 24.2 | 20.13 | 12.54 | 0.50244 |

The $U^{235}$ loading in each core region, as represented by the factor $s_\ell$, the ratio of actual U concentration (atom percent) to the nominal, is also given in Table XXVI. The nominal concentration is obtained with plates containing 37 w/o $UO_2$ in stainless steel cermet.

The ratio of peak power to average power in the radial direction with no sample in the internal thermal column is 1.95. The power levels in the inner seven core regions and in the outer two core regions are very nearly equal, i.e., the radial power distribution is flat throughout these regions.

The prompt neutron lifetime ($\ell_p$) and effective abundance of delayed neutrons ($\beta_{eff}$) were calculated with the use of 18 energy groups with thermal upscattering, and with 16 energy groups with no upscattering. The values obtained are given in Table XXVII.

Table XXVII. Effective Abundances of Delayed-Neutron Groups

| Delayed Neutron Group | $\beta_{eff_i}$ (18 groups) | $\beta_{eff_i}$ (16 groups) |
|---|---|---|
| 1 | 0.000255 | 0.000245 |
| 2 | 0.00170 | 0.00164 |
| 3 | 0.00152 | 0.00146 |
| 4 | 0.00308 | 0.00296 |
| 5 | 0.000896 | 0.00861 |
| 6 | 0.000325 | 0.000312 |
| | $\beta_{eff}$ = 0.00778 | 0.00747 |
| | $\ell_p$ = 9.98 $\mu$sec | 11.96 $\mu$sec |

Reactivity changes $\Delta k/k$ resulting from various perturbations have been calculated with the aid of the 16-group and 18-group cross-section sets. The values found by use of the two sets agreed for changes in water density, but not for changes in temperature. These calculations were made assuming a Type-I sample (see footnote to Table XXVIII) in the internal thermal column. Further calculations with the 18-group cross-section set are being made to resolve the discrepancy.

The flux varied slightly through the sample region. The percentage changes in the flux for various configurations going from the center out to the edge of the sample (in the radial direction) are listed in Table XXVIII. Normalized values of the average flux in the sample region (all normalized to the average value of the flux in energy group 16 in the internal thermal column with no sample in place) are also given in Table XXVIII.

## 2. Critical Experiment

AEC approval of the AARR fuel contract is still pending. Consequently, the delivery of the initial 300 foils of bare (unclad) uranium metal has been delayed one month since delivery is scheduled 90 days after contract execution.

Plans for fuel envelopment, using the electron beam welder, have progressed to the point of designing fixtures for welding a package of up to 50 fuel envelopes at a time.

Table XXVIII. Calculated Fluxes

| Designation of Energy Group | Energy Range (eV) | Configuration* | % Flux Change | Relative Flux |
|---|---|---|---|---|
| 15 | 0.64-0.4 | a | +2.54 | 0.02084 |
| | | b | +0.66 | 0.02253 |
| | | c | +0.10 | 0.02267 |
| | | d | +0.25 | 0.02370 |
| 16 | 0.4-0.1 | a | -8.67 | 1.00000 |
| | | b | +2.31 | 0.80694 |
| | | c | -2.34 | 0.93863 |
| | | d | +0.93 | 0.75542 |
| 17 | 0.1-0.02 | a | -8.78 | 0.69052 |
| | | b | +3.84 | 0.54471 |
| | | c | -2.06 | 0.64456 |
| | | d | +2.00 | 0.50827 |
| 18 | 0.02-0 | a | -8.70 | 0.06350 |
| | | b | +5.08 | 0.04953 |
| | | c | -1.82 | 0.05919 |
| | | d | +2.61 | 0.04624 |

* a. No sample.
b. Type-I sample: this sample mocks up a massive californium irradiation sample.
c. Type-II sample: this sample mocks up a low cross-section irradiation sample.
d. Type-I sample surrounded by Type-II sample.
The sample region ranges from 0 to 2.65962 cm in the radial direction.

Installation of the beryllium reflector for the critical experiment is complete except for retainers to prevent lateral creep. The reactor console now appears to be in good working order throughout. Significant reduction in electrical-circuit noise, as reported previously, was obtained by replacing unstable relays which fluttered or bounced when closed. One relay was so unstable that fluttering could be started by bumping the console. Some feedback is still present between activating circuits and switched circuits, and efforts are being made to eliminate this problem.

3. Shielding

Operating experience, particularly with heavy water reactors, indicates the feasibility of operating AARR with a contaminated coolant which is not flushed from the system after a moderate fuel meltdown, providing

decontaminating factors on the order of 100 can be realized. The Canadian NRU reactor has operated successfully with nonuniform concentrations of $> 8 \times 10^{-5}$ g U (natural) plus $2 \times 10^{-4}$ g Al/g $D_2O$.[7] A 10% AARR fresh core melting followed by 99% particle separator decontamination results in a total impurity concentration of $6.7 \times 10^{-7}$ g $U^{235}O_2$ plus $4 \times 10^{-6}$ g structure/g $H_2O$ in the primary coolant. Re-startup of AARR with these impurities results in less than a 100% increase in the dose rate levels for occupied areas adjacent to the primary coolant system. Fouling of heat exchange surfaces has not been investigated, but it would not appear to be a problem.

The magnitude of radiation escaping the AARR spent core during transfer operations indicates the need for calculations of transient heat transfer for the transfer chute region. Steady-state considerations indicate a steel thermal shield having a thickness greater than 4 in. would be required to preclude excessive thermal stresses in the concrete surrounding the fuel transfer chute. Such a shield would be useful as complementary shielding at other locations as well.

## B. Rocket Fuel Test Reactor

The parametric design study on the Rocket Fuel Test Reactor is progressing. Major attention is being devoted to varying the concentration of fuel and moderator to achieve optimum performance. The four combinations of fuel and moderator being considered are: $UO_2$-BeO-Fe-Na, U-Zr-$ZrH_2$-Na, $UO_2$-$D_2O$-Fe, and $UO_2$-$H_2O$-Fe. Reactivity and neutron spectrum calculations were performed for reactors having the volume percentages of fuel and moderator as shown in Table XXIX.

Table XXIX. Composition of Four Test Reactors, v/o

| No. | A. $UO_2$-BeO-Fe-Na Type | | | | B. U-Zr-$ZrH_2$-Na Type | | | | C. $UO_2$-$H_2O$-Fe Type | | | D. $UO_2$-$D_2O$-Fe Type | | |
|---|---|---|---|---|---|---|---|---|---|---|---|---|---|---|
| | $UO_2$ | BeO | Fe | Na | U | Zr | $ZrH_2$ | Na | $UO_2$ | $H_2O$ | Fe | $WO_2$ | $D_2O$ | Fe |
| 1 | 1 | 20 | 29 | 50 | 2 | 48 | 0 | 50 | 1 | 30 | 69 | 1 | 30 | 69 |
| 2 | 3 | 20 | 27 | 50 | 4 | 46 | 0 | 50 | 3 | 30 | 67 | 3 | 30 | 67 |
| 3 | 5 | 20 | 25 | 50 | 6 | 44 | 0 | 50 | 5 | 30 | 65 | 5 | 30 | 65 |
| 4 | 1 | 25 | 24 | 50 | 2 | 46 | 2 | 50 | 1 | 40 | 59 | 1 | 40 | 59 |
| 5 | 3 | 25 | 22 | 50 | 4 | 44 | 2 | 50 | 3 | 40 | 57 | 3 | 40 | 57 |
| 6 | 5 | 25 | 20 | 50 | 6 | 42 | 2 | 50 | 5 | 40 | 55 | 5 | 40 | 55 |
| 7 | 1 | 30 | 19 | 50 | 2 | 44 | 4 | 50 | 1 | 50 | 49 | 1 | 50 | 49 |
| 8 | 3 | 30 | 17 | 50 | 4 | 42 | 4 | 50 | 3 | 50 | 47 | 3 | 50 | 47 |
| 9 | 5 | 30 | 15 | 50 | 6 | 40 | 4 | 50 | 5 | 50 | 45 | 5 | 50 | 45 |

[7] Transactions of the American Nuclear Society, Reactor Operations Division Meeting, October 21-23, 1963, Ottawa, Ontario, p. 45.

A preliminary set of design calculations was developed for a reactor and a typical test section for use with the four types of systems. The designs were bounded by some of the following criteria. The composition of the test reactor should limit the ratio of power density between the test section and the reactor to a value of 4 or more. The power output of the test reactor should be held to a minimum. The reactor composition for the innermost regions was limited to a uranium concentration four to five times less than the test section and a moderator concentration which most closely reproduces the neutron spectrum of the test section. For the outer regions a uranium concentration was selected which yielded a flat or slightly decreasing power density and a moderator concentration which gradually softened the neutron spectrum. The calculations were then studied to determine possible design changes which would further reduce the power output.

Some preliminary results are reported here. The light and heavy water types of the test reactor cannot achieve a power density ratio of four or more with a typical test section. This is due to large differences between the neutron spectrum of the test section and of the test reactor. For a power density ratio of four, a test reactor with varying concentration of fuel and moderator produced a slightly smaller amount of power than the test reactor with a uniform concentration.

## C. Magnetohydrodynamics (MHD)

### 1. MHD AC Generator - Flashing Cycle

One type of energy-conversion system under study is the AC liquid metal MHD generator (see Progress Report for October 1963, ANL-6801, p. 69). Figure 24 shows a schematic of the experiment which was performed with this type of generator. Figure 25 shows a Lucite model for experiments at room temperature.

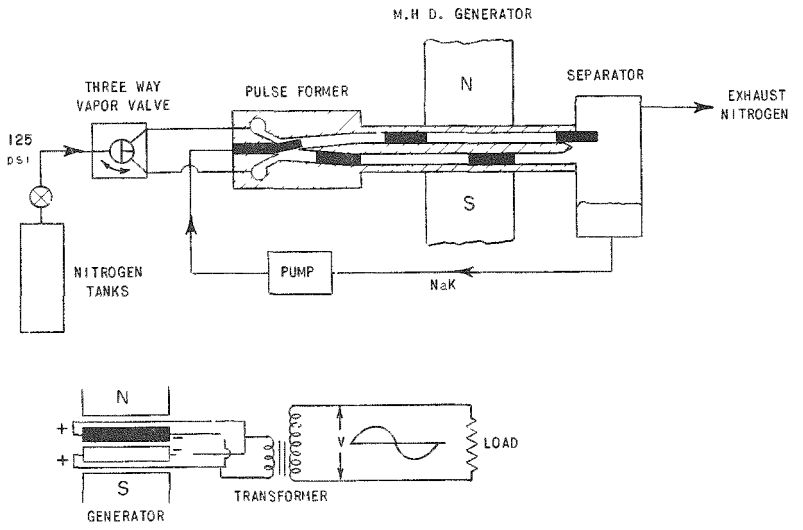


Figure 24. Schematic Arrangement of Layout of Experiment with AC Liquid Metal MHD Generator

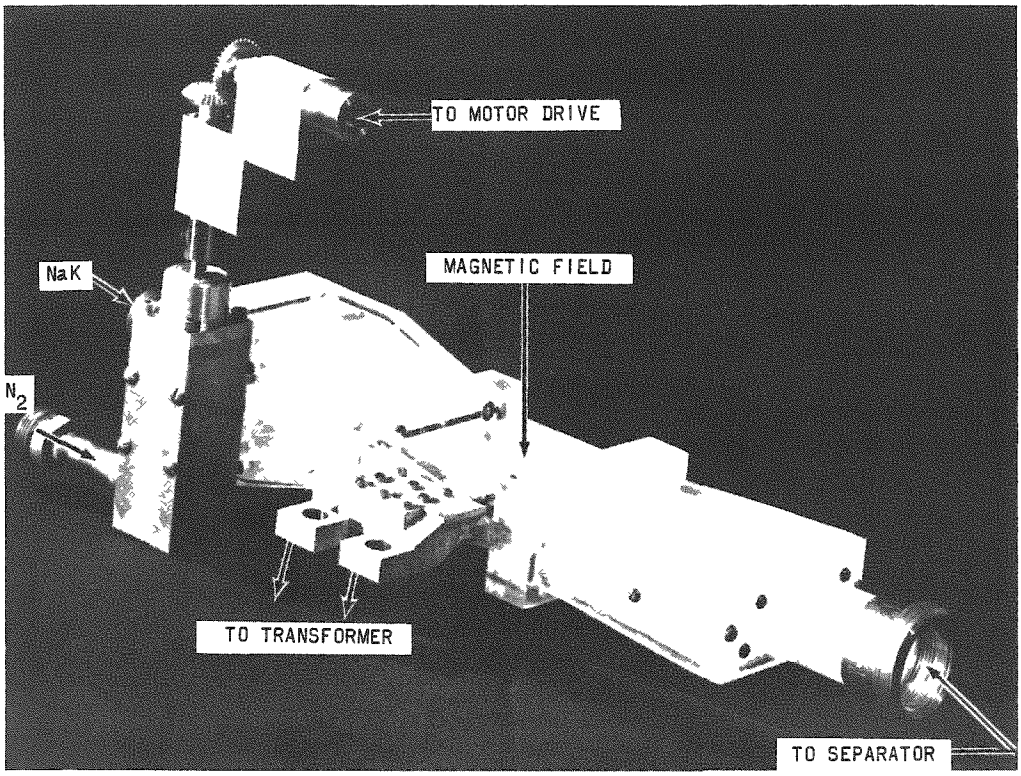


Figure 25. Lucite Model of AC Liquid Metal MHD Generator

The generator experiment operates as follows: By means of the three-way vapor valve, nitrogen is alternately switched from one duct to the other. This causes a stream of liquid NaK to be deflected from one duct to the other, with slugs of liquid being followed by slugs of gas. As the slugs move through a magnetic field, a voltage is induced perpendicularly to the field and the motion of the slugs. The current which flows in the slugs of liquid creates a force opposing the motion of the slug, but the pressure of the nitrogen forces the slug through the generator. The electrodes in the generator are connected so that a positive pulse is followed by a negative pulse, and a transformer is used to increase the voltage. As shown in Figure 24, when one set of electrodes is in contact with the slug, the other set must be open.

Figure 26 shows for one of the experiments the voltage trace across the load resistor. The incomplete lower pulse resulted from the fact that one duct leaked badly during this run. Figure 27 shows the voltage trace across the load when power from one duct is used. A modulating force of slightly more than 4 cycles/sec was found on the voltage trace; the cause for this phenomenon is unresolved.

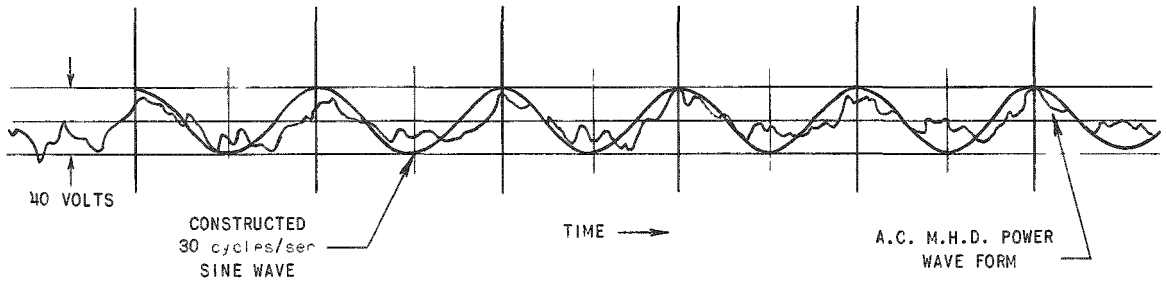


TIME = 50 in./sec
1 in. .02 sec
1 cycle .033 sec

FREQUENCE 30 cycles/sec
POWER 0.7 watts

Figure 26. Voltage Trace Across Load Resistor

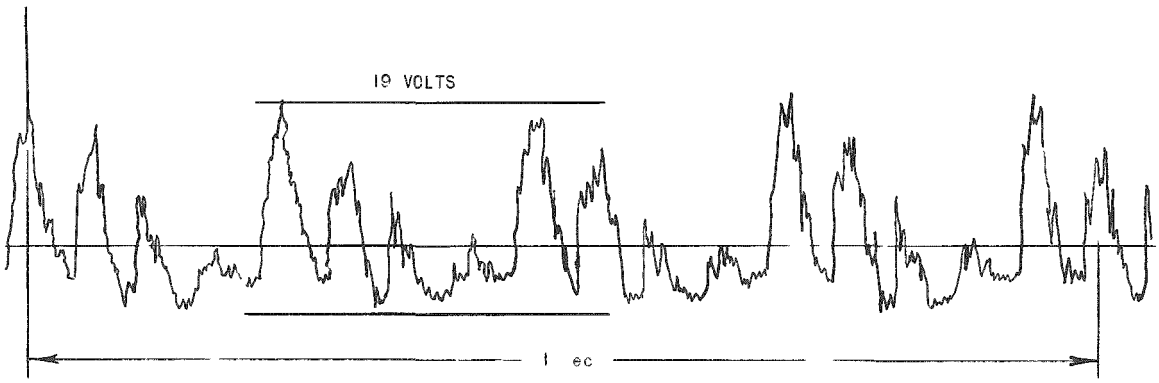


FREQUENCE 17 cycles/ secr

M-5000 GALVO IN SERIES WITH 270Ω LOAD TOTAL 305Ω
CS 10 n /sec

Figure 27. Voltage Trace Across Load with Power from One Duct

The Lucite model is not strong enough for continued use and is being replaced with a steel duct lined with an insulating material. Problems which need further investigation are:

1. increase of efficiency;
2. sizing of ducts so that hydraulic losses are minimized while maintaining integrity of the slugs;
3. spacing of pulses to give a more usable wave form;
4. development of a high-temperature system;
5. cycle analysis for two-fluid systems and also for a one-fluid system.

## 2. MHD Power Generation - Jet Pump Cycle

The new nozzle and combiner design was operated at a proper pumping location (see Progress Report for December 1963, ANL-6810, p. 44). The velocity obtained with the $\frac{1}{4}$-in. restriction was 49.9 ft/sec, a value that did not present any significant advantages over previous tests.

The various components of the loop have been investigated in order to provide improved performance. The thrust and discharge rate of the nozzle were measured and the total energy appearing in the discharge compared with the power expended in pumping. The pumping power was calculated from the measured pressure drops and mass flow rate figures.

These investigations yielded the following results.

1. The thrust of the nozzle was measured at 0.485 lb with a steam discharge rate of 0.0235 lb/sec. This corresponds to a discharge velocity of 663 ft/sec.

2. The measured discharge velocity was considerably less than theoretical. Subsequent examination showed that two valves in the steam line were throttling down the steam supply.

3. The pumping power expended amounted to 109.6 ft-lb/sec; the kinetic energy in the discharge steam was equal to 159.7 ft-lb/sec. This corresponds to a mechanical pumping efficiency of 68.6%. The ratio of water velocity to steam velocity at this time was equal to 61/663 = 0.092. When this figure is compared with the Mark's handbook value given by the curve for steam bucket to steam velocity vs. efficiency, one finds that at a value of 0.1, the efficiency is close to 60%. Thus, it can be seen that the results are consistent.

4. After removal of the valves that were producing throttling (see point 2), the nozzle thrust and discharge rate were redetermined. The thrust was raised to 4.8 lb and the discharge rate increased to 0.0662 lb/sec. This corresponds to a steam discharge velocity of 2332 ft/sec. The nozzle efficiency for these conditions amounted to 79.9% of theoretical.

Following this determination, the loop was again reassembled and the optimum operating position located for the new discharge. At this time, the maximum velocity was not appreciably greater than that obtained with the lower velocity exhaust. For this pumping rate, the velocity ratio was only 0.0261 and the conversion efficiency dropped to 1.97%. This is again consistent with turbine-efficiency curves and demonstrates the original premise that reasonably good velocity matching is necessary for good operation.

In addition, a heat balance taken over the loop for the new discharge conditions showed that the recirculating water entered the jet pump at a fairly high temperature. The heat balance also indicated that a considerable amount of vapor carryover was encountered at the diffuser. This condition would result in a large slip loss and lack of formation of the condensing shock, which would certainly be responsible for a lowered efficiency. Present modifications are aimed at trying to secure a proper condensing shock and a more favorable velocity ratio.

## D. Regenerative EMF Cells

### 1. Bimetallic Cells

Studies were continued on the development of thermally regenerative emf cells which, in a closed cycle, would have the net effect of converting heat from a nuclear reactor or from some other source into electricity. One type of cell under consideration is a bimetallic cell, consisting of two liquid metal electrodes in contact with an electrolyte which contains only the salts of the more active metal.

Previous studies (see Progress Report for November 1963, ANL-6808, pp. 65-69) indicated that the promising lithium-bismuth cell (current density of 450 amp/sq ft at 0.46 V) would be difficult to regenerate thermally. The difficulties stem from the facts that, at regeneration temperatures, the partial pressure of lithium is too low and the difference between the partial pressures of lithium and bismuth is small over the Li-Bi alloy formed in the cathode during cell operation. Thus, over a 0.60 atom fraction lithium alloy with bismuth at 1273°K, the estimated partial pressure of lithium is 0.24 mm Hg, while that of bismuth is 0.15 mm Hg. Because of the problem of thermal regeneration encountered with the Li-Bi system, other systems which may be more amenable to thermal regeneration are being investigated, namely, Li-Sn, Na-Sn, Na-Bi, and Rb-Bi systems.

The results of exploratory experiments on the thermal regeneration of the Li-Sn and Na-Sn systems have been reported previously (ANL-6808, p. 69). A similar experiment has been carried out with the Na-Bi system. A 70 a/o Na-30 a/o Bi alloy prepared with activated bismuth was contained in a closed tube. The end of the tube containing the alloy was heated for 6 hr at 920°C while the other end of the tube was maintained at 515°C. About 50 percent of the sodium was recovered in the distillate after the 6-hr distillation period. Analysis of the distillate revealed the sodium to be of high purity, the bismuth content being less than 3 ppm. These results indicate that the regeneration of the reactants in a Na-Bi cell could be accomplished effectively by thermal decomposition of the cathodic alloy and distillation at practical temperatures.

In cooperation with the Physics Division, a mass-spectrometric study of the rubidium-bismuth system was carried out to determine some of the thermodynamic characteristics of this system. The amounts of the monomeric species, $Rb^+$ and $Bi^+$, evaporated from $Rb_3Bi$ were measured in a week-long experiment. The results revealed that rubidium evaporated from the alloy at a much higher rate than bismuth, thereby indicating that thermal regeneration of the Rb-Bi system is feasible.

## 2. Lithium Hydride Cell

A second type of thermally regenerative emf cell being considered for the direct conversion of heat to electricity is the lithium hydride cell. The overall reaction of this cell is $Li(liq) + 1/2\ H_2(g) \rightarrow Li^+ + H^-$. Recent measurements with the hydrogen gas-hydride ion electrode gave a cell voltage at about 570°C that was approximately 100 mV greater than the voltages previously measured. This measurement was made with a new cell configuration, which introduced a junction potential. The cell configuration was as follows:

$$Li(liq),\ Li^+ \left| \begin{matrix} LiCl \\ LiF \end{matrix} \right\| \begin{matrix} LiCl \\ LiH \end{matrix} LiH(s) \left| H_2,\ H^-,\ Fe \right.$$

A calculation of the magnitude of this potential resulted in a value of about 100 mV.

A new cell is now being constructed in which the lithium metal electrode will be isolated from the electrolyte by a beryllium oxide (BeO) protection tube. A 0.006-in.-diameter hole drilled into the side of the protection tube will serve as a bridge. A second lithium electrode will be introduced into the lithium hydride-saturated electrolyte after the emf measurements with the BeO-protected lithium anode have been made. The initial voltage developed between these two lithium electrodes will be due to the junction potential in the system. As the second lithium electrode becomes saturated with lithium hydride, the voltage will change owing to the resulting decrease in activity of the second lithium anode. Careful time-voltage measurements between the two lithium anodes should make it possible to measure the activity of lithium saturated with lithium hydride. This will then allow the appropriate corrections to be made of the overall cell voltage to give a value of $E°$.

# V. NUCLEAR SAFETY

## A. Thermal Reactor Safety Studies

### 1. Metal Oxidation and Ignition

a. Oxidation of Uranium-10 w/o Molybdenum Alloy. A uranium-10 w/o molybdenum alloy is being considered for use as core material in a critical assembly, "Super Kukla," at the Lawrence Radiation Laboratory. Short studies of the oxidation and ignition behavior of this alloy are being undertaken at Argonne to aid in the assessment of possible hazards that might be associated with the use of the alloy. The samples for the studies are being provided by the Lawrence Radiation Laboratory.

Previous studies (see Progress Report for December, 1963, ANL-6810, p. 49) were extended to include isothermal oxidation experiments with bare alloy samples (1-cm cubes) in moist air (20,000 ppm $H_2O$) at 300, 400, 450, 500, 600, and 700°C. At 300°C, the oxidation rate was linear at $1.74 \times 10^{-3}$ mg $O_2$/(sq cm)(min) for the first 80 to 100 min, after which the reaction became parabolic. This transition is attributed to the formation of a protective oxide coating (about 1.5 $\mu$ thick after 80-100 min). At 400 and 450°C, the reaction was parabolic with rate constants of 5.5 and 14 (mg $O_2$/sq cm)$^2$/min, respectively. At 500 and 600°C, the reactions were linear throughout the runs, with rate constants of 0.039 and 0.31 mg $O_2$/(sq cm)(min), respectively. At 700°C, a very protective oxide coating was formed which resulted in a nearly cubic oxidation process for the first 200 min. This was followed by an accelerating reaction leading to a final rate of about 0.07 mg/(sq cm)(min).

The oxidation rates for the uranium-10 w/o molybdenum alloy were, in general, at least lower by an order of magnitude than those for unalloyed uranium. It should be noted, however, that thermal cycling might alter the oxidation behavior of the alloy. Once the conditions of cycling are established in "Super Kukla," a reappraisal of the oxidation behavior of the alloy under these cycling conditions might be appropriate.

b. Thermal Conductivity of Metal Powders. The study of thermal conductivities of metal powders has been undertaken to gain a better understanding of the mechanisms of ignition of metal powders, which, in turn, should lead to the formulation of sound preventive measures against accidental ignitions.

Previous studies (see Progress Report for December 1963, ANL-6810, p. 51) indicated that the thermal conductivities of unoxidized, 1.4% oxidized, and 2.3% oxidized uranium particles (-70 +80 mesh) were $8.0 \times 10^{4}$, $6.8 \times 10^{-4}$, and $6.4 \times 10^{-4}$ cal/(cm)(sec)(°C), respectively, at 24°C and 1000 mm Hg nitrogen pressure. In additional experiments, it was found that the decrease in thermal conductivity became more gradual as

the extent of oxidation was increased. At about 4.5, 12, 52, and 90% oxidation, the thermal conductivities were $6.2 \times 10^{-4}$, $5.4 \times 10^{-4}$, $4.4 \times 10^{-4}$, and $3 \times 10^{-4}$ cal/(cm)(sec)(°C), respectively.

2. Metal-Water Reactions

a. Reaction of Aluminum-Uranium Alloy (SL-1 Material) with Steam. The reaction of an aluminum-uranium alloy having the composition of SL-1 material (X-8001 aluminum with 17 w/o uranium) with steam is being studied by the levitation method.[9] The levitation method consists of simultaneously heating and levitating a pellet of the alloy in a radiofrequency field while steam is passed over the sample. The method allows the sample to be heated rapidly to the test temperature, held at this temperature for the desired time, and rapidly cooled. Preliminary studies at 1600°C have shown that the extent of oxidation of the aluminum-uranium alloy was nearly the same as that observed in previous studies with pure aluminum.[10] The data for pure aluminum conformed to a linear rate law, whereas the preliminary data for the alloy appear to deviate from linearity. Additional data are needed before the rate law for the aluminum-uranium alloy can be established.

b. Laser-beam Heating Applications. Research on the application of laser-beam heating to metal-water reactions was continued (see Progress Report for December 1963, ANL-6810, p. 52). Additional studies were performed with 1 x 1 x 0.13-mm-thick foils of zirconium. The foils were subjected to laser outputs of 4, 5, and 6 cal while submerged under a water column about 20 cm high. On melting, the foils were transformed to spherical particles. Microscopic examination of the particles revealed that the thickness of the oxide coating was independent of the laser energy. This is consistent with the results obtained in studies of the zirconium-water reaction by the condenser-discharge method and supports the diffusion-control theory of reaction proposed in the analysis of zirconium-water reaction studies by the condenser-discharge method.[11]

c. Studies in TREAT. Three experiments were completed in TREAT with oxide-core ($UO_2$), metal-clad fuel pins. The objectives of the experiments were to extend the information on the extent of metal-water reaction as a function of energy, to obtain reliable pressure-rate data, and to determine the particle size distribution of both the fragmented core and cladding. Results concerning the first two objectives are reported below. Particle size distribution data, however, are not yet available.

---

[9] Chemical Engineering Division Summary Report, Oct-Dec 1962, ANL-6648, p. 198.

[10] Chemical Engineering Division Research Highlights, May 1962-April 1963, ANL-6766, p. 101.

[11] L. Baker, Jr., and L. C. Just, Studies of Metal-Water Reactions, Part III, ANL-6548 (May 1962).

The conditions and the results of the experiments are given in Table XXX. The oxide core attained a temperature of 3300°C in each of the three runs; this temperature is the vaporization point of the $UO_2$ in the core. Each pin underwent total destruction with the formation of globules and fine particles. It is noteworthy that, although the fuel pins were subjected to extremely energetic excursions while submerged in water, only about one-third of the molten metal reacted with the water.

Table XXX. High-energy Metal-Water Experiments in TREAT with Oxide-core, Metal-clad Fuel Pins

(Unirradiated fuel pins submerged in water at 20°C)

| | CEN Transient Number | | |
|---|---|---|---|
| | 168 | 169 | 170 |
| **Characteristics of Reactor Pulse** | | | |
| Integrated Power, MW-sec | 985 | 768 | 606 |
| Peak Power, MW | 4142 | 4338 | 2570 |
| Period, ms | 41 | 42 | 51 |
| **Characteristics of Fuel Pin** | | | |
| Core Material, % $UO_2$ | 8.7 | 100 | 100 |
| Enrichment, % $U^{235}$ | 93.5 | 11.2 | 20.0 |
| Cladding Metal (20 mils thick) | Zr-2 | SS-304 | SS-304 |
| **Results** | | | |
| Computed Energy Input, cal/g of core | 787 | 617 | 655 |
| Estimated Peak Adiabatic Core Temp, °C | 3300 | 3300 | 3300 |
| Peak Recorded Pressure in Autoclave, psi | 102 | >300 | 670 |
| Final Recorded Pressure in Autoclave, psi | 102 | 114 | 164 |
| Max Recorded Rate of Pressure Rise, psi/ms | 0.26 | 3.75 | 6.00 |
| Ratio: Peak Pressure/Final Pressure | 1.0 | >2.6 | 4.1 |
| Measured Extent of Metal-Water Reaction, % | 29.6 | 29.8 | 31.7 |

## B. Fast Reactor Safety Studies

### 1. Scanning Device for Mockup of Prompt-neutron Meltdown

Two key safety features characteristic of typical fast power reactor designs are the short prompt-neutron lifetime and the quantity of fissionable material, which is usually sufficient to provide a number of critical masses. Because of these, a class of "meltdown" accidents can be postulated in which (a) some operating abnormality triggers some degree of fuel failure, (b) the fuel moves into a super-prompt critical configuration, and (c) a destructive burst of nuclear energy results. However, because of the short neutron lifetime, such a power burst would have a duration of the order of a few milliseconds or less. Hence, rates of reactivity addition are more important for accident analysis than total conceivable reactivity addition. Thus, a device capable of directly observing fuel movement during a meltdown experiment

is of great importance. For this purpose, high-speed optical photography has been employed usefully in experiments on dry samples, but is of limited worth for study of EBR-II pins, which release an opaque cloud of sodium upon failure, and cannot be used for experiments on samples in a sodium coolant.

A multichannel meltdown scanner has been proposed which would use detection of prompt neutrons from fuel samples. The basic theoretical calculations have been checked by tests at TREAT with a mockup of a single collimator channel of the proposed multichannel device to view typical experimental arrangements of meltdown. Analysis of the tests showed that the spatial resolution of the channel (0.38 cm at the meltdown sample location) was satisfactory and in agreement with prediction. Signal strengths and signal-to-background ratios were acceptable for the three basic experiments of the mockup: dry opaque meltdown, dry transparent meltdown, and package sodium loop meltdown (see Progress Report for October 1962, ANL-6635).

Two types of neutron detectors were tried; both were satisfactory. Test results will be used to fix the design of the full-scale device including shielding, multichannel collimation, detectors, and readout. Figure 28 shows relative counting rates as a function of collimator position for a

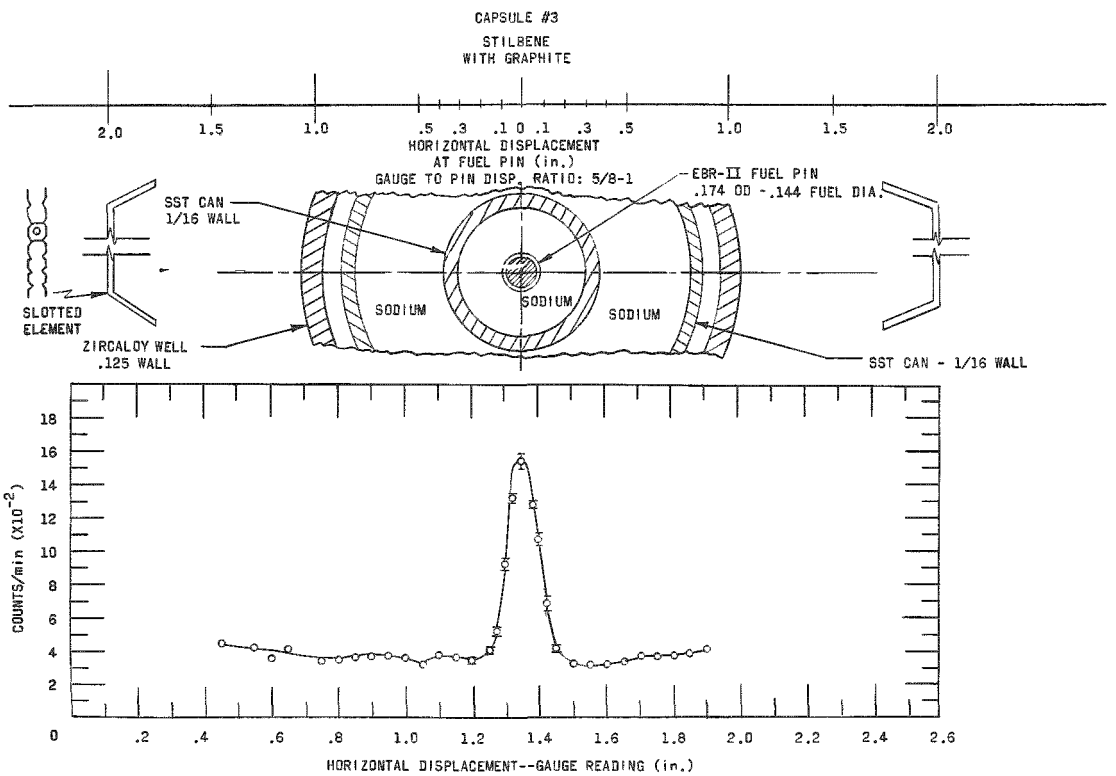


Figure 28. Counting Rate as a Function of Collimator Position for a 6% Enriched EBR-II Pin inside a Mockup of the Package Sodium Loop. For clarity in presentation, position is designated by horizontal location of collimator aiming point in the test hole on the TREAT centerline. The collimator position is indicated by an attached gauge.

6% enriched EBR-II sample inside a simulated package sodium loop. Although some background from the container (see Figure 28) is apparent, it is much less than that obtained from the trials of a gamma-ray scanning device which was tested earlier and found to have both unsatisfactory signal strength and signal-to-background ratio.[12]

## C. TREAT

### 1. Small TREAT Loop

A test of the integrity of the lower silicone "O" ring seal for the small-loop dummy element was performed. Sodium at 500°C was poured into one of the assemblies followed by several hours of heating to a maximum temperature of 343°C. The seal operated satisfactorily under these extreme conditions and was considered an adequate demonstration of its suitability for use with the small loop.

### 2. Large TREAT Loop

The 4-in. P-K ball valves under repair and modification are approximately 80% complete at this time. Three valves are under helium leak test following the final assembly, and the remaining two are being prepared for final test.

Construction of the vessels is proceeding according to schedule. ANL personnel have inspected interior welds and cleanliness and have reported that these are satisfactory. Shipment to Idaho is expected for the week of February 3, 1964.

An additional flowmeter is being added to monitor flow in the cold trap. A spare 2-in. model has been located. The flowmeters are being prepared for calibration.

Calculations were completed on the non-transient thermal stresses in this large loop. The design was found to be adequate.

Preliminary studies for draining sodium from the test section after removal from the reactor has been started. The results of this study will dictate the location of suitable services for the performance of this operation at TREAT.

---

[12] L. A. Beach, A. G. Pieper, and M. P. Young, Gamma-ray Scanning Techniques for Fast Breeder Reactor Safety Studies, NRL-5625 (July 12, 1961).

# VI. PUBLICATIONS

## Papers

AN EFFICIENT COMPOSITE FORMULA FOR MULTIDIMENSIONAL QUADRATURE
Henry C. Thacher, Jr.
Comm. ACM 7(1), 23-25 (January 1964)

EXPEDITING DANGER-COEFFICIENT MEASUREMENTS BY MEASURING TWO SAMPLES AT ONCE
Charles Erwin Cohn
Nucl. Sci. and Eng. 18, 140-142 (January 1964)

ELASTIC SCATTERING OF FAST NEUTRONS FROM $U^{235}$
A. B. Smith
Nucl. Sci. and Eng. 18, 126-129 (January 1964)

NEUTRON ACTIVATION CROSS SECTIONS FOR $Br^{79}$, $Br^{81}$, $Rh^{103}$, $In^{115}$, $I^{127}$, AND $Ta^{181}$
S. A. Cox
Physical Review 133 (2B), B-378-B383 (January 27, 1964)

SCATTERING OF FAST NEUTRONS FROM NATURAL Zr AND Nb
Daniel Reitman, C. A. Engelbrecht, and A. B. Smith
Nucl. Phys. 48(4), 593-607 (1963)

SUBNANOSECOND RC RISE TIMES FROM IONIZATION COUNTERS
Alexander DeVolpi, K. G. Porges, and C. J. Rush
Bull. Am. Phys. Soc. 9, 46 (January 1964) Abstract

NUCLEAR PHOTOPRODUCTION OF NEUTRAL PIONS
C. A. Engelbrecht
Bull. Am. Phys. Soc. 9, 80 (January 1964) Abstract

THE $Fe^{54}$ (d,n) $Co^{55}$ REACTION
D. S. Gemmell, L. L. Lee, Jr., J. P. Schiffer, and A. B. Smith
Bull. Am. Phys. Soc. 9, 92 (January 1964) Abstract

CALCULATIONS FOR LATTICE PARAMETERS
B. I. Spinrad
Heavy Water Lattices: Second Panel Report, Vienna, February 18-22, 1963. Tech. Report Ser. No. 20. Intern. Atomic Energy Agency, Vienna, 1963. pp. 39-41

WORLD STATUS AND FUTURE OF FAST REACTORS
L. J. Koch
Proc. Am. Power Conf., March 26-28, 1963, Chicago, Illinois Illinois Institute of Technology, Chicago, 1963. Vol. 25, pp. 178-188

PERFORMANCE CHARACTERISTICS OF EBWR FROM 0-100 MWt
E. A. Wimunc, Michael Petrick, W. C. Lipinski, and H. P. Iskenderian
Proc. IAEA Conf. on Operating Experience with Power Reactors, Vienna, June 4-10, 1963. Intern. Atomic Energy Agency, Vienna, 1963. pp. 355-404

TITANIUM AND TITANIUM ALLOYS IN MERCURY - SOME OBSERVATIONS ON CORROSION AND INHIBITION
J. Y. N. Wang
Nucl. Sci. Eng. 18, 18-30 (January 1964)

THE REACTIONS OF URANIUM HEXAFLUORIDE WITH HYDROGEN SULFIDE AND WITH CARBON DISULFIDE
L. E. Trevorrow, Jack Fischer and W. H. Gunther
Inorg. Chem. 2, 1281-1284 (1963)

ANL Reports

ANL-5719 (Addendum) ADDENDUM TO HAZARD SUMMARY REPORT, EXPERIMENTAL BREEDER REACTOR-II (EBR-II)
L. J. Koch, W. B. Loewenstein, and H. O. Monson

ANL-6103 EXAMINATION OF IRRADIATED RaLa SOURCE FUEL ROD (PROTOTYPE NO. 2) FOR LOS ALAMOS SCIENTIFIC LABORATORY
S. H. Paine, W. F. Murphy, and F. L. Brown

ANL-6632 NONDESTRUCTIVE TESTS OF COMPONENTS OF EBR-I, CORE IV
R. H. Selner, C. J. Renken, R. B. Perry, and K. Balaramamoorthy

ANL-6691 CRITICAL EXPERIMENT WITH BORAX-V. Internal Superheater
K. E. Plumlee, Q. L. Baird, G. S. Stanford, and P. I. Amundson

ANL-6695 TIME-OPTIMUM CONTROL OF NUCLEAR REACTORS WITH VELOCITY-LIMITED CONTROL DEVICES
Thomas P. Mulcahey

ANL-6697 A PRIMER ON THE ACT-III COMPILER FOR THE LGP-30 DIGITAL COMPUTER
H. C. Thacher, Jr. and R. E. Grench

ANL-6763 LABORATORY INVESTIGATIONS IN SUPPORT OF FLUID BED FLUORIDE VOLATILITY PROCESSES.
Part IV. The Fluid Bed Fluorination of $U_3O_8$
R. L Jarry, A. V. Hariharan, G. Manevy, J. Fischer, J. J. Stockbar, J. G. Riha, T. D. Baker, and G. W. Redding